



Non-Equilibrium Phase Diagrams: Interference between the gas-liquid, glass, and gel transitions

Tesis que para obtener el grado de Doctor en Ciencias Interdisciplinarias presenta
Jesús Benigno Zepeda López

Línea de investigación

Física de Materiales

Codirectores de Tesis

Dr. Magdaleno Medina Noyola

Dr. Luis Fernando Elizondo Aguilera



POSGRADO
EN CIENCIAS
INTERDISCIPLINARIAS





Non-Equilibrium Phase Diagrams: Interference between the gas-liquid, glass, and gel transitions

A thesis submitted as a requirement for the obtainment of the degree Doctor en Ciencias Interdisciplinarias presented by

Jesús Benigno Zepeda López

Investigation Line

Material Physics

Thesis co-advisors

Dr. Magdaleno Medina Noyola

Dr. Luis Fernando Elizondo Aguilera



**POSGRADO
EN CIENCIAS
INTERDISCIPLINARIAS**





Non-Equilibrium Phase Diagrams: Interference between the gas-liquid, glass, and gel transitions por Jesús Benigno Zepeda López se distribuye bajo una [Licencia Creative Commons Atribución 4.0 Internacional](https://creativecommons.org/licenses/by/4.0/).

Resumen

En este trabajo estudiamos la dependencia temporal en la transformación de estados de no-equilibrio utilizando la teoría de no-equilibrio de la ecuación generalizada de Langevin (NE-SCGLE por sus siglas en inglés) en un sistema fluido que interactúa a través de un potencial repulsivo de esfera dura más una atracción de pozo cuadrado (HSSW por sus siglas en inglés). Existe una inmensa cantidad de materiales utilizados en la vida cotidiana que no pueden ser descritos utilizando métodos de termodinámica clásica ni estadística. Los geles y los vidrios, son ejemplo de esta clase de materiales. En particular, estos tipos de materiales exhiben comportamientos tales como el envejecimiento de sus propiedades estructurales y dinámicas, lo cual hace complicado su estudio por medio de teorías de equilibrio. Por ello, la teoría NE-SCGLE, una teoría de primeros principios, es utilizada como alternativa al estudio de procesos evolutivos en sistemas fuera de equilibrio termodinámico.

Una forma de modelar estos materiales es a través de sistemas tipo Lennard-Jones, caracterizados por un juego entre interacciones repulsivas y atractivas de corto alcance, como es el caso del fluido HSSW. Al someter este tipo de sistemas a procesos de no-equilibrio, tales como enfriamientos súbitos, uno puede obtener sólidos amorfos tales como los geles y vidrios. En este sentido, una forma de modelar dichos procesos de no-equilibrio es a través de la teoría NE-SCGLE, la cual nos permite introducir el protocolo de preparación de los sistemas mediante el conocimiento de los parámetros termodinámicos. De esta forma, uno puede obtener los resultados principales de la teoría NE-SCGLE de estos procesos, los cuales pueden ser resumidos en los cambios temporales de propiedades estructurales y dinámicas que caracterizan al sistema.

En particular, estos procesos de solidificación amorfa son descritos a través de sistemas que sufren un arresto dinámico, en el cual las partículas que lo conforman, esencialmente pierden su capacidad de difundirse. Por ello, el estudio de las propiedades dinámicas resulta especialmente crucial en la formación de sólidos amorfos, mientras que las propiedades estructurales nos permiten entender el ordenamiento entre las partículas que conforman a un sistema. El estudio de ambos tipos de propiedades nos permiten no sólo conocer la existencia de estados dinámicamente arrestados, sino que también nos permite clasificarlos. Esto es por ejemplo, a través de la identificación de comportamientos característicos que nos permiten distinguir entre vidrios y geles.

De esta manera, el presente trabajo se centra en mostrar la capacidad predictiva de la teoría NE-SCGLE en términos de algunas de las características principales en la formación de geles y vidrios. En particular, estas características son mostradas en términos de su dependencia temporal, la cual nos permite entender los procesos de transformación de estos materiales. A su vez, esto nos permite proponer una predicción práctica para el tiempo en el cual las transformaciones a sólidos amorfos ocurren. Tal propuesta es considerada la contribución más relevante del presente trabajo, la cual tiene como resultado principal la primer derivación de un diagrama de no-equilibrio dependiente del tiempo a través de una teoría de primeros principios.

Abstract

In this work, we study the time dependency of non-equilibrium states through the use of the non-equilibrium generalized Langevin equation theory (NE-SCGLE) for a fluid with a repulsive hard sphere plus an attractive square well interaction potential (HSSW). There exist a huge amount of daily life materials which can not be fully described through classical and statistical thermodynamics methods. Gels and glasses are an example of these kind of materials. These kind of materials exhibit non-equilibrium behaviors, such as aging in structural and dynamical properties, which makes their study difficult through equilibrium theories. Thus, the NE-SCGLE theory, as a first principle theory, is employed as an alternative for the study of evolution processes of out of thermodynamic equilibrium systems.

One way to model these kind of materials is through Lennard-Jones-like systems, characterized by the interplay of repulsive and attractive short-range interactions, such as the HSSW fluid. By submitting these kind of systems to non-equilibrium processes such as sudden quenches, one can obtain amorphous solids such as gels and glasses. In this sense, a scheme to model such non-equilibrium processes can be devised within the NE-SCGLE theory, which allow us to input the preparation protocol of the systems through the knowledge of the thermodynamic parameters. Thus, we can obtain the NE-SCGLE main results of such processes, which can be summarized by the temporal description of the structural and dynamical properties that allow us to characterize the system.

In particular, such amorphous solidification processes are described through systems dynamically arrested in which, their conforming particles essentially lose their capacity to diffuse. Thus, the study of dynamical properties is particularly crucial in the formation of amorphous solids, while the structural properties allow us to understand the ordering between particles that conform the system. The study of these both kind of properties allow us not only to recognize the existence of dynamically arrested states, but also to classify them. This is done for example, by identifying signature behaviors which allow us to distinguish between gels and glasses.

Thus, the present work focuses on exhibiting the predictive capacity of the NE-SCGLE theory in terms of signature characteristics in the formation of gels and glasses. In particular, such characteristics are shown in terms of their temporal dependence, which allow us to understand the transformation processes of these materials. In return, this enable us to propose a practical prediction for the time in which the transformations towards an amorphous solid occurs. Such proposal is considered the most relevant contribution of the present work, which leads to the main result: the first time-dependent non-equilibrium diagram from a first principles theory.

Acknowledgments

I would like to thank all of my family members, specially Concepción López Rosas, José Zepeda Martínez and José Eduardo Zepeda López, whose full support has allowed me to commit and finish this work. In addition, I would like to thank my closest colleagues and collaborators, Leticia López Flores, José Manuel Olais Govea, Ernesto Cortés Morales, Edilio Lázaro Lázaro, Patricia Mendoza Méndez, Mariana Eugenia Farías Anguiano, Pablo Fernando Zubieta Rico, Luis Fernando Elizondo Aguilera, Yuto Kimura, Pedro Ezequiel Ramírez González and Alexis Torres Carbajal, María Inés Valenzuela Carrillo, Paulina Alejandra Ojeda Martínez, Ana Gabriela Carretas Talamante, Ricardo Peredo Ortiz, Orlando Joaquin, Jan Carlo, as well as my advisor Magdalena Medina Noyola, whose fruitful discussions and invaluable friendship do not go under appreciated across the development of this work, as well as CONACyT, who financially supported me through the grants Becas Nacionales No. 455426, LANIMFE 314881 and CB A1-S-22362.

Lastly, I would like to thank my colleagues and friends that accompanied me along this stage of my life, with whom I cherished precious moments, Erick Sarmiento Gómez, María de Jesús Martínez, Beatriz Morales Cruzado, Jesús Hector Castillo Sotelo, Carlos Robles, Cristian Rodríguez Escalante, Gabriel Corella, Zaid Ignacio, Maximino Perez, Elizabeth Flores, Daniel López, Cristian Omar Aguilar, Fernando Aldair Pérez González, Nohemi Atquetzali Pérez Gómez, Francisco Álvarez, Alma Rosales, Sandra Zapata, Rafael Dávila, Eva Wong, Fidel Martínez, Luis Trujillo, Daniela Blanco, Regina Sanchez, José Zárate, Ulises Torres Herrera, Weiquan Zhan, Yuan Yuan, Manuel Meza, Silvia del Carmen Jonguitud Flores, Fidel Ibarra and Rafael Osvaldo Dávila.

Contents

1	Introduction	11
2	The NE-SCGLE theoretical framework	17
2.1	The mathematical nature of the generalized Langevin equation (GLE)	17
2.2	SCGLE Theory	19
2.2.1	Memory functions approximations	21
2.3	Derived dynamical properties and relevant asymptotic limits	23
2.4	NE-SCGLE Theory	25
2.5	Summary	28
3	Stationary diagrams of the HSSW fluid system.	29
3.1	Thermodynamic equilibrium phase diagram	30
3.2	<i>Glass transition</i> phase diagram	34
3.3	<i>Non-equilibrium</i> glass transition phase diagram	36
3.4	Summary	39
4	The kinetic perspective of the glass, gel and gas-liquid transitions and their interference.	41
4.1	NE-SCGLE results & discussion	41
4.2	Summary	47
5	Waiting-time dependent non-equilibrium glass transition diagrams	49
5.1	The mobility function $b(t)$ as a dynamical arrest parameter	50
5.2	The time dependent non-equilibrium glass transition diagram of the HSSW fluid	51
5.3	Summary	58
6	NE-SCGLE description of density linear deviations.	59
6.1	Theoretical approximation.	59
6.2	Initial state condition of a hard sphere system.	61
6.3	Evolution of density fluctuations.	63
6.4	Summary	79
7	Conclusions	81
	Appendices	83
A	Solution algorithm for the SCGLE equations	85
B	Additional data treatment for the density fluctuations	91

Chapter 1

Introduction

This thesis proposes a fundamental definition and practical determination of *non-equilibrium phase diagrams*, and offers them as a novel tool for the theoretical interpretation of the widespread empirical reports of the experimental evolution of suddenly quenched liquids (or melts) in the process of fabrication of amorphous solid materials. This proposal is based on the application of the *non-equilibrium Self-Consistent Generalized Langevin Equation (NE-SCGLE)* theory to the description of the irreversible evolution of the structural and dynamical properties of suddenly quenched model liquids. This non-equilibrium theory [1] was developed only one decade ago in another Ph. D. Thesis at Universidad Autónoma de San Luis Potosí (UASLP), and still remains as the first and only first-principles statistical mechanical theory reported in the international literature, capable of explaining and predicting the most relevant features of the non-equilibrium amorphous solidification of liquids. In this context, the present thesis presents the first and only statistical mechanical description of the irreversible evolution of the properties of a liquid in the process of formation of non-equilibrium amorphous solids, in a format that extends the ordinary notion of equilibrium phases and phase diagrams to the full non-equilibrium regime.

To better explain the actual contributions of this work as well as its relevance, let us start by providing the pertinent contextual material. The basic problem of thermodynamics is to understand and predict the changes of the thermodynamic variables which describe the thermodynamic state of a system, let it be water, alcohol, carbon or any other substance. In general, this problem is solved when the associated *fundamental thermodynamic relation* (FTR [2]), $\mathcal{S} = \mathcal{S}[E, X_1, X_2, \dots]$, describing the system, is known. Here \mathcal{S} is the entropy of the system, E is the internal energy, and X_i is the i th extensive variable with which one describes the system (*e.g.*, the volume V and the number of particles N for monocomponent liquids and gases). Such general formalism allows us to describe not only changes within the same phase of the system, but in general, the physical transformation between phases, such as the condensation of gases into liquids, the freezing of liquids into crystalline solids or other possible phase transformation that the system may undergo. Hence, thermodynamics is a fundamental tool to understand and characterize a system, at least under conditions of full thermodynamic equilibrium [2, 3].

From classical thermodynamics, one learns that the FTR of a system may be determined primarily by empirical means. On the other hand, from statistical thermodynamics, one learns that the FTR can actually be derived from the fundamental interactions between particles through Boltzmann's expression $\mathcal{S} = k_B \ln \Omega$, which writes the entropy \mathcal{S} (a macroscopic quantity) in terms of the number Ω of microscopic states of the N -particle system [4]. Statistical thermodynamics thus provides what is thought to be a complete framework that allows us to understand the thermodynamics of the system starting from the knowledge of fundamental interactions, which

can be applied to a great variety of systems. However, in reality we only know how to apply this formalism in full detail for (thermodynamic) equilibrium states, whose properties are determined by the solution of a set of equations that derive from, and expresses in mathematical form, the equilibrium condition of maximum entropy. In this manner, the full catalog of thermodynamic equilibrium phases of the system, and the conventional *thermodynamic equilibrium phase diagram*, are determined.

The problem arises, however, when trying to describe systems that do not satisfy thermodynamic equilibrium conditions. One of the most fundamental features of *equilibrium* thermodynamics is that the state of a system is time independent, *i.e.*, that the thermodynamic properties of a system in equilibrium remain constant in time. Furthermore, thermodynamic equilibrium also implies the absence of fluxes. Such conditions lead to several universal conclusions, one of the most relevant being that these equilibrium properties are independent of the preparation protocol employed to drive the system to a given equilibrium state. In real life, however, it is known that changes in the non-equilibrium production process of materials may produce changes in their final physical properties, one of the most ancient examples being the tempering of steel [5]. A more colloquial analogy would be the comparison between frying scrambled eggs and scrambling fried eggs.

Dynamically arrested states constitute a broad category of macroscopic states of materials that cannot be explained by equilibrium statistical thermodynamics, for the simple reason that they are not in equilibrium. The evidence for this is the fact that they exhibit aging (*i.e.*, their properties depend on the time after preparation), and the fact that these properties actually depend on the very process of preparation. In dynamically arrested states the constituent particles are almost unable to diffuse. In a more practical and relaxed definition, their mean particle diffusion coefficient is found to decrease by several orders of magnitude with respect to that of its fluid or gas counterpart. As a result, the system solidifies, and yet, its *structural* properties remain closer to those of a fluid than to those of a crystalline solid. Examples of such states are in every day materials in the form of gels and glasses, such as yogurts[6], ceramic materials[7] and stained glasses[8].

The description of dynamically arrested materials is typically given in terms of dynamic (rather than thermodynamic) properties. Theories that explain the dynamics of liquids at equilibrium exist, such as the so-called mode coupling theory (MCT) [9, 10] and the self-consistent generalized Langevin equation (SCGLE)[11]. In spite of their limitation to equilibrium conditions, these theories have long been used to understand and predict several features of dynamical arrest phenomena [9, 10, 12]. Fundamentally, the two aforementioned theories are able to link the structure (*i.e.*, the average local arrangement of the fluid particles) with the dynamics of the system. Since the structure is characterized by the elementary or effective interaction forces between the constituent particles, these theories serve as an extension of statistical thermodynamics to the description of the macroscopic dynamic properties of the system. It is then within these kind of theories that the dynamics of fluids still in equilibrium, but near dynamically arrested states, have commonly been studied [13]. Both MCT and SCGLE provide two major prediction for glass forming liquids, namely, the existence of an idealized arrest transition (involving strictly non diffusive states) and of a power-law increase of the relaxation times near arrested states [13, 14, 15, 16, 12].

It is the prediction of such idealized arrested states what allows these theories to determine the region of a state space (*e.g.*, temperature-density plane), where the system will be able to reach equilibrium, and the region where the system will become dynamically arrested (in which case it may become a glass or a gel, depending on the molecular interactions). The locus of these regions in the control parameters space, along with the corresponding boundaries (or “dynamical arrest

lines”) indicating the transition from ergodic (equilibrium fluid) to non-ergodic (glass, gel, etc.), is referred to as the *glass transition diagram*, a recurring term that will be employed along the present work for historical reasons [17]. In general, a *glass transition diagram* complements the ordinary thermodynamic equilibrium phase diagram with information of kinetic nature. Thus, the equilibrium phase diagram indicates the phases attained in the absence of kinetic barriers, whereas the glass transition diagram predicts the regions where this may not be possible. Unfortunately, the idealized sharp dynamical arrest transitions predicted by both MCT and SCGLE is never observed in practice, as experiments always reveal the existence of a residual small diffusion, even for glassy states well beyond the dynamical arrest transitions predicted by these theories. In addition, since these theories were developed under equilibrium assumptions, they are unable to explain essential non-equilibrium fingerprints of arrested materials, such as aging, which consists of the increasingly slow but endless evolution of the system’s properties, such as their viscoelastic or structural response, commonly observed in the formation of gels and glasses [14, 15, 18].

In this context, the extension of these (or other) theories to the description of non-equilibrium states remains as a major theoretical challenge for modern statistical thermodynamics. Historically, at the end of the last century A. Latz launched the first attempt to extended MCT to the description of aging[19], whereas a *non-equilibrium* extension of the self-consistent generalized Langevin equation (NE-SCGLE) theory was developed one decade later [1]. Unfortunately, the endeavor started by Latz, in the context of structural glass formers, was not really continued by the MCT community, as demonstrated by the lack of concrete applications in the context of structural glass forming liquids. In the meanwhile, in spite of the considerably smaller scientific community behind it, the NE-SCGLE theory immediately succeeded in demonstrating its usefulness in the detailed description of non-equilibrium processes, by means of its successful application in several concrete directions. Some examples are the aging of soft mono- and multi-component repulsive systems[20, 21, 22], as well as dipole-dipole interacting systems[23, 24].

One recent application of the NE-SCGLE theory that will be particularly relevant for the present thesis is its application to Lennard-Jones-like systems [25]. These systems involve a short range attractive interaction plus a strong shorter-ranged repulsion (such as the hard sphere plus attractive Yukawa (HSAY) interaction potential), and hold a special place in the study of classical fluids due to their role in the understanding of the nature of the gas-liquid transition. Conventional statistical thermodynamics allows us to outline the corresponding coexistence and spinodal lines in the thermodynamic state space of this system. The coexistence line determines the region in which the two phases (*i.e.* gas and liquid) are expected to coexist under equilibrium conditions, while the spinodal line is the boundary of stability of uniform metastable states within such coexistence region. Thus, inside the spinodal region, the small inherent thermal fluctuations of the system become unstable and are amplified to grow in size through what is commonly known as spinodal decomposition, whose effective final result is the complete phase separation of the system [3]. As it happens, however, for sufficiently fast and deep quenches, such spinodal decomposition processes may be interrupted by the emergence of dynamic arrest conditions, leading to the formation of physical gels, which are rather common non-equilibrium amorphous materials [26, 27].

It is precisely these dynamically arrested spinodal decomposition processes experimentally observed in systems represented by Lennard-Jones-like models what emphasizes the relevance of the NE-SCGLE framework [28, 27]. As said above, one of the main results of both, MCT and the equilibrium SCGLE theory, is their prediction of the so-called glass transition diagrams. These glass transition diagrams, however, do not include a description of dynamically arrested states inside the thermodynamically unstable spinodal region, where the input required by these theories (the structure factor of the homogeneous equilibrium state) does not exist. This limitation

was removed by the NE-SCGLE framework, whose most fundamental input is not the equilibrium structure factor, but the second functional derivative of the entropy \mathcal{S} with respect to the local density.

As described in detail in Refs. [25, 29], this subtle but relevant difference allowed the NE-SCGLE theory to yield the first fundamental theoretical description of arrested spinodal decomposition. This was first obtained from the analysis of the long-time asymptotic limit of the solution of the NE-SCGLE main equations for specific non-equilibrium instantaneous isochoric quenching processes. Outside the spinodal region, this method confirmed the glass transition diagram originally provided by the equilibrium (MCT and SCGLE) theories. Inside the spinodal region, however, its predictions unveiled a complex and fascinating scenario describing the formation of non-equilibrium arrested phases with sponge-like structures, typical of gels and porous glasses. The resulting diagram, enriched with these predicted amorphous solid states, was thus referred to as the *non-equilibrium glass transition diagram*. Its long-time asymptotic nature allowed the direct comparison of such novel diagrams, with the ordinary equilibrium phase diagrams, and to spell out the interference between an ordinary gas-liquid phase transition and the more mysterious and fascinating transitions to glass and gel states.

Summarizing these non-equilibrium predictions only in terms of the long-time asymptotic (equilibrium or non equilibrium) diagrams comes at the cost of ignoring the rich and relevant time dependence of the processes of formation of non-equilibrium amorphous phases. This information, however, is precisely the most relevant fingerprint of the glass and the gel transitions, as demonstrated by the comparison of the full time-dependent solutions of the NE-SCGLE equations with simulation and experimental results for a few illustrative quench processes [29, 30, 22]. The practical and fundamental relevance of the full time dependence of these processes, however, can hardly be overestimated. Every day enormous amounts of experimental information is produced in the world, which reports the time-dependent phase transformation of many materials during their process of fabrication.

The information thus obtained is reported in empirical non-equilibrium *time-dependent “phase diagrams”*, in which the time after preparation is a fundamental variable. In such reports, the time is frequently expressed in logarithmic scale, due to the strikingly slow relaxation involved in the aging of dynamically arrested materials. Illustrative examples are the so-called time-temperature-transformation (TTT) diagrams, widely employed in metallurgical processes and in the fabrication of borosilicate glasses [31], or the phase separation, gelation and vitrification processes of colloidal clay suspensions[32]. In these cases, relevant delayed effects in the material response are commonly observed prior to the observation of notable changes in their properties. These experimental data are especially relevant for virtually every industrial sector that depends on the precise fabrication or transformation of amorphous materials. It is in this context that the need arises of a fundamental theory capable of predicting and describing the intricate evolution of these non-equilibrium materials.

Addressing precisely this issue is, thus, the main aim of the present dissertation, whose most important contribution is the development of a fundamental statistical mechanics description of the experimentally-determined *time-dependent non-equilibrium* glass transition diagrams illustrated by the referred time-temperature-transformation (TTT) diagrams. For this, we apply the non-equilibrium Self-Consistent Generalized Langevin Equation (NE-SCGLE) theory to a generic model fluid with well-defined interparticle interactions described by a pair potential $u(r)$. In this manner we describe the non-equilibrium evolution of the structural and dynamical properties of the system as a function of the (waiting) time t after it was suddenly quenched to a point (n, T) of its density-temperature state space. This work builds upon previous developments involving

several specific model systems [1, 20, 25, 30, 29]. Such previous works, however, focused only in the description of a single quench, whereas in the present contribution we discuss the physics that emerges when considering a collection of quenches to state points in a finite region of the (n, T) plane.

A second major aim of this thesis is to reveal the time-dependent scenario predicted by the NE-SCGLE theory regarding the interference between the gas-liquid equilibrium phase transition, and the non-equilibrium glass- and gel-transitions that lead to the amorphous solidification of liquids, into glasses, gels, and porous glasses. This expanded scenario constitutes a natural extension of the ordinary scenario of equilibrium phases predicted by statistical thermodynamics, starting with van der Waals' theory of the gas-liquid transition. Like van der Waals, here we shall also have in mind a simple model fluid whose particles interact with a pair potential composed of a strong short-ranged repulsion plus a longer-ranged attraction (from now on, systems of this kind will be referred to as Lennard-Jones-like liquids).

Finally, a third main contribution of this thesis refers to the theoretical description of the growth and arrest of density heterogeneities during the process of arrested spinodal decomposition. These heterogeneities describe the non-equilibrium evolution of the morphology of the system. These three aims of the present thesis thus map onto three main contributions, described in three technical manuscripts. The first major scientific contribution is summarized in reference [33] and the second in reference [29]. A manuscript that summarizes the theoretical description of morphological evolution is still in preparation for publication.

Hence, in order to fully exhibit these contributions, the present thesis is divided in seven chapters. In chapter 2, we present a general overview of the equations that constitute the essence of the NE-SCGLE theoretical framework. These general equations describe the time evolution of the relevant properties, such as the local mean density, its covariance, the (waiting) time dependent intermediate scattering function and the local mobility. Along the chapter, we discuss the derivation and approximations leading to such set of equations. Given a noticeable absence of a careful review of the fundamentals of the theory, filling this gap is also a relevant contribution of this chapter.

Chapter 3 focuses on the precise background of the *glass transition diagrams* for Lennard-Jones-like systems within the NE-SCGLE framework. Thus, in this chapter some of the asymptotic relations derived in chapter 2 are applied for a model system, namely, a hard sphere plus square well (HSSW) fluid. It is worth to notice that this is the first time that this model system is described within the NE-SCGLE framework. The relevance in considering this model comes from the fact that it exhibits a gas-liquid spinodal line, thus delimiting an inaccessible region to any equilibrium theory such as MCT or SCGLE. As shown in this chapter, this is not an impediment for the NE-SCGLE theory, which is employed to determine the corresponding *non-equilibrium glass transition diagram*, that includes a hard-sphere-like glass-transition (also predicted by the SCGLE) and two competing dynamical arrest transitions inside the spinodal region.

Chapter 4 discusses the full waiting -time evolution of the HSSW fluid for an ensemble of non-equilibrium processes, allowing to emphasize various fundamental non-equilibrium fingerprints involved in the interference of the gas-liquid, gel and glass transitions. These fingerprints are related to the prediction of different aging and latency effects in the dynamical properties of the HSSW liquid, which are systematically studied across the non-equilibrium glass transition diagram. Thus, this chapter paves the way for one of our main contributions, namely, the proposal and derivation of a waiting-time non-equilibrium glass transition diagrams.

Chapter 5 deals with the main objective of the present dissertation. This is done across two sections. In the first one, the practical threshold for the mobility to describe dynamical arrested

states and its context are discussed. In the second one, the main results leading to the *waiting-time dependent non-equilibrium glass transition diagrams* are presented. Specifically, these diagrams are obtained through the full waiting-time description of the NE-SCGLE framework across an extensive set of thermodynamical parameters. Thus, it is precisely the capacity to connect the ideas behind such analysis, as well as its implementation, what distinguish the present work from previous contributions. In particular, the resulting diagrams are in stark contrast with the asymptotic diagrams shown in 3, as the time dependency is explicitly stated. On the other hand, the resulting time dependent diagram are embedded around the concepts discussed in chapters 3 and 4, allowing us to present a clear view of the involved dynamical arrest phenomena.

Chapter 6 addresses the third contribution of our work, organized in three sections. In the first of them, an equation for the evolution of a locally dependent mean density $\bar{n}(\mathbf{r}, t)$ is derived, a property which is expected to describe the system's morphology. This equation is obtained through a linear approximation performed for one of the main equations of the theory, whose solution requires an initial condition. In the second section, a simple theoretical approach for the initial condition is explained and employed. Then, on the third section, the theoretical predictions are displayed and discussed.

Finally, in chapter 7 we provide our concluding remarks. The achievement of the presented objective conforms what is thought to be the next step in the understanding of non-equilibrium materials with what is hopefully an unified first principle theoretical framework, capable of extending the equilibrium concepts given by statistical thermodynamics. Such understanding is the principal justification of the present work and all advances made for this understanding are far from falling short. For perspective, two and a half decades have passed since the famous quote of the Nobel prize physicist P. W. Anderson " *The deepest and most interesting unsolved problem in solid state theory is probably the theory of the nature of glass and the glass transition. This could be the next breakthrough in the coming decade.*" [34]. This statement was, as a matter of fact, made without the added complexity of competing behaviors with other non-equilibrium states, and yet such clear breakthrough is still to be seen.

Chapter 2

The NE-SCGLE theoretical framework

This chapter summarizes the fundamental basis of the *non-equilibrium self-consistent generalized Langevin equation* (NE-SCGLE) theoretical framework. Such fundamental basis lie in areas of statistical and thermal physics as diverse as the classical theory of equilibrium homogeneous and non-uniform liquids, the thermodynamic and hydrodynamic theory of irreversible processes, and the stochastic description of physical fluctuations. Building the NE-SCGLE theoretical framework upon such diverse fundamental basis has been a rather slow process, requiring many specific steps, which have been reported in a correspondingly long series of apparently disconnected reports. There is, thus, an urgent need for a unifying review, and this chapter describes our attempt to fill such a gap.

With this purpose in mind, let us start by noticing that the NE-SCGLE theory was developed in two distinct sequential stages, and its formulation involved two hierarchical levels of abstraction and generality. The first stage involves the application of the fundamental perspective provided by Onsager's general and abstract formalism for the relaxation and thermal fluctuations description in equilibrium systems, for the derivation of the SCGLE theory, which describes the dynamics in fully ergodic states. The second stage refers to the extension of this equilibrium theory to the non-equilibrium domain, leading to the full NE-SCGLE theory, which turns out to be a general non-equilibrium theory of irreversible processes in liquids with temporal and spatial molecular resolution. To review the main steps in the construction the NE-SCGLE theory, this chapter is divided into four main sections, the first three being composed around the equilibrium version of the theory, where relevant theorems involving theory of fluctuations are briefly summarized for reasons of self-containedness. Then the core set of equations for the SCGLE theory are derived and some relevant limits and properties are obtained. In the last section, the non-equilibrium version is explained in terms of two main equations, one for the evolution of the mean local density and another one for its covariance. Due to the intricacies of the solution of these two equations, which involves a generalization of the SCGLE core equations, the actual NE-SCGLE theory is left at the end of the chapter.

2.1 The mathematical nature of the generalized Langevin equation (GLE)

In this section, the fundamental basis of the self-consistent generalized Langevin equation (SCGLE) theory is summarized. We refer to a relevant mathematical theorem that imposes strong and general conditions on the stochastic models employed to describe thermal fluctuations. This leads

to the so-called generalized Langevin equation (GLE), whose mathematical structure incorporates these imposed mathematical conditions as important and exact relationships between the physical properties involved. Many times these exact conditions, such as the fluctuation-dissipation relation, are perceived merely as phenomenological results. Being exact conditions, however, they are instrumental in deriving other important exact or approximate equations describing the relaxation of thermal fluctuations of specific physical properties in concrete systems. A detailed example will be found in the next section, which refers to the description of density fluctuations in a liquid. Here we only state the content of these theorems, whose mathematical proof can be found elsewhere[35].

Let \mathbf{a} be a n -dimensional vector of stochastic variables

$$\mathbf{a}(t) = \begin{bmatrix} a_1(t) \\ a_2(t) \\ \vdots \\ a_n(t) \end{bmatrix}, \quad (2.1)$$

described by the most general linear stochastic equation with additive noise, of the form

$$\frac{d\mathbf{a}(t)}{dt} = - \int_0^t \mathbf{G}(t-t')\mathbf{a}(t')dt' + \mathbf{f}(t), \quad (2.2)$$

with initial condition $\mathbf{a}_0 = \mathbf{a}(0)$ of zero mean $\langle \mathbf{a}_0 \rangle = 0$, driven by a stochastic n -dimensional vector $\mathbf{f}(t)$ of also zero mean $\langle \mathbf{f}(t) \rangle = 0$ and uncorrelated with \mathbf{a}_0 , *i.e.* $\langle \mathbf{a}_0 \mathbf{f}^T(t) \rangle = \langle \mathbf{f}(t) \mathbf{a}_0^T \rangle = 0$. The formal solution of (2.2) is

$$\mathbf{a}(t) = \chi(t)\mathbf{a}_0 + \int_0^t \chi(t-t')\mathbf{f}(t')dt', \quad (2.3)$$

where $\chi(t)$ is the propagator defined by the inverse Laplace transform (LT) of

$$\hat{\chi}(z) = \left(z\mathbf{I} + \hat{\mathbf{G}}(z) \right)^{-1}. \quad (2.4)$$

For this stochastic process, the following three statements are equivalent:

Statement A: $\mathbf{a}(t)$ is stationary, *i.e.*

$$\langle \mathbf{a}(t+s)\mathbf{a}^T(t'+s) \rangle = \langle \mathbf{a}(t)\mathbf{a}^T(t') \rangle \quad (2.5)$$

Statement B: $\mathbf{f}(t)$ is stationary and $\mathbf{G}(t)$ is such that generalized Langevin equation can be written as

$$\frac{d\mathbf{a}(t)}{dt} = -\boldsymbol{\omega} \circ \chi^{-1} \circ \mathbf{a}(t) - \int_0^t \mathbf{L}(t-t') \circ \chi^{-1} \circ \mathbf{a}(t')dt' + \mathbf{f}(t), \quad (2.6)$$

where

$$\chi = \langle \mathbf{a}(0)\mathbf{a}^T(0) \rangle, \quad (2.7)$$

and \mathbf{L} is defined as

$$\mathbf{L}(t-t') = \mathbf{L}^T(t'-t) = \langle \mathbf{f}(t)\mathbf{f}^T(t') \rangle \quad (2.8)$$

Statement C: an exact fluctuation-dissipation relation exists between $\mathbf{L}(t-t')$ and $\mathbf{G}(t-t')$, namely,

$$\mathbf{L}(t-t') = (\mathbf{G}(t-t')\boldsymbol{\omega} - 2\delta(t-t')\boldsymbol{\omega})\theta(t-t') + (\mathbf{G}(t'-t)\boldsymbol{\omega} - 2\delta(t'-t)\boldsymbol{\omega})\theta(t'-t). \quad (2.9)$$

2.2 SCGLE Theory

In this section we derive the set of equations that conform the SCGLE theory for the description equilibrium dynamics. This set consist of an equation for the intermediate scattering function $F(k, t)$ (ISF), another for the self part of the ISF $F_s(k, t)$, and a third for an unknown memory function. For the ISF and its self part, the expressions are first derived for a general multi-component system. For clarity and simplicity, however, a closure relation for the memory functions is derived only for a monocomponent system.

In the last section, several theorems that stochastic variables which are described by the generalized Langevin equation were summarized. Now, in order to derive general expressions for the ISF and its self part, the local density fluctuations

$$\delta \mathbf{n}(\mathbf{r}, t) = \begin{bmatrix} \delta n_1(\mathbf{r}, t) \\ \delta n_2(\mathbf{r}, t) \\ \vdots \\ \delta n_\nu(\mathbf{r}, t) \end{bmatrix}, \quad (2.10)$$

along with its fluxes (also referred to as current density)

$$\delta \mathbf{j}(\mathbf{r}, t) = \begin{bmatrix} \delta j_{1,x}(\mathbf{r}, t) \hat{\mathbf{x}} + \delta j_{1,y}(\mathbf{r}, t) \hat{\mathbf{y}} + \delta j_{1,z}(\mathbf{r}, t) \hat{\mathbf{z}} \\ \delta j_{2,x}(\mathbf{r}, t) \hat{\mathbf{x}} + \delta j_{2,y}(\mathbf{r}, t) \hat{\mathbf{y}} + \delta j_{2,z}(\mathbf{r}, t) \hat{\mathbf{z}} \\ \vdots \\ \delta j_{\nu,x}(\mathbf{r}, t) \hat{\mathbf{x}} + \delta j_{\nu,y}(\mathbf{r}, t) \hat{\mathbf{y}} + \delta j_{\nu,z}(\mathbf{r}, t) \hat{\mathbf{z}} \end{bmatrix}, \quad (2.11)$$

are selected as said stochastic variables, in which

$$\delta n_i(\mathbf{r}, t) \equiv \sum_{j=1}^{N_i} \delta[\mathbf{r} - \mathbf{r}_j(t)] - n_i, \quad (2.12)$$

is the local density fluctuation of the N_i identical particles of the i species for a mixture of ν species, and where $n_i \equiv N_i/V$ is the mean particle density of the i specie in the system, and

$$\delta j_{i,z}(\mathbf{r}, t) \equiv \sum_{l=1}^{N_i} \hat{\mathbf{k}} \cdot \mathbf{v}_l(t) \delta[\mathbf{r} - \mathbf{r}_l(t)] - \langle \mathbf{j}_i \rangle_z, \quad (2.13)$$

where $\mathbf{v}_l \equiv \partial \mathbf{r}_l / \partial t$ is the velocity of the l particle of species i and $\langle \mathbf{j}_i \rangle$ stands for the ensemble average of the flux of species i and where $\hat{\mathbf{k}}$ stands for the unit wave-vector. These variables allow to define the stochastic vector

$$\delta \mathbf{a}(\mathbf{k}, t) = \begin{bmatrix} \delta \hat{\mathbf{n}}(\mathbf{k}, t) \\ \delta \hat{\mathbf{j}}(\mathbf{k}, t) \end{bmatrix}, \quad (2.14)$$

in which

$$\delta \hat{\mathbf{n}}_l(\mathbf{k}, t) = \frac{1}{\sqrt{N_l}} \sum_{k=1}^{N_l} e^{i\mathbf{k} \cdot \mathbf{r}_k}, \quad (2.15)$$

$$\delta \hat{\mathbf{j}}_l(\mathbf{k}, t) = \frac{1}{\sqrt{N_l}} \sum_{k=1}^{N_l} \hat{\mathbf{k}} \cdot \mathbf{v}_k e^{i\mathbf{k} \cdot \mathbf{r}_k}, \quad (2.16)$$

are the Fourier transform (FT) of $\delta\mathbf{n}_l(\mathbf{r}, t)$ and $\delta\mathbf{j}_l(\mathbf{r}, t)$ times $1/\sqrt{N_l}$, respectively, and *where the ensemble average* (denoted by $\langle \rangle$) of the particle flux is considered zero $\langle \mathbf{j} \rangle = \mathbf{0}$, in other words, the particles movement occur without any directional preference.

This stochastic variable follows the general form expressed by Eq. (2.6), for which the problem now becomes the identification of each of the terms. For example, when considering *an homogeneous and isotropic system*, the static correlation matrix $\chi \equiv \langle \mathbf{a}(0)\mathbf{a}^T(0) \rangle$ must have the form

$$\chi = \begin{bmatrix} \mathbf{S}(k) & \mathbf{0} \\ \mathbf{0} & \chi_{jj} \end{bmatrix}, \quad (2.17)$$

where $\mathbf{S}(k) \equiv \langle \delta\mathbf{n}(k, 0) \circ \delta\mathbf{n}^T(-k, 0) \rangle$ with \circ being the matrix multiplication operator, and where $\chi_{jj} \equiv \langle \delta\mathbf{j}(k, 0) \circ \delta\mathbf{j}^T(-k, 0) \rangle = k_B T \mathbf{M}^{-1}$ (where the equipartition theorem is being employed), with k_B being the Boltzmann constant, T the temperature and \mathbf{M} the diagonal matrix of masses for multiple particle species with $\mathbf{M}_{ij} \equiv \delta_{ij} M_i$ entries.

In addition to the last consideration, through a *contraction of the description* [36], a single equation for one of the variables can be obtained. Such contraction is, in general, proposed in terms of a known phenomenological relation between the variables, such as the continuity equation for a system in which the number of particles is conserved

$$\frac{d\delta n_i(\mathbf{r}, t)}{dt} \equiv ik\delta j_i. \quad (2.18)$$

Besides its use in the aforementioned contraction of the description, this equations allows to gain insight about the memory and the entries of the anti-symmetric matrix ω terms, which are now constrained to the structures

$$\mathbf{L} = \begin{bmatrix} \mathbf{L}_{nn} = \mathbf{0} & \mathbf{L}_{nj} = \mathbf{0} \\ \mathbf{L}_{jn} = \mathbf{0} & \mathbf{L}_{jj} \end{bmatrix}, \quad (2.19)$$

and

$$\omega = \begin{bmatrix} \mathbf{0} & \omega_{nj} = -ik\chi_{jj} \\ \omega_{jn} = ik\chi_{jj} & \mathbf{0} \end{bmatrix}. \quad (2.20)$$

The conditions imposed over the terms of Eq. (2.6) allow us to write the set of equations

$$\frac{d\delta\mathbf{n}(\mathbf{k}, t)}{dt} = -\omega_{nj}\chi_{jj}\delta\mathbf{j}, \quad (2.21)$$

$$\frac{d\delta\mathbf{j}(\mathbf{k}, t)}{dt} = -\omega_{jn} \circ \chi_{nn}^{-1} \circ \delta\mathbf{n}(\mathbf{k}, t) - \int_0^t \mathbf{L}_{jj}(t-t') \circ \chi_{jj}^{-1} \circ \delta\mathbf{j}(\mathbf{k}, t') + \mathbf{f}_j(\mathbf{k}, t), \quad (2.22)$$

which in return leads for the contraction of the description. In Laplace space, such contraction reads

$$\begin{aligned} \delta\hat{\mathbf{n}}(\mathbf{k}, z) - \delta\mathbf{n}(\mathbf{k}, 0) &= -\omega_{nj} \circ \chi_{jj} \circ \left\{ \mathbf{I} + \hat{\mathbf{L}}_{jj}(z) \circ \chi_{jj}^{-1} \right\}^{-1} \circ \\ &\left\{ \mathbf{j}(\mathbf{k}, 0) - \omega_{jn} \circ \chi_{nn}^{-1} \circ \delta\hat{\mathbf{n}}(\mathbf{k}, z) + \hat{\mathbf{f}}_j(\mathbf{k}, z) \right\}, \end{aligned} \quad (2.23)$$

where the flux term has been replaced by

$$\delta\hat{\mathbf{j}}(\mathbf{k}, z) = \left\{ \mathbf{I} + \hat{\mathbf{L}}_{jj}(z) \circ \chi_{jj}^{-1} \right\}^{-1} \circ \left[\mathbf{j}(\mathbf{k}, 0) - \omega_{jn} \circ \chi_{nn}^{-1} \circ \delta\hat{\mathbf{n}}(\mathbf{k}, z) + \hat{\mathbf{f}}_j(\mathbf{k}, z) \right]. \quad (2.24)$$

Equation 2.23 can be written in terms of the ISF, defined for stationary systems as $\mathbf{F}(\mathbf{k}, \tau) \equiv \langle \delta\mathbf{n}(\mathbf{k}, t) \circ \delta\mathbf{n}^T(-\mathbf{k}, t') \rangle$, where $\tau \equiv |t - t'|$ is the elapsed time between states at t and t' , and for

which the arbitrary initial condition can be set at $t' = 0$. Thus, an equation for the ISF is obtained by multiplying Eqn. 2.23 by $\delta \mathbf{n}^T(k, 0)$, and then taking the ensemble average, leading to

$$\mathbf{F}(k, z) = \left\{ z\mathbf{I} + \left[\mathbf{I} + \hat{\mathbf{L}}_{jj}(z) \circ \mathbf{D}_0^{-1} \right]^{-1} k^2 \mathbf{D}_0 \mathbf{S}^{-1}(k) \right\}^{-1} \mathbf{S}(k), \quad (2.25)$$

where $\mathbf{S}(k)$ is the initial condition of $\mathbf{F}(k, \tau)$. This same procedure can also be applied to a tracer particle instead of all the particles, which leads to the same kind of equation for the self part, namely

$$\mathbf{F}_s(k, z) = \left\{ z\mathbf{I} + \left[\mathbf{I} + \hat{\mathbf{L}}_{jj}^{(s)}(z) \circ \mathbf{D}_0^{-1} \right]^{-1} k^2 \mathbf{D}_0 \right\}^{-1}. \quad (2.26)$$

2.2.1 Memory functions approximations

As the general expressions for the ISF and its self part were just derived, the question is now how to compute the memory functions $\mathbf{L}_{jj}^{(s)}(z)$ and $\mathbf{L}_{jj}(z)$ appearing in Eqs. (2.25) and (2.26). To answer this question, the derivation of reference [12] for a memory kernel, along with the approximations used for the simplified version of the theory [37] are followed for the simplified case of a mono component system.

Let us consider a slightly different set of stochastic variables $\delta n^*(\mathbf{r}, t)$, and the velocity of the tracer particle \mathbf{v}_T , where the difference is that for these variables the frame of reference is now centered around a tracer particle. For this set of variables, the set of equations given by the generalized Langevin equation formalism are now [12]

$$m \frac{d\mathbf{v}_T}{dt} = -\zeta^0 \mathbf{v}_T(t) + \mathbf{f}_T(t) + \int d\mathbf{r} \nabla u(\mathbf{r}) \delta n^*(\mathbf{r}, t), \quad (2.27)$$

$$\frac{d\delta n^*(\mathbf{r}, t)}{dt} = [\nabla n^{eq}(\mathbf{r}, t) \cdot \mathbf{v}_T(t)] - \int_0^t dt' \int d\mathbf{r}' D^*(\mathbf{r}, \mathbf{r}', t) \delta n^*(\mathbf{r}', t') + \mathbf{f}(\mathbf{r}, t), \quad (2.28)$$

where m corresponds to the mass of the tracer particle, ζ^0 is the friction produced by the solvent, $u(\mathbf{r})$ is the interaction potential between the tracer and the other particles, $\mathbf{f}_T(t)$ is the random force produced by the solvent, f is the fluctuation term associated with D^* through the fluctuation-dissipation theorem (see eq. (2.8)) with $\omega = \langle \delta n^*(\mathbf{r}, 0) \delta n^*(\mathbf{r}', 0) \rangle$ and where D^* plays the role of the unknown memory function \mathbf{G} in equation (2.2).

By substituting in Eq. (2.27) the formal solution of Eq. (2.28), the expression

$$m \frac{d\mathbf{v}_T}{dt} = -\zeta^0 \mathbf{v}_T(t) + \mathbf{f}_T(t) - \int_0^t \Delta \overset{\leftrightarrow}{\zeta}(t') dt' \cdot \mathbf{v}(t') + F(t), \quad (2.29)$$

is obtained, where the fluctuating force $\mathbf{F}(t)$ is a fluctuation given by the tracer interaction with the other particles, related to the friction memory kernel $\delta \zeta$ through the fluctuation-dissipation theorem (Eq. (2.9)), and where $\Delta \overset{\leftrightarrow}{\zeta}$ is given by the exact result[12]

$$\Delta \overset{\leftrightarrow}{\zeta} = - \int d\mathbf{r} \int d\mathbf{r}' [\nabla u(\mathbf{r})] \chi(\mathbf{r}, \mathbf{r}'; t) [\nabla' n^{eq}(\mathbf{r}')] \quad (2.30)$$

in which the propagator χ^* is solution the of Eq. (2.4). Then, by denoting the convolution of two functions $\int d\mathbf{r}'' F(\mathbf{r}, \mathbf{r}'') G(\mathbf{r}'', \mathbf{r}') \equiv F \circ G$ and by using the Wertheim-Lovett relation $[\nabla n^{eq}] = -\beta \sigma \circ [\nabla u]$, the exact solution for $\Delta \overset{\leftrightarrow}{\zeta}$ can be expressed as

$$\Delta \overset{\leftrightarrow}{\zeta} = k_B T [\nabla n^{eq \dagger}] \circ \omega^{-1} \circ G^*(t) \circ \omega^{-1} \circ [\nabla n^{eq}], \quad (2.31)$$

where $G^*(t) \equiv \chi^* \omega$ is the Van Hove function referred to the tracer particle.

The functions G^* and ω^* are referred to the tracer particles, with an explicit dependence on \mathbf{r} and \mathbf{r}' . This implies that these functions are, in general, three particle correlation functions. Nevertheless, one could think in these two properties just as the common two particle correlation functions with a perturbation held by the tracer particle. When such perturbation is neglected, the "homogeneous fluid approximation" is recovered [12, 36], for which $\omega(\mathbf{r}, \mathbf{r}') = \omega(|\mathbf{r} - \mathbf{r}'|)$ and $G^*(\mathbf{r}, \mathbf{r}') = G^*(|\mathbf{r} - \mathbf{r}'|)$. This approximation allows us to express the tensor $\Delta \overset{\leftrightarrow}{\zeta}$ in terms of the traced framed ISF $F^* \equiv \langle \exp\{i\mathbf{k} \cdot [\mathbf{r}_T(t) - \mathbf{r}_T(0)]\} \cdot (\sum_{ij} \exp\{i\mathbf{k} \cdot [\mathbf{r}_i(t) - \mathbf{r}_j(0)]\}) \rangle$, where $\mathbf{r}_T(t)$ and $\mathbf{r}_i(t)$ are the position of the traced and the i -th particle from a laboratory-fixed frame. With such definition, then the decoupling approximation is employed, for which $F^* \approx F(k, t)F_s(k, t)$.

Finally, by considering spherical interacting particles, the tensor $\Delta \overset{\leftrightarrow}{\zeta}$ must be diagonal, such that the tensor $\Delta \overset{\leftrightarrow}{\zeta} = \Delta \zeta(t) \Delta \overset{\leftrightarrow}{\mathbf{I}}$, along with Eq. (2.31), the following expression for $\Delta \zeta^* \equiv \Delta \zeta / \zeta^0$ is obtained

$$\Delta \zeta^*(\tau) = \frac{D_0}{24\pi^3 \bar{n}} \int_V k^2 \left[\frac{S(k) - 1}{S(k)} \right]^2 F(k, \tau) F_s(k, \tau) d\mathbf{k}, \quad (2.32)$$

which is an expression that now relates a memory function with the ISF and its self part. As the exact relation of the memory kernel just derived with the memory functions $\mathbf{L}_{jj}^{(s)}$ and $\mathbf{L}_{jj}(z)$ remains unknown, and in order to close the system of equations, various approximate closure relations have been proposed [12, 37]. In this work, we will adopt the simplest the proposals, which as shown in Ref. [37], can be summarized by the following equations

$$\mathbf{L}_{jj}^{(s)} = \mathbf{L}_{jj}, \quad (2.33)$$

$$\mathbf{L}_{jj}^{(s)} = \Delta \zeta^*(\tau) \lambda(k), \quad (2.34)$$

where

$$\lambda(k) = \frac{1}{1 + (k/k_c)^2}, \quad (2.35)$$

is an interpolating function, with k_c being the theory only adjustable parameter, which in this work is set as $k_c = 1.305 \times 2\pi$ in order to conform with previous results [25].

This set of approximations leads to the evolution equations for the LT of the ISF and its self part

$$F(k, z) = \frac{S(k)}{z + \frac{k^2 D_0 S^{-1}(k)}{1 + \lambda(k) \Delta \zeta(z)}}, \quad (2.36)$$

$$F_s(k, z) = \frac{1}{z + \frac{k^2 D_0}{1 + \lambda(k) \Delta \zeta(z)}}. \quad (2.37)$$

These equations, along with Eqs. (2.32) and (2.35) form a complete and self consistent set of equations that summarizes the SCGLE formalism. The only external input in this set of equations comes in the form of the static structure factor $S(k)$, which is just the initial condition of the ISF. Once this external input is known, an iterative method, such as the one explained in Appendix A can be employed in order to give solutions to obtain the solution of these coupled equations.

2.3 Derived dynamical properties and relevant asymptotic limits

Once the central equations for the dynamical variables $F(k, \tau)$, $F_s(k, \tau)$ and $\Delta\zeta^*(\tau)$ have been derived, let us emphasize that the SCGLE theory is able to provide other important dynamical properties. The most relevant of such properties, which will also play a central role in the description of the non-equilibrium version of the SCGLE to be discussed in what follows, is the long-time diffusion coefficient D . This property is directly related to the mean-squared displacement (MSD) $W(\tau)$

$$W(\tau) \equiv \langle |\mathbf{r}(\tau) - \mathbf{r}(0)|^2 \rangle, \quad (2.38)$$

through the (correlation) time dependent diffusion coefficient

$$D(\tau) \equiv \frac{1}{6} \frac{dW(\tau)}{d\tau}, \quad (2.39)$$

in the limit

$$D \equiv \lim_{\tau \rightarrow \infty} D(\tau). \quad (2.40)$$

In particular, a relationship between these properties and the memory function $\Delta\zeta(\tau)$ can be derived from the general Langevin equation for a tracer particle. Taking the inner product of Eq. (2.29) with $\mathbf{v}(0)$ and using the LT it follows

$$m(z\hat{v}(z) - v_0^2) = \zeta^0\hat{v}(z) - \Delta\hat{\zeta}(z)\hat{v}(z), \quad (2.41)$$

where $\hat{v}(z)$ is the Laplace transform \mathfrak{L} of $\langle \mathbf{v}(t) \cdot \mathbf{v}(0) \rangle$, namely $\hat{v}(z) \equiv \mathfrak{L}[\langle \mathbf{v}(t) \cdot \mathbf{v}(0) \rangle]$, and with $v_0^2 \equiv \langle \mathbf{v}(0) \cdot \mathbf{v}(0) \rangle$. From the last equation, one can solve for $\hat{v}(z)$, which yields

$$\hat{v}(z) = \frac{v_0^2}{mz + \zeta^0 + \Delta\hat{\zeta}(z)}, \quad (2.42)$$

which in the over-damped limit can be approximetly written as

$$\hat{v}(z) \approx \frac{v_0^2}{\zeta^0 + \Delta\hat{\zeta}(z)}. \quad (2.43)$$

In this equation both, the equipartition theorem ($v_0^2 = 3k_B T$, with k_B being the Boltzmann's constant), along with the Stokes-Einstein relation ($\zeta^0 = k_B T/D_0$, where D_0 is the free particle diffusion coefficient) can be employed to rewrite the last equation as

$$\hat{v}(z) \approx \frac{3D_0}{1 + \Delta\hat{\zeta}^*(z)}. \quad (2.44)$$

Finally, by taking into account the relationship between the velocity auto correlation and the diffusion equation derived from its definition, we may write

$$\hat{D}(z) = \frac{\hat{v}(z)}{zd}. \quad (2.45)$$

Hence, an equation for $D^* \equiv D(\tau)/D_0$ can be written as

$$\hat{D}^*(z) = \frac{1}{z(1 + \Delta\hat{\zeta}^*(z))}, \quad (2.46)$$

whose inverse Laplace transformation (ILT) is

$$D^*(\tau) = 1 - \int D^*(\tau') \Delta\zeta^*(\tau - \tau') d\tau'. \quad (2.47)$$

A similar procedure can be done in order to obtain an equivalent expression for the MSD, *i.e.* by considering $z\hat{W}(z) = \hat{D}(z)$. As for the long time diffusion coefficient, the limit can be easily evaluated in Eq. (2.46) as $\lim_{z \rightarrow 0} z\hat{D}^*(z)$, which yields

$$b = \frac{1}{1 + \int_0^\infty \Delta\zeta^*(\tau) d\tau}, \quad (2.48)$$

with $b \equiv D/D_0$ being the mobility of the system. This equation then becomes an operative way to calculate the system mobility once the history of the memory function $\Delta\zeta^*(\tau)$ is known. On the other hand, this equation allows for a straightforward interpretation of $\Delta\zeta^*(\tau)$ as correlation time dependent friction function.

Finally, from the main set of equations (Eqs. (2.32) and (2.35)-(2.37)), it is possible to derive asymptotic long-time equations which play the role of order parameters in the determination of dynamically arrested states. By defining the non-ergodicity parameters

$$f(k) = \lim_{\tau \rightarrow \infty} F(k, \tau), \quad (2.49)$$

$$f_s(k) = \lim_{\tau \rightarrow \infty} F_s(k, \tau), \quad (2.50)$$

from Eqs. (2.36) and (2.37), the limits $\lim_{z \rightarrow 0} zF(k, z)$ and $\lim_{z \rightarrow 0} zF_s(k, z)$ can be evaluated. Such procedure results in

$$f(k) = \frac{S(k)}{1 + \frac{k^2 S^{-1}(k) \gamma}{\lambda(k) \Delta}}, \quad (2.51)$$

$$f_s(k) = \frac{1}{1 + \frac{k^2 \gamma}{\lambda(k)}}, \quad (2.52)$$

where $\gamma \equiv D_0 / \lim_{\tau \rightarrow \infty} \Delta\zeta^*(\tau)$. These limits are used to evaluate $\lim_{\tau \rightarrow \infty} \Delta\zeta^*(\tau)$ in Eq. (2.32), leading to

$$\gamma^{-1} = \frac{1}{3(2\pi)^3 \bar{n}} \int d\mathbf{k} \frac{k^2 + [S(k) - 1]^2 \lambda^2(k)}{[\lambda(k)S(k) + k^2 \gamma][\lambda(k) + k^2 \gamma]}, \quad (2.53)$$

a relatively simple equation that can be solved once the structure factor $S(k)$ is known. **Physically, the parameter γ is nothing but the square localization length, which plays the role of a dynamic order parameter within the SCGLE.**

For equilibrated fluids, these non ergodicity parameters are equal to zero, which is equivalent to state that the system fully relaxes to equilibrium. This behavior is then observed as a divergence for the value of γ and a non-zero value for the mobility. Conversely, for dynamical arrested states, the non-ergodicity parameters and memory function are expected to have non-zero values, a behavior typical of solid materials, where particles are not free to diffuse. In this case, γ becomes finite, while the asymptotic long value of the mobility is zero. The described behavior can also be explained in terms of the MSD, as $\gamma = \lim_{\tau \rightarrow \infty} W(\tau)$, a relationship derived from the definition of γ , $D(\tau)$ and Eq. (2.46).

2.4 NE-SCGLE Theory

This section provides a brief review of the generalization of the SCGLE description of the dynamic properties of liquids, now to systems undergoing non-equilibrium processes, which results in what we refer to as the non-equilibrium self-consistent generalized Langevin equation (NE-SCGLE) theory [1]. The NE-SCGLE framework is set upon the Onsager-Machlup's linear response theory, for which the main ideas are first presented. Onsager-Machlup's theory basically states that when considering a M -dimensional vector $\mathbf{a}(t)$, whose M elements are a set of extensive variables, one can represent the state of $\mathbf{a}(t)$ as a multivariate stochastic process[38, 39]. Although, in general, such process is non-stationary, it might be partitioned into small intervals that are locally stationary [40]. For each of the resulting locally stationary process, still represented by the vector $\mathbf{a}(t)$, the mean value $\overline{\mathbf{a}(t)}$ is described by a non-linear equation of the form

$$\frac{d\overline{\mathbf{a}(t)}}{dt} = \mathcal{R}[\overline{\mathbf{a}(t)}], \quad (2.54)$$

while its fluctuation around an equilibrium value $\delta\hat{\mathbf{a}}(t) \equiv \hat{\mathbf{a}}(t) - \mathbf{a}^{eq}$ can be modeled by Onsager linear response theory. Hence, the expression

$$\frac{d\overline{\delta\mathbf{a}(t)}}{dt} = -\mathbf{L}[\mathbf{a}^{eq}] \cdot \boldsymbol{\varepsilon}[\mathbf{a}^{eq}] \cdot \overline{\delta\mathbf{a}(t)}, \quad (2.55)$$

describes the evolution of the fluctuations, where $\mathbf{L}[\mathbf{a}^{eq}] \equiv -(\partial\mathcal{R}[\mathbf{a}^{eq}]/\partial\mathbf{a})_{\mathbf{a}=\mathbf{a}^{eq}} \cdot \boldsymbol{\varepsilon}^{-1}[\mathbf{a}^{eq}]$ is the kinetic matrix, and where $\boldsymbol{\varepsilon}$ is the thermodynamic matrix with elements

$$\varepsilon_{ij}[\mathbf{a}] = -\frac{1}{k_B} \left(\frac{\partial^2 \mathcal{S}[\mathbf{a}]}{\partial a_i \partial a_j} \right), \quad (2.56)$$

in which $\mathcal{S}[\mathbf{a}]$ corresponds to the entropy of the system in terms of the extensive variables conforming the vector $\mathbf{a}(t)$. With such premise, two main results that conforms the core of the NE-SCGLE formalism, can be derived. The first is an equation for the covariance matrix $\boldsymbol{\sigma}(t) \equiv \overline{\delta\mathbf{a}(t)\delta\mathbf{a}^\dagger(t)}$, which can be written as

$$\frac{d\boldsymbol{\sigma}(t)}{dt} = -\mathbf{L}[\mathbf{a}(t)] \cdot \boldsymbol{\varepsilon}[\mathbf{a}(t)] \cdot \boldsymbol{\sigma}(t) - \boldsymbol{\sigma}(t) \cdot \boldsymbol{\varepsilon}[\mathbf{a}(t)] \cdot \mathbf{L}^\dagger[\mathbf{a}(t)] + \mathbf{L}[\mathbf{a}(t)] + \mathbf{L}^\dagger[\mathbf{a}(t)]. \quad (2.57)$$

The second result states that, for locally stationary fluctuations $\delta\mathbf{a}(t+\tau) = \mathbf{a}(t+\tau) - \overline{\mathbf{a}(t)}$, the variable $\delta\mathbf{a}(t+\tau)$ follows the description made by the most general linear stochastic differential equation

$$\frac{d\delta\mathbf{a}(t+\tau)}{d\tau} = -\boldsymbol{\omega}[\overline{\mathbf{a}(t)}] \cdot [\boldsymbol{\sigma}(t)]^{-1} \cdot \delta\overline{\mathbf{a}(t+\tau)} - \int_0^\tau d\tau' \mathbf{L}[\tau - \tau'; \overline{\mathbf{a}(t)}] \cdot \delta\overline{\mathbf{a}(t)} + \mathbf{f}(t+\tau). \quad (2.58)$$

This last expression, as a matter of fact, perfectly resemble the generalized Langevin equation (Eq. (2.6)). When comparing these two equations, the difference resides in the time dependency of the mean value of \mathbf{a} for the above one. On the other hand, the theorem presented in the first section of this chapter still holds true [1].

The NE-SCGLE is obtained when when one considers the local density $n(\mathbf{r}, t)$ as the only entry of the abstract vector $\mathbf{a}(t)$. For such variable, the evolution equation is given by the empirical Fick's law, which in its most general description is given by

$$\frac{\partial \bar{n}(\mathbf{r}, t)}{\partial t} = D_0 \nabla \cdot b(\mathbf{r}, t) \bar{n}(\mathbf{r}, t) \nabla \beta \mu[\mathbf{r}; \bar{n}(\mathbf{r}, t)], \quad (2.59)$$

where D_0 is the free particle diffusion coefficient, $b(\mathbf{r}, t)$ is the local mobility, whose dependence on the position (non-homogeneous fluid) and time is explicitly stated, with $\beta \equiv (k_B T)^{-1}$ and where $\mu \equiv \partial \mathcal{S} / \partial n(\mathbf{r}, t)$ is the chemical potential. For such variable, the linearization of Eq. (2.59) leads to the identification of \mathbf{L} as

$$\mathbf{L} \equiv -D_0 \nabla \cdot \bar{n}(\mathbf{r}, t) b(\mathbf{r}, t) \nabla \delta(\mathbf{r} - \mathbf{r}'). \quad (2.60)$$

The last expression allow us to write the evolution of the covariance as

$$\begin{aligned} \frac{\partial \sigma(\mathbf{r}, \mathbf{r}'; t)}{\partial t} &= D_0 \nabla \cdot \bar{n}(\mathbf{r}, t) b(\mathbf{r}, t) \nabla \int d\mathbf{r}_2 \varepsilon[\mathbf{r}, \mathbf{r}_2; \bar{n}(t)] \sigma(\mathbf{r}_2; \mathbf{r}'; t) + \\ &D_0 \nabla \cdot \bar{n}(\mathbf{r}', t) b(\mathbf{r}', t) \nabla \int d\mathbf{r}_2 \varepsilon[\mathbf{r}', \mathbf{r}_2; \bar{n}(t)] \sigma(\mathbf{r}_2; \mathbf{r}; t) - \\ &2D_0 \nabla \cdot \bar{n}(\mathbf{r}, t) b(\mathbf{r}, t) \nabla \delta(\mathbf{r} - \mathbf{r}'). \end{aligned} \quad (2.61)$$

Eqs. (2.59) and (2.61) are the most general description of the NE-SCGLE framework, and allow us to describe the evolution of the mean local density along with the evolution of the covariance. On the other hand, a general solution to these expressions becomes a highly involved problem to solve, as they are coupled by the system's dynamics through $b(\mathbf{r}, t)$. To solve this proble, thus, one requires a closure relation allowing to also solve for the non-equilibrium mobility. The mobility is then the only unknown variable besides the externally known chemical potential (directly related with the entropy and ε).

In order to solve for the mobility $b(\mathbf{r}, t)$, a local isotropy and homogeneity approximation is employed, hence allowing us to find a similar expression as Eq. (2.48). For the covariance, this approximation is expressed as $\sigma(\mathbf{r} + \mathbf{x}, \mathbf{r} + \mathbf{x}', t) \approx \sigma(|\mathbf{x} - \mathbf{x}'|, \mathbf{r}, t)$, which allow us to write the FT of Eq. (2.61) as

$$\frac{\partial \sigma(k, \mathbf{r}; t)}{\partial t} = -2k^2 D_0 b(\mathbf{r}, t) \bar{n}(\mathbf{r}, t) \hat{\varepsilon}(k; \bar{n}(\mathbf{r}, t)) \sigma(k; \mathbf{r}, t) + 2k^2 D_0 b(\mathbf{r}, t) \bar{n}(\mathbf{r}, t). \quad (2.62)$$

Another way of expressing the above equation is in terms of the static structure factor, through the relation $S(k; \mathbf{r}, t) = \sigma(k; \mathbf{r}, t) / \bar{n}(\mathbf{r}, t)$, leading to

$$\frac{\partial S(k, \mathbf{r}; t)}{\partial t} = -2k^2 D_0 b(\mathbf{r}, t) \bar{n}(\mathbf{r}, t) [S(k; \mathbf{r}, t) - 1 / \bar{n}(\mathbf{r}, t) \hat{\varepsilon}(k; \bar{n}(\mathbf{r}, t))]. \quad (2.63)$$

On the other hand, the locally stationary approximation permit us to express Eq.(2.46) in terms of nonstationary time-correlation functions $C(\mathbf{x}, \tau; \mathbf{r}, t) \equiv \delta n(\mathbf{r} + \mathbf{x}, t + \tau) \delta n(\mathbf{r}, t)$ [40, 1]. This, along with the fact that the derivation of the SCGLE main set of equations (Eqs. (2.32), (2.36)-(2.37)) can be done without the use of any equilibrium condition, but just a clever identification of terms in stationary conditions [1], leads to the generalization of such set, which reads

$$F(k, z; \mathbf{r}, t) = \frac{S(k; \mathbf{r}, t)}{z + \frac{k^2 D_0 S^{-1}(k; \mathbf{r}, t)}{1 + \lambda(k) \Delta \zeta(z; \mathbf{r}, t)}}, \quad (2.64)$$

$$F_s(k, z; \mathbf{r}, t) = \frac{1}{z + \frac{k^2 D_0}{1 + \lambda(k) \Delta \zeta(z; \mathbf{r}, t)}} \quad (2.65)$$

$$\Delta \zeta^*(\tau; \mathbf{r}, t) = \frac{D_0}{24\pi^3 \bar{n}} \int_V k^2 \left[\frac{S(k; \mathbf{r}, t) - 1}{S(k; \mathbf{r}, t)} \right]^2 F(k, \tau; \mathbf{r}, t) F_s(k, \tau; \mathbf{r}, t) d\mathbf{k}. \quad (2.66)$$

Likewise, the mobility holds the same relation with the nonstationary time-correlation memory function reading

$$b(\mathbf{r}, t) = \frac{1}{1 + \int_0^\infty \Delta\zeta^*(\tau; \mathbf{r}, t) d\tau}. \quad (2.67)$$

Thus, this coupled set of equations allow us to close the relationship between the evolution of the mean density and the structure (Eqs. (2.59) and (2.63)).

Nevertheless, a general solution for these general equations is non-trivial. It is only for specific processes that semi analytic solutions have been found, as it is the case of instantaneous transformation processes. For example, let us consider an instantaneous isochoric quenching process of an homogeneous and isotropic system. The conditions imposed by this process follows the consideration $\bar{n}(\mathbf{r}, t) = \bar{n}$, thus, the solution of (2.59) becomes trivial. In addition, the evolution of the static structure factor simplifies as

$$\frac{\partial S(k; t)}{\partial t} = -2k^2 D_0 b(t) \bar{n} [S(k; t) - 1/\bar{n} \hat{\varepsilon}_f(k; \bar{n})], \quad (2.68)$$

where the suffix in $\hat{\varepsilon}_f$ denotes the evaluation of the thermodynamical property $\hat{\varepsilon}$ at the final state (see Eq. (2.56)), and where the mobility is expected to be homogeneous $b(\mathbf{r}, t) = b(t)$. With such simplification, a solution for $S(k; t)$ can be given when considering the variable transformation

$$u(t) = \int_0^t b(t') dt', \quad (2.69)$$

which allow us to write (2.68) as

$$\frac{\partial S(k; u)}{\partial u} = -2k^2 D_0 \bar{n} [S(k; u) - 1/\bar{n} \hat{\varepsilon}_f(k; \bar{n})], \quad (2.70)$$

whose solution reads

$$S(k; u) = [\bar{n} \hat{\varepsilon}_f]^{-1} + \{S_0(k) - [\bar{n} \varepsilon_f]^{-1}\} e^{-2k^2 D_0 \bar{n} \hat{\varepsilon}_f u(t)}, \quad (2.71)$$

where $S_0(k) \equiv S(k, t = 0)$ is the initial static structure factor, related with the thermodynamical ε property by $S(k; \bar{n}, T) = \bar{n}/\hat{\varepsilon}(k; \bar{n}, T)$ under equilibrium conditions. In this solution, the u time shrouds the corresponding evolution time, nevertheless, the simplicity of the solution allow us to evaluate (2.64)-(2.67) for any value of u . This allow us to trace the time once the evolution of the mobility is solved in the u -space. In addition, the transformation also allows to determine the time of arrest u_a , predicted through the solution of [1, 41]

$$\gamma^{-1}(u_a) = \frac{1}{3(2\pi)^3 \bar{n}} \int d\mathbf{k} \frac{k^2 + [S(k; u_a) - 1]^2 \lambda^2(k)}{[\lambda(k) S(k; u_a) + k^2 \gamma(u_a)][\lambda(k) + k^2 \gamma(u_a)]}, \quad (2.72)$$

where u_a is the first u value for which a finite value of the **non-equilibrium dynamic order parameter** γ is found. The complete derivation of this last expression can be found elsewhere [1], nevertheless, the same mathematical steps employed to derive its equilibrium counterpart Eq. (2.32), can be employed for the now waiting-time dependent dynamical properties, namely Eqs. (2.64)-(2.66). Given the definition of u (Eq. (2.69)), u_a is actually found for infinite waiting times $t \rightarrow \infty$ as $b(u_a)$ converges to 0. Such prediction, inherent to the solution, remarks the subtle difference between the equilibrium dynamics and the non-equilibrium process dynamics, for which the waiting time is now relevant to the description.

In this section, we have presented the NE-SCGLE theory as an extension to the SCGLE theory. Nevertheless, one could start directly from the non-equilibrium perspective and consider the SCGLE theory as a particular case in which both the mean local density and its covariance, are constant. For such consideration, the set of equations that conforms this non-equilibrium theory are reduced to the equilibrium expressions derived in the previous sections.

2.5 Summary

In this section we have reviewed the fundamental basis and derivation of the NE-SCGLE theory of irreversible processes in liquids, which is obtained from the extended non-equilibrium version of Onsager's abstract and general description of thermal fluctuations and is then complemented with a set of simplifying approximations. This first led to the equilibrium SCGLE theory of the dynamic properties of liquids, analogous to the well-known mode coupling theory (MCT), with both theories restricted to equilibrium condition. The SCGLE theory was latter extended to full non-equilibrium conditions, leading to the NE-SCGLE theory, which has no counterpart in the literature.

In particular, the NE-SCGLE formalism is distinguished by Eq. (2.59) and Eq. (2.68), which describe the non-equilibrium evolution of the mean value and the covariance of the fluid's local particle density $\bar{n}(\mathbf{r}, t)$. On the other hand, the solution of these equations requires to first solve the problem already posed by the SCGLE set of equations (Eqs. (2.64)-(2.67)). The concrete application of the NE-SCGLE framework for instantaneous isochoric quenches starts with the formal solution of Eq. (2.68) given in Eq. (2.71), while the trivial solution of Eq. (2.59) ($\bar{n}(\mathbf{r}, t) = cte.$) is imposed. For this formalism, the only external input is given in terms of the free energy functional derivatives. Concretely, such derivatives are expressed in terms of the chemical potential μ and the thermodynamic matrix ε (related to the static structure factor under thermodynamic equilibrium). In the next chapters, the solution of these equations is discussed for a concrete system.

Chapter 3

Stationary diagrams of the HSSW fluid system.

In the previous chapter the fundamental bases of the NE-SCGLE framework were described, and its main equations were discussed. The main purpose of the present chapter is to introduce and define with precision the concept of *non-equilibrium glass transition diagram*, and to explain its relationship with its predecessor, the *equilibrium glass transition diagram* (generated by equilibrium dynamical theories such as MCT or the SCGLE theory), and with conventional and long established *thermodynamic equilibrium phase diagram*. These three different diagrams provide different and complementary perspectives of the location of the various equilibrium and non-equilibrium phases, in the state space of the system.

Thus, this chapter is divided in three major sections and a summary. The first of them illustrates the concept of equilibrium phases and phase diagram with the classical description of gases and liquids and their equilibrium coexistence, very much as van der Waals explained it more than one century ago. Here, however, we frame van der Waals arguments on the identification of a simple (mean field) approximation for the free energy functional for the specific class of model systems referred to as Lennard-Jones-like fluids. These concepts may be textbook material in conventional course of classical and statistical thermodynamics.

We cannot say the same regarding the concept of equilibrium *glass transition diagram*, developed only within the last three decades. As explained in the second section, this diagram describes the boundary in the thermodynamic state space of the system between the region where no kinetic barriers are met, hence being able to reach thermodynamic equilibrium, and the region where it is predicted to become dynamically (or kinetically) arrested. Such predictions, however, do not derive solely from free energy considerations. Instead, they are determined from dynamic arrest conditions such as Eq. (2.53), provided by equilibrium dynamical theories (MCT or SCGLE). These theories require as an input the equilibrium static structure factor of the homogeneous fluid, which does not exist inside the spinodal region.

As explained below in section three, however, this limitation is eliminated by the non-equilibrium SCGLE theory. The NE-SCGLE unveils the precise manner in which, the emergence of kinetic impediments to reach thermodynamic equilibrium, leads to the formation of unexpected non-equilibrium amorphous states. The identification of these non-equilibrium phases and the regions of state space where they are expected to be formed constitutes the *non-equilibrium glass transition diagram*.

As mentioned before, here we shall restrict our discussion to Lennard-Jones like systems, whose particles interact through a strong short range repulsion plus a longer-ranged attraction.

The *non-equilibrium glass transition diagram* of Lennard-Jones like systems was first proposed in reference [25], in the context of the hard-sphere plus attractive Yukawa (HSAY) model fluid. The present chapter mostly reviews the work explained in that reference. However, our own original contribution here is to perform a similar systematic discussion employing a different Lennard-Jones like model system, namely, the analytically simpler hard-sphere plus square well (HSSW) fluid, which will be studied in the rest of the present thesis.

3.1 Thermodynamic equilibrium phase diagram

This section illustrates the classical concept of equilibrium phases and phase diagrams with van der Waals theory of the gas-liquid transition, which we derive from a simple (modified mean field, MMF) free energy, applied to a specific Lennard-Jones-like fluid, namely, the HSSW model. The reason to start this discussion at the level of the MMF free energy, and not from van der Waals equation of state itself, is that a free energy functional also generates the equilibrium static structure factor $S^{eq}(k)$, which is the input in the equilibrium (MCT and SCGLE) dynamical theories. In addition, its second functional derivative is the fundamental input of the NE-SCGLE theory. Using the same free energy and the same model potential, provides the same basis for the determination of the three diagrams that we wish to compare.

The MMF approximation can be summarized as an approximation done to the free energy \mathcal{F} , which we write as the superposition of a hard core part \mathcal{F}_{HS} and an attractive part \mathcal{F}_A , such as

$$\mathcal{F}[n, T] = \mathcal{F}_{HS}[n, T] + \mathcal{F}_A[n, T], \quad (3.1)$$

and in which the hard core part is its *exact* solution when \mathcal{F}_A is neglected. Within the MMF approximation, the attractive part is then approximated as

$$\mathcal{F}_A[n, T] = -\frac{k_B T}{2} \int d\mathbf{r} \int d\mathbf{r}' n(\mathbf{r}) f_A(|\mathbf{r} - \mathbf{r}'|) n(\mathbf{r}'), \quad (3.2)$$

where

$$f_A(r) = [e^{-\beta u(r)} - 1] \theta(r - \sigma), \quad (3.3)$$

with

$$\theta(r - \sigma) = \begin{cases} 0 & r < \sigma \\ 1 & \sigma < r \end{cases}, \quad (3.4)$$

and in which $u(r)$ is the two particle interaction potential.

This approximation allow us to write down the second functional derivative of the free energy, which in return leads to the the direct correlation function $c(r)$ [42]

$$c(r) = c_{HS}(r) + f_A(r), \quad (3.5)$$

where $c_{HS}(r)$ is the *exact* direct correlation function of the Hard Sphere system. Within this approximation, $c_{HS}(r)$ is given by the analytical expression obtained by Wertheim using the Percus-Yevick approximation [43] along with the Verlet-Weiss correction [44]. This approximation then leads to the structure factor $S(k)$

$$S(k) = \frac{1}{1 - n\hat{c}(k)}, \quad (3.6)$$

where $\hat{c}(k)$ is the FT of $c(r)$

$$\hat{c}(k) = \hat{c}_{HS}(k_{VW}; \phi_{VW}) + \hat{f}_A(k), \quad (3.7)$$

with

$$\hat{c}_{HS}(k) = \frac{24\phi}{k^*} \left[\alpha \left(\frac{a(k^*) + a'(k^*)}{k^{*2}} \right) + \beta \left(\frac{b(k^*) + b'(k^*)}{k^{*3}} \right) + \delta \left(\frac{d(k^*) + d'(k^*)}{k^{*5}} \right) \right], \quad (3.8)$$

in which

$$\alpha = -(1 + 2\phi)^2 / (1 - \phi)^4, \quad (3.9)$$

$$\beta = 6\phi(1 + \frac{1}{2}\phi)^2 / (1 - \phi)^4, \quad (3.10)$$

$$\delta = -\phi(1 + 2\phi)^2 / 2(1 - \phi)^4, \quad (3.11)$$

$$a(k^*) = \sin(k^*) \quad (3.12)$$

$$a'(k^*) = -k \cos(k^*) \quad (3.13)$$

$$b(k^*) = 2k^* \sin(k^*) - 2 \quad (3.14)$$

$$b'(k^*) = (-k^{*2} + 2) \cos(k^*) \quad (3.15)$$

$$d(k^*) = (-k^{*4} + 12k^{*2} - 24) \cos(k^*) \quad (3.16)$$

$$d'(k^*) = (4k^{*3} - 24k^*) \sin(k^*) + 24 \quad (3.17)$$

$$k_{VW} = k(\phi_{VW}/\phi)^{1/3} \quad (3.18)$$

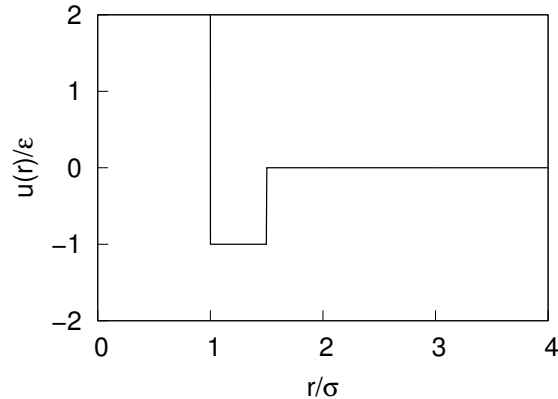
$$\phi_{VW} = \phi(1 - \phi/16) \quad (3.19)$$

and where $k^* \equiv k\sigma$ is the dimensionless wave vector magnitude, $\phi \equiv n\pi\sigma^3/6$ is the volume fraction and $T^* \equiv k_B T/\epsilon$ is the dimensionless temperature.

Let us now properly introduce the Hard Sphere Square Well interacting fluid system used to exemplify the theories capabilities. The two particle interaction is given by a hard core spherical interaction of diameter σ plus an attractive well of depth ϵ and range $\lambda\sigma$ (with $\lambda > 1$), which reads

$$u(r) = \begin{cases} \infty & r < \sigma \\ -\epsilon & \sigma \leq r < \lambda\sigma \\ 0 & \lambda\sigma \leq r \end{cases} \quad (3.20)$$

A schematic representation of this potential is shown in Fig. 3.1 for the case $\lambda = 1.50$. Within the current work, the case $\lambda = 1.50$ will be fixed for no other reason that to conform to equivalent attractive lengths of other Lennard-Jones like potential previously studied within the theory [25].

Figure 3.1: HSSW potential with $\lambda = 1.50$

The election of this interaction potential yields to the attractive part of the direct correlation function

$$\hat{f}_a(k) = \frac{4\pi F(T^*)}{k^*} \left[\frac{\cos(k^*) - \lambda \cos(k^*\lambda)}{k^*} + \frac{\sin(k^*\lambda) - \sin(k^*)}{k^{*2}} \right], \quad (3.21)$$

in which

$$F(T^*) = e^{1/T^*} - 1, \quad (3.22)$$

that closes the scheme in order to compute both $S(k)$ and $\varepsilon(k)$.

Within this approximations, it is possible to draw the equilibrium phase diagram of the system. For such purpose the mechanical equation state of the system must be derived. From statistical thermodynamics, it is known that the thermodynamics properties can be linked to the distribution of particles. In particular, the relation $S(k=0) = nk_B T \chi_T \equiv \chi_T^*$ [42] is used in order to link the structure factor with the isothermal compressibility of the system χ_T . From this relation the isothermal compressibility of the system is obtained as

$$\chi_T^* = \frac{1}{\chi_{T,HS}^{*-1} - 8\phi(\lambda^3 - 1)F(T^*)}, \quad (3.23)$$

which yields the mechanical equation of state, namely

$$P_{HSSW}^* = P_{HS}^* - \frac{24}{\pi}(\lambda^3 - 1)T^*F(T^*), \quad (3.24)$$

where $P^* = \sigma^3 P/\epsilon$,

$$P_{HS}^* = \frac{6\phi T^*}{\pi(1-\phi)^3}(1 + \phi + \phi^2 - \phi^3) \quad (3.25)$$

$$\chi_{T,HS}^* = \frac{6T^*}{\pi} \left[\frac{8\phi - 2\phi^2}{(1-\phi)^4} + 1 \right], \quad (3.26)$$

thus allowing us to estimate both, the binodal (also known as coexistence) and the spinodal lines.

It is a common understanding that the binodal or coexistence line traces the limit between single thermodynamic phase states and the coexistence of two phases. For the current HSSW model, it traces down the thermodynamic state limit between gas and liquid coexistence states and single phase states. On the other hand, meta-stable homogeneous states inside the binodal

line, are commonly acknowledge to be stable homogeneous phases of the system. Being the current model for the structure a mean field model, such homogeneous meta-stable phases are the ones under consideration within the current work. Nevertheless, the binodal line can still be identified through Maxwell construction for isotherms below the critical temperature $T^{*(c)}$ [3].

On the other hand, the spinodal line delimits the region in which meta-stable homogeneous phases can be found. For states inside the spinodal line, the internal fluctuations of the system are expected to grow to macro sizes through what is known as a spinodal decomposition process, which inevitably separates the system in the corresponding phases [2]. This spinodal line can be theoretically computed when the compressibility of the system is expected to change its sign [2]. Thus, for the current model, the condition reads

$$-8(\lambda^3 - 1)\phi_s(1 - \phi_s)^4 F(T_s^*) + 8\phi_s - 2\phi_s^2 + (1 - \phi_s)^4 = 0. \quad (3.27)$$

In Fig. 3.2 the resulting equilibrium phase diagram is presented, where the black solid and black dashed lines corresponds to the spinodal and binodal lines, respectively.

In addition to the spinodal and binodal lines, the freezing line is also represented in this figure by two different criteria. One is the Hansen-Verlet criterion [45] represented by the gray dashed line, which is a structural condition in which the main peak of the structure factor reaches a given height, for which the value $S(k_{max}) = 3.1$ is employed. The other freezing criterion is Löwen's freezing criterion [46], in which instead of using the structure of the system, the condition states that freezing occurs when the long time diffusion coefficient is approximately 10% that of the free particle. Hence, Löwen's freezing criterion, indicated by the gray solid freezing line, is found by solving the SCGLE equations for the states described by $D^* = 0.10$.

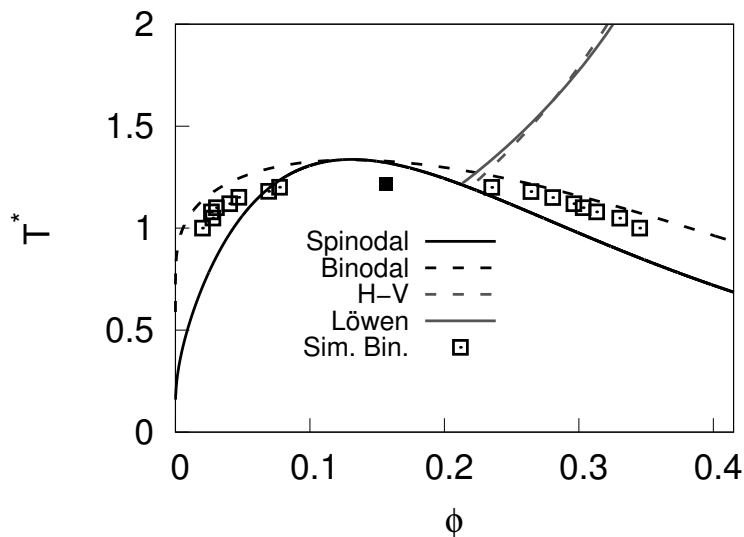


Figure 3.2: HSSW equilibrium phase diagram for $\lambda = 1.50$. The spinodal (black solid line) is traced by solving Eq. (3.27), the binodal (black dashed line) is traced by Maxwell equal area rules[2]. For the freezing line we compare the structural empirical Hansen criterion $S(k_{max}) = 3.1$ with the Löwen's dynamic empirical criterion $D^* = 0.10$

3.2 *Glass transition* phase diagram

As explained in detail in chapter 2, both the SCGLE and its non-equilibrium extension are capable to derive asymptotic equations for the system dynamics. The solution of such asymptotic equations are commonly employed to find regions in the parameters space of a system where dynamically arrested states are predicted to exist. Within the literature, these diagrams are commonly known as *glass transition diagrams*, firstly named after the Mode Coupling theory results[17]. On the other hand, these non-equilibrium phase diagrams have been extended to what we now call *non-equilibrium glass transition diagrams* within the NE-SCGLE framework. The subtle difference between these two is that the last diagrams are obtained through an explicit preparation protocol, *i.e.* a non-equilibrium instantaneous quenching process. In this section, we shall only refer to the *glass transition diagrams* obtained by the SCGLE theory in order to highlight the relevant differences when the NE-SCGLE is employed instead.

Let us now use the HSSW system to illustrate the *glass transition phase diagrams*. Within the SCGLE perspective, the *glass transition phase diagrams* can be obtained through the dynamical parameter γ (see Eq. (2.53)) once the equilibrium structure factor has been determined. Hence, for such purpose, the recently explained MMF is employed. In Fig. 3.3 the resulting *glass transition* phase diagram is shown. In this diagram, the region in which γ acquires a finite value is delimited by the black solid line, denominated as the dynamical arrest transition line. The states below such line and above the spinodal corresponds to dynamically arrested states (black squares). Additionally in Fig. 3.3, the value of the mobility b is presented for several states through a color scale of state centered squares, where the black color is used for $b = 0$. As a consequence, each state inside the dynamically arrested region is represented with a black color.

Just as explained in chapter 2, γ can be directly associated with the MSD. As a consequence of this relationship, γ is interpreted as the squared localization length. Thus, for a system of diffusive particles this quantity diverges, whereas for dynamical arrest γ becomes finite. For the latter cases, this localization length is often compared with Lindemann's melting criterion [12, 47, 25]. Lindeman's criterion states that, for crystalline solids, melting occurs when the system particles vibrates a distances comparable to 10% the inter-particle distance. Compared to such criterion, the square root of γ for the glass transition in a purely HS system is found to be around $\sqrt{\gamma} \approx 0.1\sigma$ at the transition isochore $\phi_{HS}^{(g)} \approx 0.582$, where the inter-particle distances is roughly $l \approx \sigma$, a value that results reminiscent of Lindemann's melting criterion. This reminiscence is, as a matter of fact, maintained along the glass transition curves for multiple systems, such as the HSAY [29].

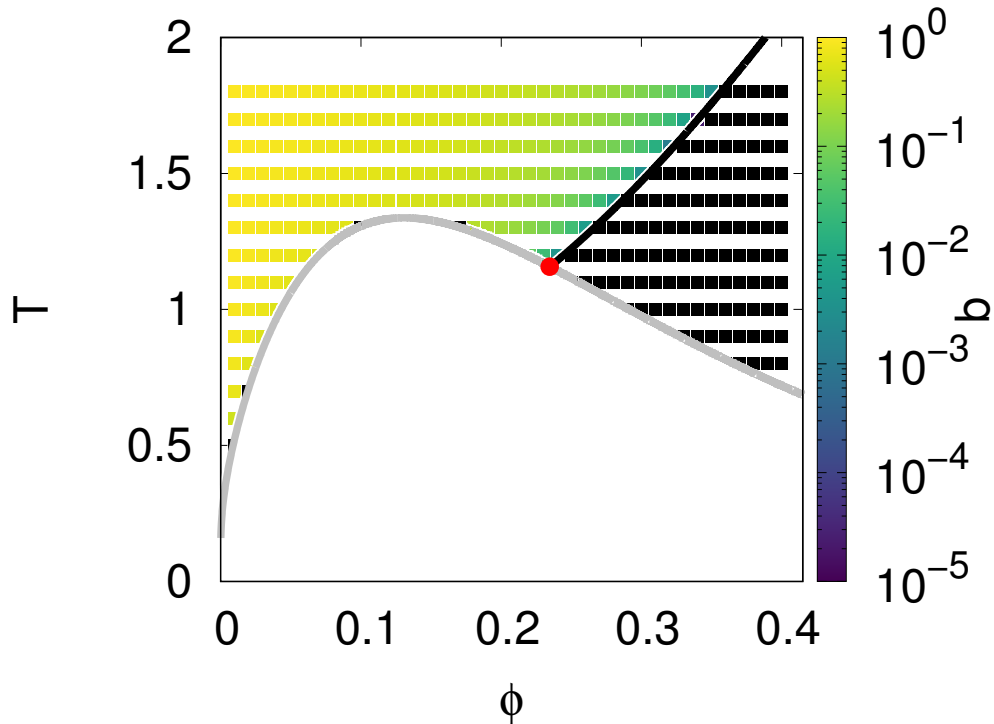


Figure 3.3: HSSW *glass transition* phase diagram for $\lambda = 1.50$. The mobility $b \equiv D_L^*$ value is represented for different states with a color scale, where the black is used for $b = 0$. The black solid line marks the glass transition line, while the gray solid line represent the spinodal line. The red circle is the bifurcation point, where the glass transition line meets the spinodal line.

In Fig. 3.4 a) the behavior of γ along the the dynamical arrest transition line is considered. As seen in this figure, this line extends from the HS limit to the bifurcation point. The value of $\gamma^{1/2}$ normalized by the interparticle distance $l \approx n^{-1/3}$ along the dynamical arrest transition line is shown in Fig. 3.4 b). In this figure it is observed that although $\gamma^{1/2}/l$ is not a constant, its value ranges in between 0.1 and 0.15, supporting the comparison between its value and Lindemann's melting criterion for the current HSSW system.

Up to this point, the SCGLE theory has only been used to describe the predicted dynamical scenario presented in a phase diagram. Nevertheless, any equilibrium theory does have predicting limitations for attractive systems in which spinodal regions arise, a region in which the theory cannot be used to make any sort of reliable predictions due to the lack of an equilibrium structural input such as $S(k, n, T)$. As already mentioned, however, within the NE-SCGLE this fundamental limitation is bypassed.

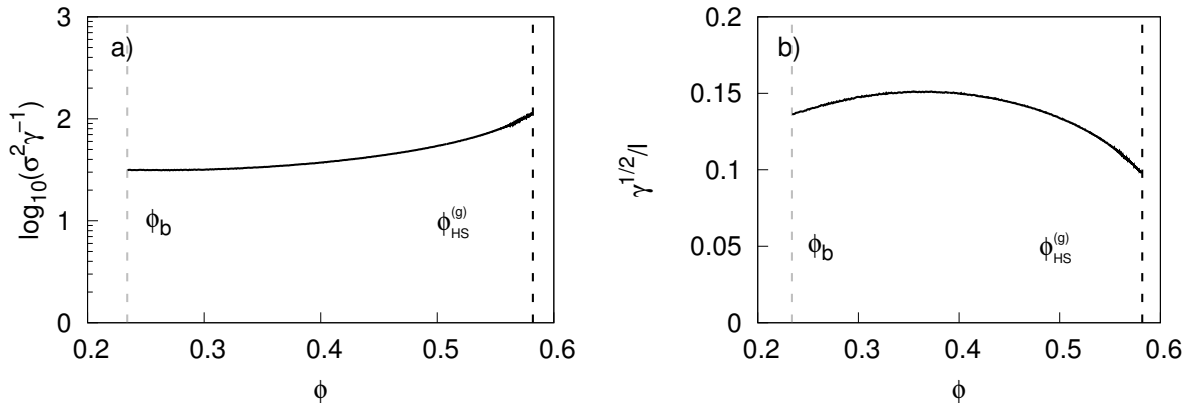


Figure 3.4: a) γ vs the volume fraction along the dynamical arrest line for the HSSW system with $\lambda = 1.50$. b) Localization length normalized by the interparticle distance $\gamma^{1/2}/l$ for the same states as a), with $l = n^{-1/3}$.

3.3 *Non-equilibrium* glass transition phase diagram

Similar to the equilibrium SCGLE theory, the non-equilibrium SCGLE theory is able to describe the asymptotic dynamics of non-equilibrium processes, which in return provide the prediction of *non-equilibrium glass transition* diagrams. For a given proposal for the thermodynamical property $n\varepsilon(k)$, this non-equilibrium formalism is able to extend the description of dynamical arrested states into spinodal regions. As mentioned before, the application of this theoretical framework for the description of systems with attractive interactions was first carried out by J/M. Olais *et al.* [29] for a HSAY fluid. Similar to the case of the *glass transition phase diagrams*, these diagrams are obtained through the solution of asymptotic limits, in which the limit $\lim_{t \rightarrow \infty} \gamma(S(k; t))$ is under consideration, hence *the waiting time of the system is not a variable*. In this section the results of this procedure on the current HSSW fluid model system are shown as a prelude to the waiting-time dependent phase diagrams to be discussed in chapter 5.

The *non-equilibrium glass transition diagram* obtained for the HSSW system is illustrated in Fig. 3.5. The results found for the system under consideration agree qualitatively with the results previously reported for the HSAY system [29], which in this work are briefly discussed and analyzed. The displayed *non-equilibrium* diagram, is obtained through the analysis of multiple instantaneous isochoric quenches within the theory. Such quenches start from an initial infinite temperature limit (*i.e.*, starting from an initial hard-sphere limit), and are then instantaneously cooled down towards different temperatures, as indicated. For states out of the spinodal region, the diagram results identical to that of the equilibrium version of the theory, where the asymptotic long-time value of the mobility is finite. However, two important differences arise when compared to the *glass transition phase diagram*. The first one is that the spinodal line is also a dynamical arrest transition line. The second one is that the glass transition line enters the spinodal line and continues inside separating the dynamical arrested states into two clearly distinctive arrested regions, leading to a diagram with a total of three identifiable regions. Region I consists in the equilibrium fluid region, while region II and III are the arrested regions. These last two regions respectively differentiate between gel-like and glass-like arrested states. Explaining how such differentiation can be made is the main goal of the current section.

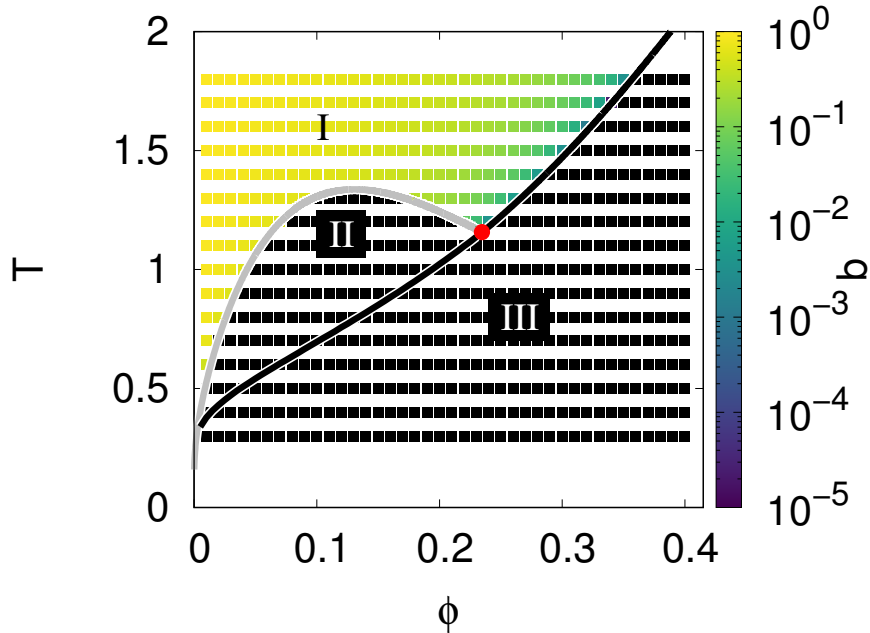


Figure 3.5: HSSW non-equilibrium *glass transition* phase diagram for $\lambda = 1.50$. The mobility $b \equiv D_L^*$ value is represented for different states with a color scale, where the black is used for $b = 0$. The black solid line marks the glass transition line, while the gray solid line represent the spinodal line. The red circle is the bifurcation point, where the glass transition line meets the spinodal line.

The boundary between regions II and III in the non-equilibrium *glass transition* diagram is mainly determined through the analysis of γ , a quantity used as an arrest order parameter. However, other properties such as the structure factor, the time-dependent MSD and mobility of the system also present distinctive signatures in these regions[29]. In Fig. 3.5, the glass transition line at the left side of the bifurcation point is identified when a discontinuity in $\gamma(T_f; \phi)$ appears. This discontinuity is observed when fixing on an isochore lower than that of the bifurcation, and then following the value of γ at different final temperatures. In Fig. 3.6 a) γ^{-1} vs the final temperature is shown for two isochores: one at the left of the bifurcation point ϕ_b ($\phi = 0.10$, empty circles), and another one at the right ($\phi = 0.25$, solid circles). For $\phi = 0.25$, for instance, one observes the features of the HS-like glass transition, where γ^{-1} jumps discontinuously from zero to the value $\sim 10^2$, which lies in the glass transition line predicted by both SCGLE and NE-SCGLE. For $\phi = 0.10$, however, one observes a different behavior, where γ^{-1} becomes finite at the spinodal temperature $T_s(\phi = 0.10)$ and increases continuously below. At a critical value $T_c(\phi = 0.10)$, however, the parameter γ^{-1} jumps discontinuously and acquires essentially the same value of $T_c(\phi = 0.25)$. This behavior, in fact, is what reveals that the glass transition line actually penetrates the spinodal region.

Following the previous discussion of the *glass transition phase diagram*, in Figs. 3.6 b) and c), the description of the T_c discontinuity is now extended for states inside the spinodal region. Such states are now highlighted with dashed lines, which allow us to follow the discontinuity in $\gamma(T_f)$ for states inside the spinodal region as one quenches into a T_c final temperature. In Figs. 3.6 b) and 3.6 c), the T_c temperature is approached from below (*i.e.* $\lim_{\epsilon \rightarrow 0} \gamma(T_f - \epsilon)$ with $\epsilon > 0$) in order to follow the glass-like behavior of γ . For temperatures $T_f < T_c$ a small localization length still comparable to 10% of the particles mean distance is found. This allow us to interpretate

the discontinuity as the continuation of the glass transition line inside the spinodal. Hence, the resulting behavior of γ serves as a reinforcement of the idea that the high density dynamical arrest transition is followed inside the spinodal for states below T_c the discontinuity.

On the other hand, recalling the behavior of γ for final states inside region II within Fig. a), the arrest is thought to be comparably "loose", as much larger localization lengths are found. In this region, the localization length is at least comparable to the particles mean distance, meaning at least one magnitude greater than that of typical glass-like arrested states. In addition, the value of the localization length is found to increase and diverge as the final temperature meets the spinodal temperature T_s , as shown in Fig. 3.6 a) for the $\phi = 0.10$ isochore. In summary, the NE-SCGLE predicts that the spinodal temperature is also an arrest transition line with a diverging localization length. These results are in agreement with previously reported findings for the HSAY system which exhibits this kind of behavior[25]. As a consequence, the general findings are expected to hold for systems with similar kinds of interaction potentials. Nevertheless, a work that systematically accounts for differences between multiple interaction potentials falls out of the scope of the current work and might be an investigation line worth exploring in the future.

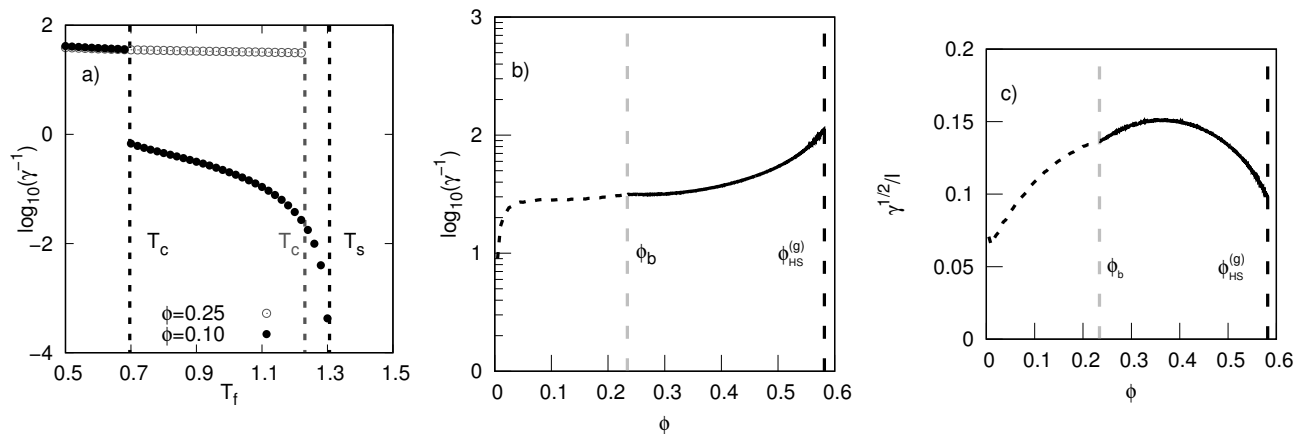


Figure 3.6: a) γ vs the final quenching temperature for an isochore below and above ϕ_b ($\phi = 0.10$ and 0.25 respectively). The dashed vertical lines correspond to the temperature glass transitions $T_c(\phi = 0.10)$ and $T_c(\phi = 0.25)$, where γ^{-1} presents a discontinuity, while the thick dashed line corresponds to the spinodal temperature $T_s(\phi = 0.10)$ b) γ vs the volume fraction along the glass transition dynamical arrest line, namely $T_c(\phi)$. The dashed line corresponds to states inside the spinodal line, while ϕ_b is the volume fraction of the bifurcation point c) Localization length normalized by the interparticle distance $\gamma^{1/2}/l$ along the glass transition line, with $l = n^{-1/3}$.

Although the behavior and analysis of γ reveals many important features of the dynamics of the HSSW system, a strict direct comparison of this quantity with experimental and simulation data is hard, if not impossible, to find. Thus, the state description with such property is obscure in nature, and insufficient to establish a connection with common gel-like systems. On the other hand, the predictions of the theory are not limited to such order parameter, and other properties such as the asymptotic structure actually reveal signatures of gel-like systems. This is illustrated in Fig. 3.7, where asymptotic long-time structure factor predicted by the NE-SCGLE along the $\phi = 0.10$ isochore for distinct final temperatures is shown. For quenches in region II ($T_f = 0.7 - 1.3$), the increase of a maximum at low wave-vectors is a fingerprint of the spinodal

decomposition process, which is predicted by the theory to be interrupted by a dynamical arrest. This behavior indicates the development of large structures, whose characteristic size increases as the final temperature approaches from below the spinodal line. This is emphasized in Fig. 3.7 by the left arrow. Notice that, in contrast, the local structure (observed in the second peak at $k\sigma \approx 2\pi$) decreases approaching the spinodal. The information revealed by the asymptotic structure factor complements that provided by the parameter γ^{-1} , emphasizing the localization of particles through the process of formation of remarkably large aggregates, which are characteristic of the development of gel states [26]. These results, allow us to interpret the dynamical arrested states of region II as gel-like states produced by a frustrated spinodal decomposition through an arrest mechanism, while reassuring the glass-like nature of region III.

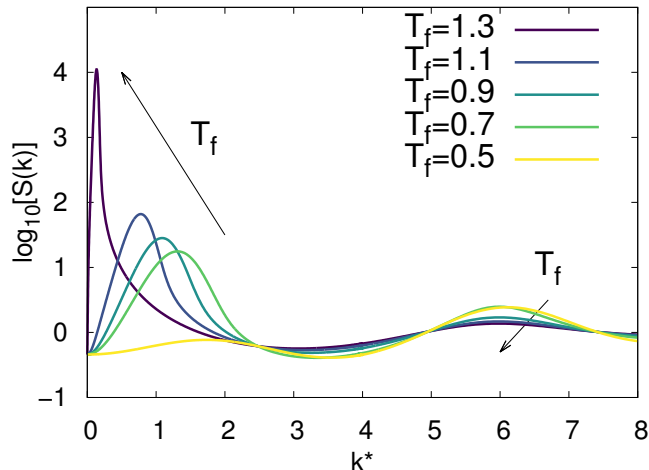


Figure 3.7: Asymptotic structure factors for the HSSW fluid system with $\lambda = 1.50$ at $\phi = 0.10$ isochore for the final temperatures $T_f = 1.3, 1.1, 0.9, 0.7$ and 0.5

Even though the presented non-equilibrium diagram is obtained as an asymptotic solution of NE-SCGLE equations, the rich landscape of arrested states predicted by the theory serves as a summary of the theoretical predictions. On the other hand, localizing the related phenomenology within the thermodynamic phase spaces allow us to discriminate and make more profound and interesting inquiries and analysis, such as the evolution of the dynamics. Finally, it becomes relevant to note the qualitative agreement of these theoretically predicted diagrams and the ones obtained by experiments[27] and simulations[48], even though differences in the particle interactions exist.

3.4 Summary

In this chapter, we have exemplified the determination of the three diagrams, the *thermodynamic equilibrium phase diagram*, the *glass transition diagram* and the *non-equilibrium glass transition diagram*, for the HSSW fluid. To obtain such diagrams, a structural approximation was proposed within the MMF formalism. In equilibrium, the structural approximation, yields to the mechanical equation of state, allowing us to trace the *thermodynamic equilibrium phase diagram*. In terms of both, the SCGLE and the NE-SCGLE theories, the structural approximation allow us to compute the dynamical arrest parameter γ , which is then employed to obtain the arrest diagrams.

In both of these diagrams, we are able to trace back the dynamical arrest transition from the HS limit. Nevertheless, for the particular case of the *glass transition diagram*, the description of the dynamical arrested states ends when the glass transition line meets the spinodal line, since the equilibrium theory cannot be applied inside the spinodal region. In stark contrast, the *non-equilibrium glass transition diagram* is able to identify the continuation of the glass transition line inside the spinodal region. Additionally, the spinodal line is also found to delimit a dynamical arrest transition for what is thought to be gel-like arrested states. These states are enclosed by the spinodal and glass transition lines (region II of the *non-equilibrium glass transition diagram*), and the identification of a gel-like state can be done in terms of the resulting structure factor. On the other hand, this chapter only attends the discussion of asymptotic properties, whereas the evolution towards these states has been postponed. It is precisely within the evolution of properties, such as the dynamics, that other typical fingerprints are presented within the formation of gels and glasses. Thus, the next chapter addresses the evolution of the predicted dynamical properties for the predicted states of the *non-equilibrium glass transition diagram*.

Chapter 4

The kinetic perspective of the glass, gel and gas-liquid transitions and their interference.

In chapter 3 the *non-equilibrium glass transition diagram* of the HSSW system, obtained by the NE-SCGLE theory, was presented. Nevertheless, such theoretical predictions do not provide the evolution of the system towards the development of an arrested state. In this regard, the present chapter aims to review the NE-SCGLE predictions for the time-evolution of the dynamical properties of the HSSW liquid towards the distinct arrested states discussed in the previous chapter. For these non-equilibrium states, complex effects such as aging and retarded responses of dynamical and structural properties, can take place, thus making their description, from a theoretical perspective, a hard problem to solve. In this chapter, the predictions on the transient dynamics and the underlying interference between the transitions described in the *non-equilibrium glass transition diagram* are discussed. A collection of such theoretical predictions for the HSAY fluid system is found within what we have referred to as the second scientific contribution of this thesis (ref. [29]). Nevertheless, for self-contained purposes, in this work is done for the HSSW system.

Concretely, this chapter reviews the latency effects and multi-step relaxations of dynamical properties predicted within the gel-like arrested states. As the name implies, the latency phenomena is characterized by the description of almost stationary properties, which present sudden changes when enough time is given. These latency have been experimentally observed, for instance in rather common physical properties like the viscoelastic modulus [18, 49, 50]. On the other hand, from the NE-SCGLE theory perspective, these latency effects have been predominately studied through the time-dependent diffusion coefficient, whereas other properties. such as the MSD and the self part of the ISF, also exhibit similar or related effects. Thus, the interference between the non-equilibrium phases is studied through the analysis of these properties along the boundaries found within the *non-equilibrium glass transition diagram*.

4.1 NE-SCGLE results & discussion

In what follows we will consider the solution of the full set of equations of the NE-SCGLE (we refer to Eqs. (2.68)-(2.67)) for isochoric quench processes, such as those discussed in the previous chapter. For such reason, a similar numerical method as the devised in reference [20] is employed. Details upon the discretization of the integro-differential coupled equations can be found

at Appendix A, while the implementation of the rest of the equations is done straightforwardly. The complete numerical implementation of all these methods resulted in a high efficiency program located in the public repository https://github.com/LANIMFE/HS_HSSW_quench_NESCGLE, available to everyone to use and modify, and from which all the results from this chapter can be reproduced.

Hence, in order to analyze the evolution of the dynamical properties of the system, we shall consider a sequence of quenches. For instance, for the $\phi = 0.15$ isochore, we consider quenches, all of which initiate at the same HS limit condition (given at $T \rightarrow \infty$), with final quenching temperatures $T_f = 0.60, 0.70, \dots, 1.40$. For such quenches, the solution of the NE-SCGLE set of equations directly leads to the evolution of the waiting-time dependent structure factor, the ISF, its self part, the MSD and the mobility. In order to describe such evolution, the dimensionless waiting time convention $t_w^* = \sigma^2/D_0 t_w$ will be employed when referring to the waiting time t_w . This convention allow us to compare the "waiting time", a laboratory time frame, with the needed time for a free particle to diffuse a distance equivalent to its own diameter.

The behavior of the inverse of the mobility for the proposed set of quenches is illustrated in Fig 4.1 a). As a reference, for the selected isochore, the predicted glass-transition temperature is around $T_c(\phi = 0.15) \approx 0.85$, while the spinodal line is found approximately at $T_s(\phi = 0.15) \approx 1.30$. From the inverse of the mobility, a clear distinction is observed for states between T_s and T_c (region II of the non-equilibrium glass transition diagram), which are highlighted by red solid circles discussed below, and states underneath T_c (region III). States inside region II and III of the non-equilibrium glass transition diagram will be from now on, simply refered as gel- and glass-like states respectively.

For the glass-like states (green curves), a power-law behavior is predicted in the evolution of the mobility since small waiting times. Such behavior is in fact the typical aging behavior predicted in repulsive glass systems [20]. Hence, it allow us to strongly corroborate a similar aging phenomena across the predicted asymptotic glass-like arrest region. In contrast, for gel-like states, a behavior similar to that of equilibration (yellow curve) is first observed, where a transient plateau develops prior to a power-law increase. This first behavior ends at the time highlighted by the red solid circles in each mobility, at a time which we denominate as latency time t_l . Such time is estimated by the condition $\frac{db(t)}{dt} \approx 1$ once the plateau is formed, and it is only found for gel-like states. Notice that t_l becomes smaller as the final temperature decreases and the latency effects disappear in the vicinity of the critical value T_c for the transition to a glass-like state.

On the other hand, the increase of t_l along the temperature is found to diverge at T_s . Such divergence is in fact described by a power law $t_l \propto (1 - T/T_s)^\alpha$, with T being the final quenching temperature. For the current HSSW system at both, $\phi = 0.15$ and $\phi = 0.20$ isochores, the exponent $\alpha \approx 2.1$ is predicted, as presented in Fig. 4.1 b). In comparison with experimental data, this kind of behavior is actually observed along the viscoelastic modulus, where a waiting time occurs prior their measurement in gel-like materials [18, 51]. For the storage modulus of silica nanocolloidal suspensions, similar power-laws behaviors are actually reported, with $\alpha \approx 2.5$ for the volume fraction $\phi = 0.20$, and $\alpha \approx 3$ for $\phi = 0.43$, where the latency time apparently diverges along a threshold temperature T_0 [18].

In this sense, the exponent predicted by the theory is actually found to be dependent on the system, as well as on the structural approximations, while, for the current HSSW fluid, the density is found to play a lesser. For example, for the HSAY system within the mean field structural approximation (MF), the exponent $\alpha = 2.5$ for the $\phi = 0.20$ isochore is found [29]. When comparing to the current HSSW fluid, the differences can be explained in terms of the non-equilibrium glass transition diagrams, where the spinodal temperature, as well as the glass transition temperature

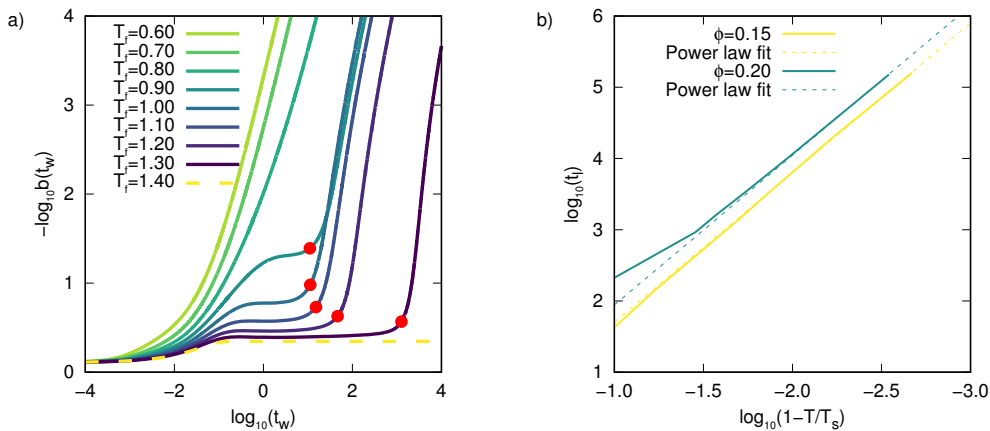


Figure 4.1: a) Inverse of the mobility for the HSSW system for the isochore $\phi = 0.15$ from the HS limit ($T \rightarrow \infty$) to $T_f = 0.60, 0.70, 0.80, 0.90, 1.00, 1.10, 1.20, 1.30$ and 1.40 . b) Latency time vs $1 - T_f/T_s$ for the isochores $\phi = 0.15$ and $\phi = 0.20$ along with the corresponding power law fit $t_l \propto (1 - T_f/T_s)^\alpha$ with $\alpha = 2.1$

are found to be dependent upon the structural approximations and interaction potential parameters. On the other hand, within the theoretical prediction, the density does seem to play a lesser role for α , where, as seen in Fig. 4.1 b), the same exponent is found for two different isochores.

Let us now discuss the NE-SCGLE predictions regarding the MSD and the self part of the ISF. In Fig. 4.2 the MSD (left column) and the self part of the ISF for $k^* = 1$ (middle column) and $k^* = 2\pi$ (right column) are presented for the same isochore $\phi = 0.15$, for three distinct final temperatures, $T_f = 0.80$ (purple lines), 0.90 (blue lines) and 1.30 (green lines), at increasing values of waiting times from left to right. To serve as a reference, the asymptotic values of each quantity for the three quenches are indicated with empty circles of the same color of each process, and where the yellow color is used to represent the initial value. Let us emphasize that the final temperature was conveniently selected in order to highlight representative features of glass-like states ($T_f = 0.80$), gel-glass interference (with $T_f = 0.90$ being just above the gel-glass transition line) and gel-like states ($T_f = 1.30$ just below the spinodal temperature). The two chosen wave vectors, $k^* = 2\pi$ and $k^* = 1$, were included in order to track the structural relaxation at (inverse) length scale of order of particle's size and larger size respectively.

Thus, Figs. 4.2 a)-c) show the evolution of the MSD and the self part of the ISF for a shallow quench inside the gel-like arrested region, where a long latency time is predicted. In terms of the MSD, negligible changes are observed for times smaller than t_l as compared to the initial value (yellow line). At $t > 10^4$, however, an aging process is observed, where the MSD evolves gradually towards its asymptotic limit (green empty circles). Hence, for sufficiently long waiting times ($t > 10^4$), the gradual development of a plateau in the MSD is observed. This plateau is a signature characteristic of dynamical arrested systems, and can be related to γ by $\gamma[u(t)] \equiv \lim_{\tau \rightarrow \infty} W(\tau; t)$, as stated in chapter 2. As a consequence, the value of this plateau is consistent with the divergent behavior of γ for quenches close below T_s . The predicted plateau for the MSD in this quench, has a much greater value than that of the glass-like state (purple empty circles), which indicates a comparably greater localization length of the system particles.

In terms of the ISF, an analogous behavior as the one described by the MSD is observed. In this quantity, for $t < t_l$, only small deviations from its equilibrium initial value are observed, while

the development of a plateau is followed afterwards. Let us emphasize that the ISFs presented in Figs. 4.2 b) and c) are shown in a log-log scale instead of the typically used normal-log scale. Such scale is employed in order to highlight the signatures present in a dynamical arrest system, which as observed for the current quench, occurs at much smaller values ($\sim 10^{-4}$ for $k^* = 2\pi$ and $\sim 10^{-2}$ for $k^* = 1$) when compared to glass-like states. In this sense, the typical arrested scenario can remain hidden when observed in a normal-log window, as it is the case for the asymptotic values of the current process observed in the rest of the ISF figures (green empty circles of Figs. 4.2 e), f), h) and i)).

The behavior of the ISF for such shallow quench close below T_s can be argued to be compatible with the physical image portrayed by the MSD and γ . For this quench, the ISF shows signs of a fairly structurally relaxed system, even at large structural scales and long waiting times. This fact, along with the high value plateau of the MSD at long waiting times, describe a system in which its particles are able to diffuse for very long distances and times prior to a solid-like response. For glasses, the dynamical arrest is commonly understood in terms of locally compact structures, where nearest-neighbor particles impede the diffusion of one and other through either caging or bonding (where the latter might occur in attractive systems) [52]. For the current process, the system particles are able to diffuse a latency distance $d_l = \sqrt{b_l t_l} \approx 18\sigma$, with b_l being the mobility value of the plateau in gel-like states. Such value is well-past the nearest-neighbor distance, hence we can conclude that the mechanism in which the dynamical arrest happens in gel-like states such as this one, differs from the typical caging or bonding mechanism.

On the other hand, and as has already been emphasized in terms of the mobility, the difference between equilibration and the formation of a gel state are difficult to be observed as the final temperature of a quench approaches the spinodal temperature from below, since the latency time becomes dramatically larger. For such cases, the divergence in the latency time implies longer waiting times in which the dynamical properties appears to be like a typical equilibrium system, while making the dynamical arrest features harder to observe (*i.e.* higher values of the MSD plateaus and lower values in the structural relaxation plateaus). In return, such behavior leads to the possibility of other non-predicted physical routes to take place, such as the complete gas-liquid spinodal decomposition process. In this regard, the theory is only able to describe the early stages of the phase separation [25]. For high enough density fluctuations values, additional effects not contained within the NE-SCGLE formalism, such as the surface tension and convection, might take place, driving the system to the expected full phase separation[25, 53].

Thus, the interplay between gelation and full phase separation of the system remains unclear. Nevertheless, an argument can be made that such interplay could be mediated in terms of the latency time. This is due to the fact that the latency time can be employed to measure the evolution of the fluctuations prior to the aging like behavior which drastically damps the evolution of the system. In return, a boundary between the gel-like arrested region and the spinodal decomposition process dependent upon the process latency time has been previously proposed [29]. On the other hand, as multiple other proposals for such boundary have been made[25], with not even a single one being corroborated by other means. Hence, we have decided not to include a more extensive discussion of such boundary in the present work.

The dynamic description just presented allow us to complement the macroscopic view of gels, thought as soft solids. The softness or rigidity of a material is commonly understood in terms of the shear or rigidity modulus, which is the ratio between a shear stress and the shear strain of a system. For gel materials, such rigidity is expected to be comparably low in contrast to other solids (small, yet finite values of shear modulus) [54]. Thus, the softness trait of gels might as well be related with the high diffusion capacity of the particles along the transient dynamics.

On the other hand, when considering lower final temperature quenches within region II, a different scenario appears. Such scenario is characterized by a competence between gel- and glass-like arrested dynamics. As illustrated in Figs. 4.2 d)-f), the interplay is highlighted by states in the neighborhood of the glass transition, where a double step relaxation is observed for the considered dynamical properties. For instance, in terms of the MSD the competing behavior traduces in a sudden change of its slope at intermediate correlation times, which for small waiting times resemble the glass-like behavior observed in the figure down below and in the asymptotic glass solution highlighted by the purple empty circles. Thus, such sudden change is actually thought to be the beginning of a caging- or bonding-like behavior in the MSD, yet at later stages, a gel-like arrested dynamics takes places. In such later stages, this feature is observed as a *double step relaxation*, where the diffusion appears to be slightly damped prior to a stronger arrest behavior. When compared with the previous case, the plateau developed at later stages is considerably smaller, indicating a comparably smaller localization length. In addition, one may also notice a faster resemblance of the MSD to its asymptotic behavior (empty blue circles). This is reminiscent of the decrease of the latency time as T_f decreases, approaching the glass transition.

At the level of the ISF, the competition between the two transitions is manifested in a stretched relaxation, more pronounced for the case $k^* = 1$. Let us take notice that, in contrast to the previous case, the y -axis of Figs. 4.2 e) and 4.2 f) is now shown in a normal scale, a convention more widely employed in reports where this quantity is presented. For $k^* = 2\pi$, the plateau formed at long waiting times have a height comparably larger than the high temperature case, yet in this scale, it remains almost imperceptible. On the other hand, at $k^* = 1$, the developed plateau can be seen within the presented window, thus indicating a structurally more compact state, which still allows for diffusion distances comparable to particle size ($d_l \approx \sigma$). In addition, for this wave-vector number, the tendency of the ISF evolution towards the glass transition is noticeable. Similar to the MSD behavior, for the largest evolution times, this tendency is observed as a double step relaxation, where at intermediate correlation times, the ISF follows after the asymptotic glass values (purple empty circles) prior to its decay towards a plateau.

Finally, in Figs. 4.2 g)-i) we illustrate the evolution of the dynamical properties for states inside the glass transition. In these states, the MSD quickly evolves towards the asymptotic γ plateau, while the self part of the ISF show signs of aging. Within the theory, this behavior is typically observed in pure repulsive glasses, such as the ones predicted in high density Lennard-Jones systems [29, 20, 22]. Hence, the observed evolution, serves as a further corroboration of the glass-like states present along region III of the asymptotic arrest diagram.

For glass-like states, the asymptotic property γ tells us about a dramatically smaller localization length when compared to gel-like states (see discussion about the T_c glass transition temperature in the previous chapter). At the level of the MSD, this change is captured by a sudden decrease in the transient plateau when compared to the previous case. Allow us to remark that, as long as a glass- and a gel-like states are compared, such change occurs in the vicinity of the gel-glass transition. This tight arrest is also observed in the ISF, where the formed plateaus are considerably higher for all wave-vector numbers when compared to the previous cases. In this sense, the now easily visible plateau formed at $k^* = 2\pi$ for the transient evolution of the ISF, tell us about a tight dynamical arrest which agrees with the scenario presented by the localization length of glasses $\gamma^{1/2} \approx 0.1\sigma$. In addition, although it is not possible to define the same latency distance for glass-like arrested, this localization length can be used as a rough estimate of one, implying diffusive distances of at least one order of magnitude lower to gel-like states.

On the other hand, and in stark contrast to the previous case, there are no visible signature features of gel-like dynamics once the glass-dynamics takes place. This is due to the glass-like

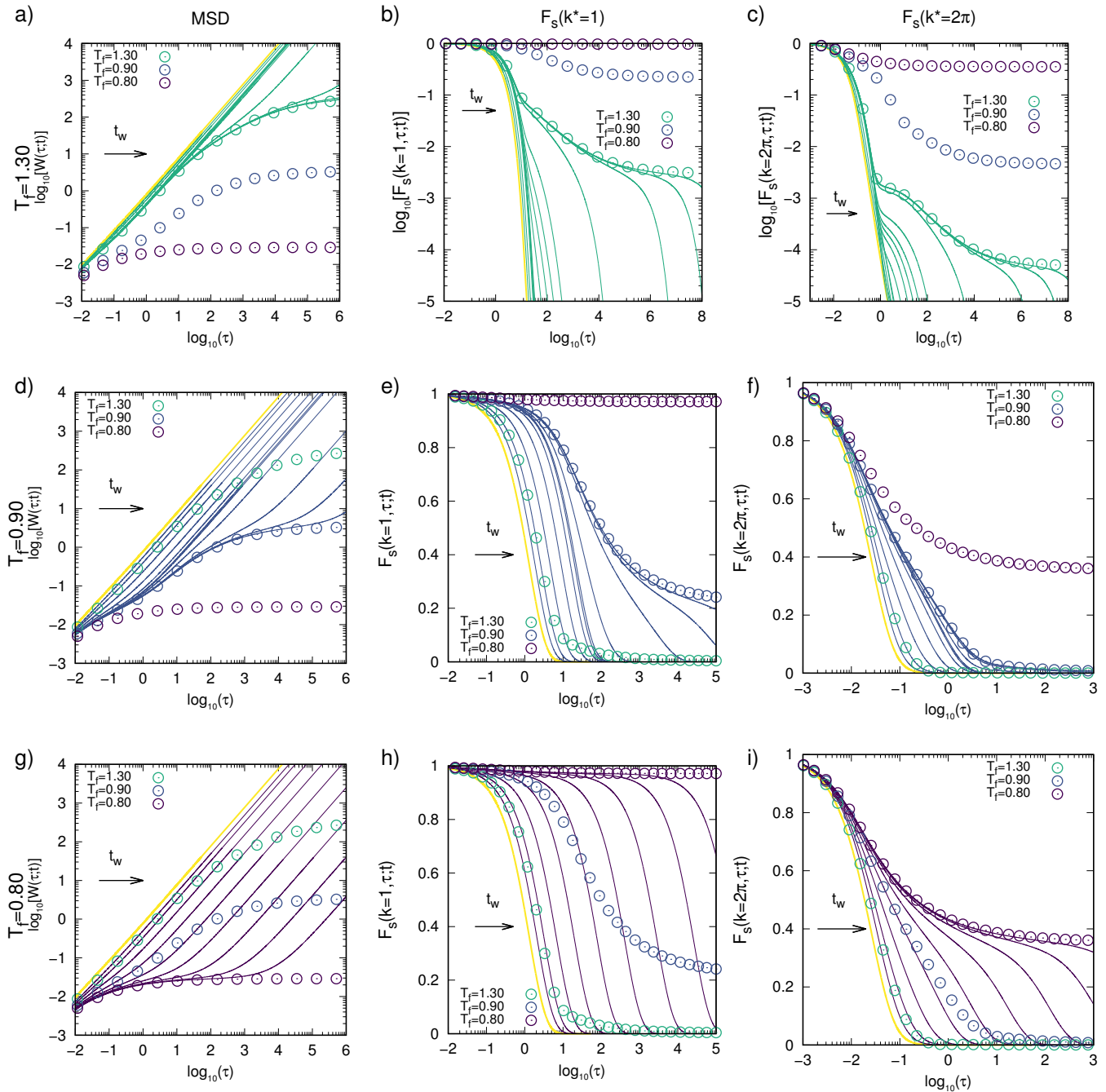


Figure 4.2: MSD (left column) and ISF for two different wave-vector numbers $k^* = 1$ (middle column) and 2π (left column) for three different final quenching temperatures $T_f = 0.80$ (purple lines), 0.90 (blue lines) and 1.30 (green lines), where the dashed lines corresponds to their respective asymptotic value, while the yellow color corresponds to the initial state condition. Each solid line, from left to right, represents the property at an increasing value of the waiting time $t = 10^{0.5n}$, with n being an integer between -4 and 6 for $T_f = 0.80$, up to 8 for $T_f = 0.90$ and up to 12 for $T_f = 1.30$.

dynamics occurs at a much faster rate than gel-like dynamics, hence the interference is only captured along gel-like states. For gel-like states, such as the previous case, the small hints that glassy dynamics are about to take place is what allow us to observe a double step relaxation behavior in the ISF and the MSD. These tendencies for the current properties has been previously reported along simulations of glass and gel former systems[55, 56, 57], thus making them a well-known fingerprint for gel-glass interplay described by the NE-SCGLE theory.

4.2 Summary

As a conclusion, the NE-SCGLE theory is able to describe many of the underlying features present within the arrested spinodal decomposition processes. Such features consist in the prediction of a power law increase in the inverse mobility as the temperature increase towards its spinodal value, the existence of a latency time and the double-step relaxation found at lower temperatures near the gel-glass transition line. The theoretical results presented in this chapter are found to qualitatively agree with those obtained for the HSAY fluid, and hence, might be generic for systems with similar interactions. On the other hand, the evolution of the kinetic properties presented in this section serves as a cornerstone in order to address the main objective of the present dissertation, where the evolution of kinetic properties must be analyzed across a multitude of states.

In addition, the presented results serve as a perspective to tackle more complex system. Particularly, the phenomenology just described is found across a variety of systems, such as hard sphere polymers[55], soft attractive interaction systems[56, 57], Laponite systems[49], and colloidal suspensions of silica[18]. Thus, a perspective of this work is to quantitatively explore the similarities and differences between experimental results and theoretical predictions when employing systems with more similar particle interactions, such as mixtures, soft cores and non-spherical interactions.

Chapter 5

Waiting-time dependent non-equilibrium glass transition diagrams

In chapter 2 a general method to predict dynamically arrested states was presented in terms of the asymptotic solutions of the NE-SCGLE equations. These solutions lead to the development of non-equilibrium glass transition diagrams, exemplified in chapter 3 using the HSSW fluid as a representative system. Such diagrams, however, do not provide a complete physical description of the predicted non-equilibrium transitions, since they do not include any specific information on the waiting time evolution of the structural and dynamical properties of the system in question. As shown in the previous chapter, this information is crucial in order to obtain a comprehensive physical picture of the different (and competing) non-equilibrium transitions predicted for the HSSW model, which includes aging and latency effects for the dynamics that are experimentally found in systems with essentially the same kind of interactions [18].

A possible manner to amend this dearth is to incorporate time as another variable in the typical thermodynamical and out-of-equilibrium representation of the HSSW system, as it has been illustrated in the context of gel and glassy states in colloidal Laponite suspensions [28, 32] or the time-temperature transformation (TTT) diagrams of borosilicate glasses [31]. Thus, in this chapter we explain how to include such time-dependent description in the previously developed non-equilibrium glass transition diagrams. More specifically, we show and explain how this can be done in terms of the mobility function $b(t)$, leading to the development of *waiting-time dependent non-equilibrium glass transition diagrams*. Let us emphasize that both the proposal and determination of such diagrams are the main scientific contributions of this work, since they provide for the very first time a first-principles description of such time-dependent non-equilibrium transitions in the thermodynamic space of a system.

generic method to predict dynamical arrested states was presented in terms of the asymptotic solutions of the NE-SCGLE formalism. Such solutions have lead to the prediction of *non-equilibrium glass transition diagrams*, exemplified in chapter 3. Although these diagrams allow us to trace the system states in terms of the thermodynamical variables, they do not take into account the complete picture of the non-equilibrium transitions. Particularly, the rich time-dependency given by the aging and latency effects just described in 4, is left out of such description. For experimental system, these effects are actually measured and taken into account when describing non-equilibrium states transitions [18]. An example of this is the consideration of time as another variable along the typical thermodynamic phase space of systems. Such is the case of colloidal Laponite suspensions [28, 32] and the time temperature transformation diagrams (TTT) of Borosilicate glasses[31].

5.1 The mobility function $b(t)$ as a dynamical arrest parameter

As discussed along chapters 3 and 4, the non-ergodicity parameter γ can be used (within both, the SCGLE or NE-SCGLE) to characterize dynamically arrested states, and also to determine the locus of different dynamical arrest transition lines in the parameter space of a given system. In particular, within the context of the NE-SCGLE approach, this parameter allow us to detect competing non-equilibrium transitions inside the spinodal region of an attractive fluid. However, this parameter is obtained from the asymptotic long time limit of the NE-SCGLE equations and, hence, does not provide any information on the waiting time evolution of a system towards the development of an amorphous arrested state. This hinders the systematic and thorough comparison of the idealized transitions predicted by the theory provided that any possible measurement must consider a finite waiting time.

In consequence, neither experiments or simulations are able to witness such idealized glassy states (as described by the asymptotic limit of the theory) and instead, only a portion of the slowly time evolving process formation of a non-equilibrium amorphous state is observed. Nevertheless, various empirical criteria have been proposed to detect the occurrence of gel and glassy states. In the former case, for instance, two properties typically employed for such characterization are the viscosity and the α -relaxation time τ_α .

The viscosity η of a system, is a physical property that allow us to quantify the resistance of a fluid to be deformed. This quantity can be thought to be inversely related to the particle's diffusion coefficient or mobility, although the exact relation is in general unknown and depends on the microscopical features and macroscopic state of the system. For example, for a colloidal dilute Hard Spheres system, the Stokes-Einstein relationship can be derived, which leads to $D_0 \propto \eta^{-1}$, with η being the fluid viscosity. On the other hand, the α -relaxation time is defined in terms of the self part of the ISF as $F_s(k, \tau_\alpha) = e^{-1}$. $\tau_\alpha(k)$ defines a structural relaxation time, in which the correlation of a particle with itself is lost. It is an experimental fact that this quantity increases dramatically during the formation of glasses [52, 14], as the diffusion of the constitutive particles significantly decreases. Thus, we can associate τ_α with the time it takes for a particle to diffuse a distance comparable to the wave length $2\pi/k$ from an initial position.

The empirical thresholds, although highly agreed within the scientific community, are not set in stone, and commonly depend on the specific system under consideration. In this regard, we might refer to two main type of glass and gel forming systems, namely, atomic and colloidal liquids, which are conformed by rather different constituent particles, whose motion is governed by interactions of distinct nature. In spite of such microscopical differences, many of the underlying features of both phase and glass transitions are acknowledged to remain rather similar for atomic and colloidal systems [58, 59, 60]. In consequence, the study of these two kinds of systems have improved our general understanding on the glass transition [60, 59].

At such, for molecular glasses, the commonly accepted threshold for the glass transition viscosity goes as high as 10^{12} Pa·s

For real molecular glasses, for instance, a commonly accepted criterion to define a glass transition is marked by an increase of the viscosity up to values 10^{12} Pa·s [61, 15, 14]. Comparatively, water's viscosity at normal condition is 10^{-3} Pa·s, while for honey is 10^2 Pa·s. Then, the difference in comparison to a glassy system is remarkably large in terms of the orders of magnitudes of the viscosity. Similarly, a commonly accepted value for the α -relaxation time, used to define a glassy state in atomic liquids is $\sim 10^2$. This is to be contrasted with the relaxation times found

for equilibrium fluids, of order 10^{-12} s [14, 15]. Hence, both the viscosity or τ_α register a similar increase during the formation of non-equilibrium glassy state.

In the case of colloidal systems, instead, the typical glass transition threshold value for τ_α is $\sim 10^5$ s [61, 59], whilst the typical equilibrium value is of order 10^0 s. A similar condition is found for the viscosity. In terms of the viscosity, such relative difference is maintained. For colloidal fluids at small concentrations, the viscosity is constrained to be that of the fluid medium, while at glassy states it typically shows an increase up to five orders of magnitude [62, 59, 61].

On the other hand, the direct study and analysis of these dynamical properties imposes a challenge within the theoretical perspective. The study of rheological properties is an area under development within the NE-SCGLE framework, while the wave-vector dependence of the α -relaxation times makes its analysis a hard problem to tackle. In return, these dynamical and rheological properties are found to be highly correlated [16, 14] among them, and also coupled with the mobility [20]. All these notions motivate thus our proposal to characterize the dynamical arrest transitions of system in terms of the function $b(t)$.

Specifically, in what follows the condition $b \leq 10^{-5}$ would be adopted to define a dynamical arrested state in a practical manner. Such condition relates to the expected colloidal threshold, which are actually the systems under consideration within the present framework. On the other hand, it is not the first time that a consideration of low mobility has actually been employed in order to follow dynamical arrest transition trends, as in the case of molecular dynamic simulations carried out by Zaccarelli *et al* [63]. In such work, the authors are able to confirm and follow predicted dynamical arrest behaviors of HSSW model systems by following the iso-diffusivity lines of values as low as $b(\phi, T) = 5 \times 10^{-6}$ [63].

In terms of the theory, this practical condition serves the purpose of localizing the aging behavior of processes leading to both, gel- and glass-like arrested states. Furthermore, the condition provides a practical way of defining each dynamical arrest transition, while also taking into account the waiting time required for their occurrence, defined as $t^a(b = 10^{-5})$. Thus, our description employs the mobility to describe waiting time dependent thermal processes. For the current system undergoing an instantaneous isochoric quenching process, when starting from a HS limit, such description is reduced to $b(\phi, T_f; t)$. Hence, the analysis of the mobility allow us to provide a reasonable description of time-dependent dynamical arrest diagrams.

5.2 The time dependent non-equilibrium glass transition diagram of the HSSW fluid

In this section the major contribution of the current dissertation is presented. To do so, the systematic solution of the NE-SCGLE is carried out for a large ensemble of possible final states, spanned by multiple values of the two control parameters ϕ and T_f . The resulting analysis of such enormous set of possible final conditions distinguish this from previous works within the NE-SCGLE theory. In practice, the multitude of final conditions consist in a combination of 40×16 densities and final quenching temperatures, going from volume fractions as small as $\phi = 0.01$ up to $\phi = 0.40$ in differences of $\Delta\phi = 0.01$, and with final temperatures ranging from $T = 0.3$ up to $T = 1.8$ in differences of $\Delta T = 0.1$. The mobility analysis of such set are the building blocks which allow us to determine the *waiting-time dependent non-equilibrium glass transition diagrams*.

Let us start by addressing the manner in which the mobility $b(t; \phi, T)$ will be displayed in terms of its three dependent variables. As shown in Fig. 5.1, the dependence of this quantity on the

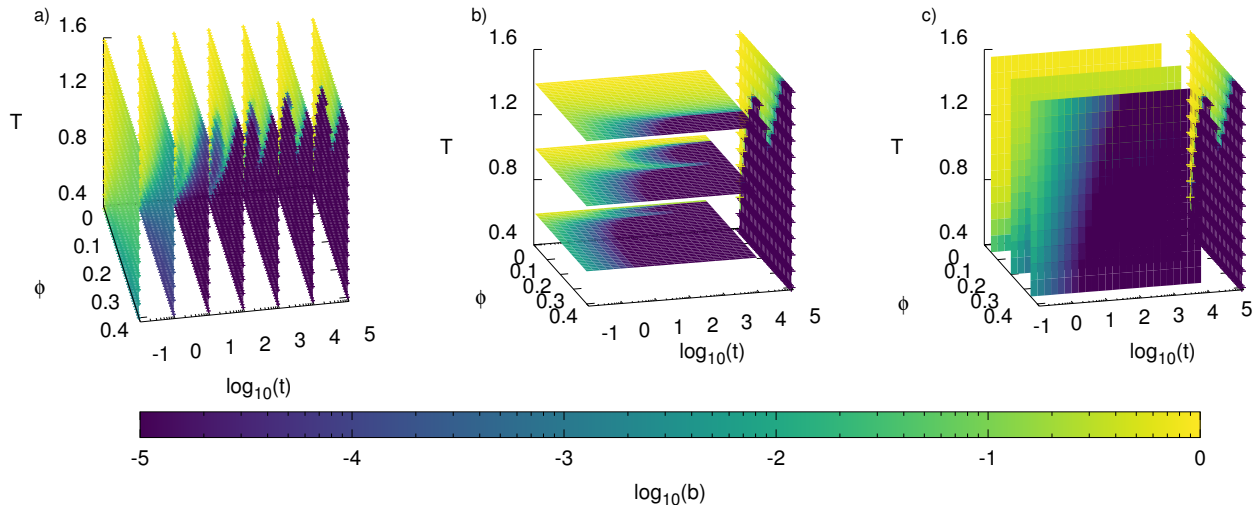


Figure 5.1: Different planes of $b(t; T; \phi)$ for instantaneous isochoric quenches within the HSSW system and where T corresponds to final quenching temperature. a) ϕ - T planes at constant $t = 10^{-1}, 10^0, 10^1, 10^2, 10^3, 10^4$ and 10^5 . b) ϕ - t planes at constant $T = 0.6, 1.0$ and 1.4 , along with the ϕ - T plane at $t = 10^5$. c) t - T planes at constant $\phi = 0.05, 0.20$ and 0.35 , along with the ϕ - T plane at $t = 10^5$.

variables ϕ , t and T can be described using a three dimensional representation, an also with a color scale that emphasizes the specific value of b for each value of the three aforementioned parameters. In this figure, the results obtained for the mobility are emphasized by following different possible planes where one of the variables is fixed. In general, each of these planes, offers a different perspective of the function $b(t; \phi, T)$, which allow us to focus on different planes depending on the application. For example, from the cuts at $t = 10^5$, a very similar scenario as the one portrayed by the *non-equilibrium glass transition diagram* (see Fig. 3.5) is observed. As a matter of fact, the main difference between this cut and its asymptotic counterpart, is that the black colored states of Fig. 3.5 are now denoted by an homogeneous purple, corresponding to a value $0 < b \leq 10^{-5}$. This subtle difference highlights the fact that the mobility of such states at the finite waiting time $t = 10^5$, is a small non-zero value.

Let us consider the evolution of the (ϕ, T) plane, described by the sequence of cuts at constant values of t shown in Fig. 5.1 a) and also displayed in detail in Fig. 5.2. These planes are of special interest as they are somehow comparable to the conventional thermodynamic state diagrams, similar to the case of the asymptotic non-equilibrium glass transition diagrams. The sequence shown in Fig. 5.2 for $t = 0, 10^{-1}, 10^0, 10^1, 10^2$ and 10^3 describes the evolution of the system during the development of both equilibrium (yellow and green colors) and arrested states (purple color $b \leq 10^{-5}$). In Fig. 5.2 the iso-diffusivity lines for $b(t) = 10^{-1}$ (black dotted lines) and $b(t) = 10^{-5}$ are also shown as a reference. Notice that in the former case, this line appears at a time scale of order 10^1 , whilst for the later this occurs at waiting times $\sim 10^1$. Also for reference, we show the asymptotic limit of these iso-mobility curves, described by the thick solid dark gray ($b^{eq} = 10^{-1}$) and light gray ($b^{eq} = 10^{-5}$) lines, as well as the asymptotic glass transition $T_c(\phi)$ (dashed thick light gray line) for inside spinodal states at densities lower than the bifurcation point (full red circle).

At the initial time, the HS limit is under consideration, which leads to an only volume de-

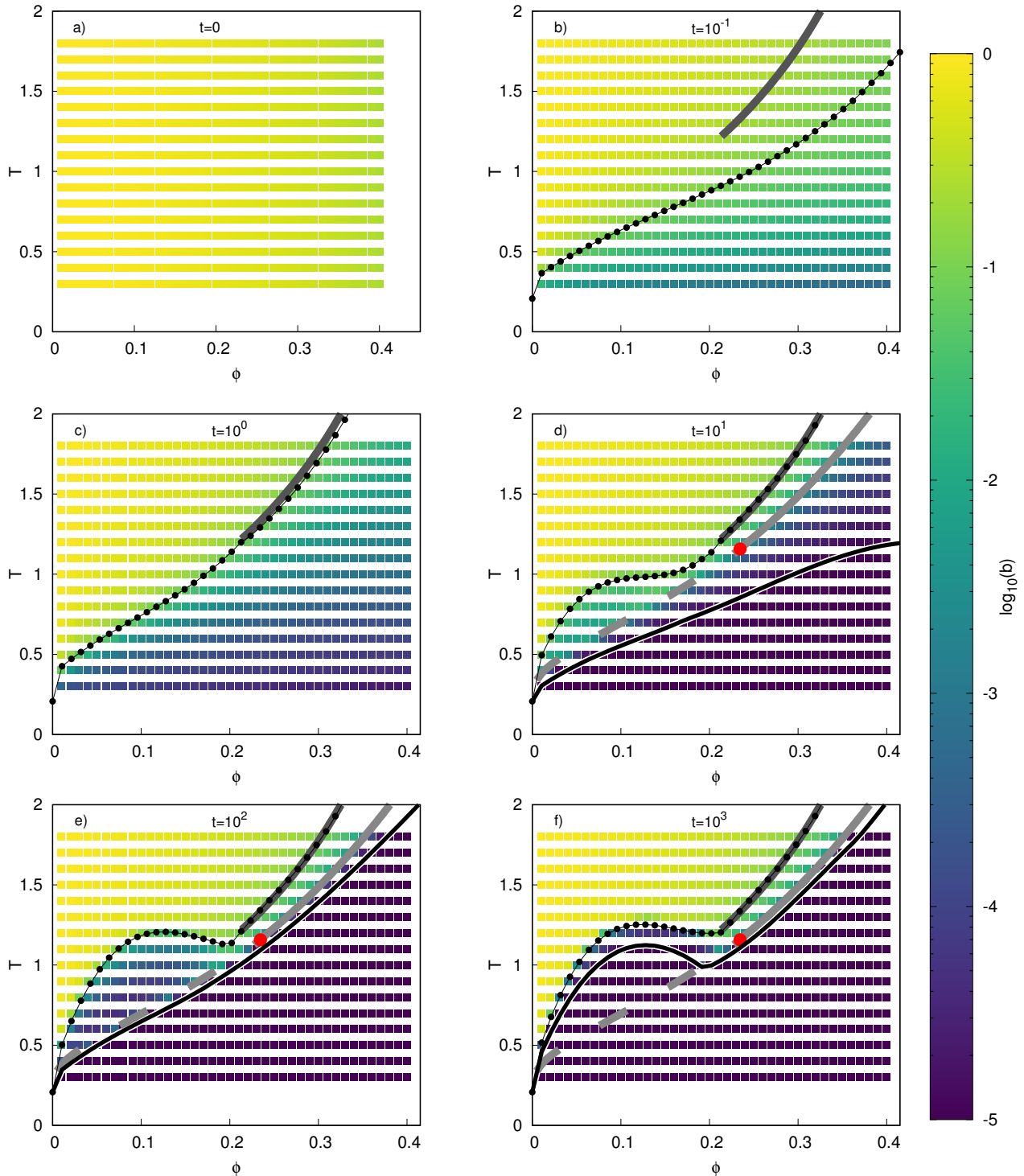


Figure 5.2: Evolution of the ϕ - T planes of $b(t; \phi, T)$ for an instantaneously-quenched HSSW model fluid at $t = 0$ a), 10^{-1} b), 10^0 c), 10^1 d), 10^2 e) and 10^3 f). The black dotted b)-f) and solid d)-f) lines corresponds to the iso-mobility (contour) lines $b(t; \phi, T) = 10^{-1}$ and 10^{-5} respectively. The thick solid dark gray b)-f) and clear gray d)-f) lines corresponds to the asymptotic equilibrium iso-mobility lines $b^{eq}(\phi, T) = 10^{-1}$ and 10^{-5} respectively, while the red dot represents the bifurcation point and the dashed thick gray line is the asymptotic glass transition inside the spinodal.

pendent mobility. Hence, in 5.2 a), columns of the same color with small variations for different density are observed. In this limit, the mobility values of the reference curves $b = 10^{-1}$ and $b = 10^{-5}$ are actually found at $\phi = 0.49$ and $\phi = 0.58$ respectively. Thus, the iso-mobility columns corresponding to the reference lines, are not visible within the presented scale.

At later times, the first thing to notice is the gradual and monotonic decrease of $b(t; \phi, T)$ with increasing waiting time in some regions of the ϕ, T plane, which are indicative of the gradual slowing down of the microscopic dynamics. This process is observed through the evolution of state points towards darker colors as t increases. In each of the presented quenches, the exact evolution of $b(t)$ depends on the specific values of the control parameters, which in return leads to a strongly inhomogeneous distribution of colors at sufficiently large waiting times. The strong contrast presented at later stages of the process allow us to glimpse at distinct evolution processes such as the ones presented in the previous chapter.

In equilibrium conditions, the asymptotic iso-mobility line (thick solid dark gray) of $b = 10^{-1}$ serves the special purpose of also being the freezing line according to a dynamic empirical criterion [46]. However, under the current framework, it simply separates the stable from the metastable liquid regions. Additionally, when the time dependence is included in the description, the iso-mobility curve (black lines with circles) describes the evolving boundary between the equilibrium and non-equilibrium regions. Notice that the iso-mobility curve $b(t) = 10^{-1}$ matches its asymptotic value at waiting times $t \approx 10^0$. Also important, during the early stage of evolution of the HSSW system, the motion of particles is presented by fast diffusion-limited clustering of nearest-neighbor particles. This, however, is only the preamble of a slowly evolving process that involves collective restructuring processes. At later stages ($t > 10^0$) many relevant features are developed in the time-dependent diagram.

A similar but noticeably slower evolution is exhibited by the iso- b line corresponding to $b_0 = 10^{-5}$ (solid line), which is only observed at waiting times $t \geq 10^1$, as illustrated in Figs. 5.2d)-f). Notice that this iso-mobility line matches its asymptotic value (thick solid gray line) at time scales of order 10^3 . Fig. 5.2 describes the continuous time-evolving pattern of the mobility on the (ϕ, T) state space, in which the time-dependent iso- b lines serve as sharp, yet artificial visual aids. At even longer times, however, this evolution becomes less and less perceptible, to the point that it eventually appears to be stationary. In fact, this already occurs at the waiting time $t = 10^5$, whose snapshot coincides, within the resolution of the figure, with the non-equilibrium glass transition diagram $b(t \rightarrow \infty; \phi, T) = b^{eq}(\phi, T)$ of Fig. 3.5.

The slow dynamic features illustrated in Figs. 5.2d)-f) and the non-equilibrium glass transition diagram helps to understand the time dependence of the experimental glass transition. The empirical criterion just proposed in this work serves as a link to the experimental thresholds proposed for the glass transition. Hence, the condition $b(t, \phi, T) \leq b^{(a)}$ provides a practical criterion to determine the occurrence of non-equilibrium transformations into gel and glassy states. This removes the fundamental difficulties to compare theoretical predictions with experimental and/or simulated results.

The whole evolution in Figs. 5.2 a)-f) and 3.5, from the beginning to the end, is what is referred to as a *time-dependent non-equilibrium phase diagram*. Its kinetic perspective, and its description of dynamically-arrested phases, constitute the most relevant difference with respect to ordinary equilibrium phase diagrams, whose proper counterpart, illustrated in Fig. 3.5, is the *non-equilibrium glass transition diagram*, now obtained at $t \rightarrow \infty$ limit of this t -dependent process.

One important question refers to the possible dependence of the kinetic scenario just presented, on the threshold value of $b^{(a)}$. In general, we found that the basic scenario is essentially the same, except that in order to observe qualitative features similar to those displayed in Figs. 5.2 d)-

f) and 3.5, much longer waiting times and much higher resolution in $b(t)$, ϕ and T , will be required as the threshold value decreases. What will not change, however, are the long-time limiting lines $b(t \rightarrow \infty; \phi, T) = b^{eq}(\phi, T) = b^{(g)}$ for $b^{(g)}$ smaller than 10^{-5} , all of which virtually superimpose (again, within the resolution of the figure) on the solid line of Fig. 3.5. Thus, this line is the stationary dynamic arrest line $b^{eq}(\phi, T) = 0$, one of the most relevant elements of the non-equilibrium glass transition diagram, first presented and explained in detail in Ref. [25].

Although the analysis done in the (ϕ, T) has been revealing enough, as it can be compared with common thermodynamical diagrams, the theoretical description allow us to focus in different chosen variables. In this regard, and as it has been previously stated, other planes might be more relevant depending on the application. Such is the case of the (T, t) plane at constant ϕ and (t, ϕ) plane at constant T . These planes are commonly seen in TTTs diagrams and experimental reports[31, 28]. The analysis done in these alternative planes is shown in Figs. 5.3 a)- c) for the (t, ϕ) plane for a supercritical ($T = 1.4$) and two subcritical ($T = 1.0, 0.6$) quenching temperatures. Additionally, the (T, t) plane is shown in Figs. 5.3 d)-f) for the isochores $\phi = 0.05, 0.15$ and 0.25 . In each of these figures, the intersection of the respective plane with the empirical dynamic arrest transition surface $b(t; \phi, T) = b^{(a)} = 10^{-5}$ is represented by the colored solid lines. These lines indicate the time required for the system to pass from a fluid state to an arrested one ($b(t; \phi, T) < b^{(a)}$). In particular, the red solid line indicates a transition to the expected glass-like states (region III of Fig. 3.5) and the pink solid line to the expected gel-like states (region II of Fig. 3.5).

Let us further discuss the isothermal diagrams. From Figs. 5.3 a)-c) it can be seen that, at a given isotherm, we only have two or three possible final states. Thus, at supercritical temperatures (Fig. 5.3 a)) the system is expected to reach equilibrium at low volume fractions, but above a critical volume fraction $\phi_g(T)$ that depends on temperature ($\phi_g(T = 1.4) \approx 0.29$), a transition will occur into an arrested state corresponding to a high-density repulsive glass. In fact, the high- T limit of $\phi_g(T)$ is precisely $\phi_g(T = \infty) \approx 0.58$.

In contrast, for subcritical temperatures, illustrated by Figs. 5.3 b) and c), a third possibility emerges, namely, the formation of arrested sinodal-decomposition gel states, corresponding to region II in the non-equilibrium glass transition diagram of Fig. 3.5. In fact, for isotherms only slightly subcritical (not illustrated here), the gel transition will be confined to a small volume fraction interval around the volume fraction ϕ_c of the critical point. For such cases, the transition is expected to occur after a very long waiting time. This is due to the previously discussed nature of the latency time, which diverges approaching the spinodal line and, hence, is not contained in the time-window employed in the present figures.

For completeness, let us focus now on the constant ϕ planes. In these isochore planes, Figs. 5.3 d) and e) have volume fractions smaller than the bifurcation point (full red circle of 5.2), while Fig. 5.3 f) represents a higher value case. In these plane, the bifurcation point plays a similar role as the critical temperature, which is the meeting state point between the spinodal and the dynamical arrest line as previously discussed in chapter 3. Hence, for densities greater than the bifurcation point, the typical glass transition is predicted, while for densities lower than that of the bifurcation point, depending on the final temperature, gel or glassy states might be found.

Finally, in Fig. 5.4, two practical applications in other kind of system are shown and qualitatively compared with the planes predicted by the theory for the HSSW model. In Fig. 5.4 a), the resulting time-dependent non-equilibrium glass transition diagram is shown for plane (t, ϕ) at $T = 1.0$. To serve as a reference, in Fig. 5.4 b) we show similar results obtained from experimental characterizations of Laponite suspensions [28]. In this figure, the transition from an equilibrium fluid state to a non-equilibrium one is highlighted by the gray circles, with black the solid line

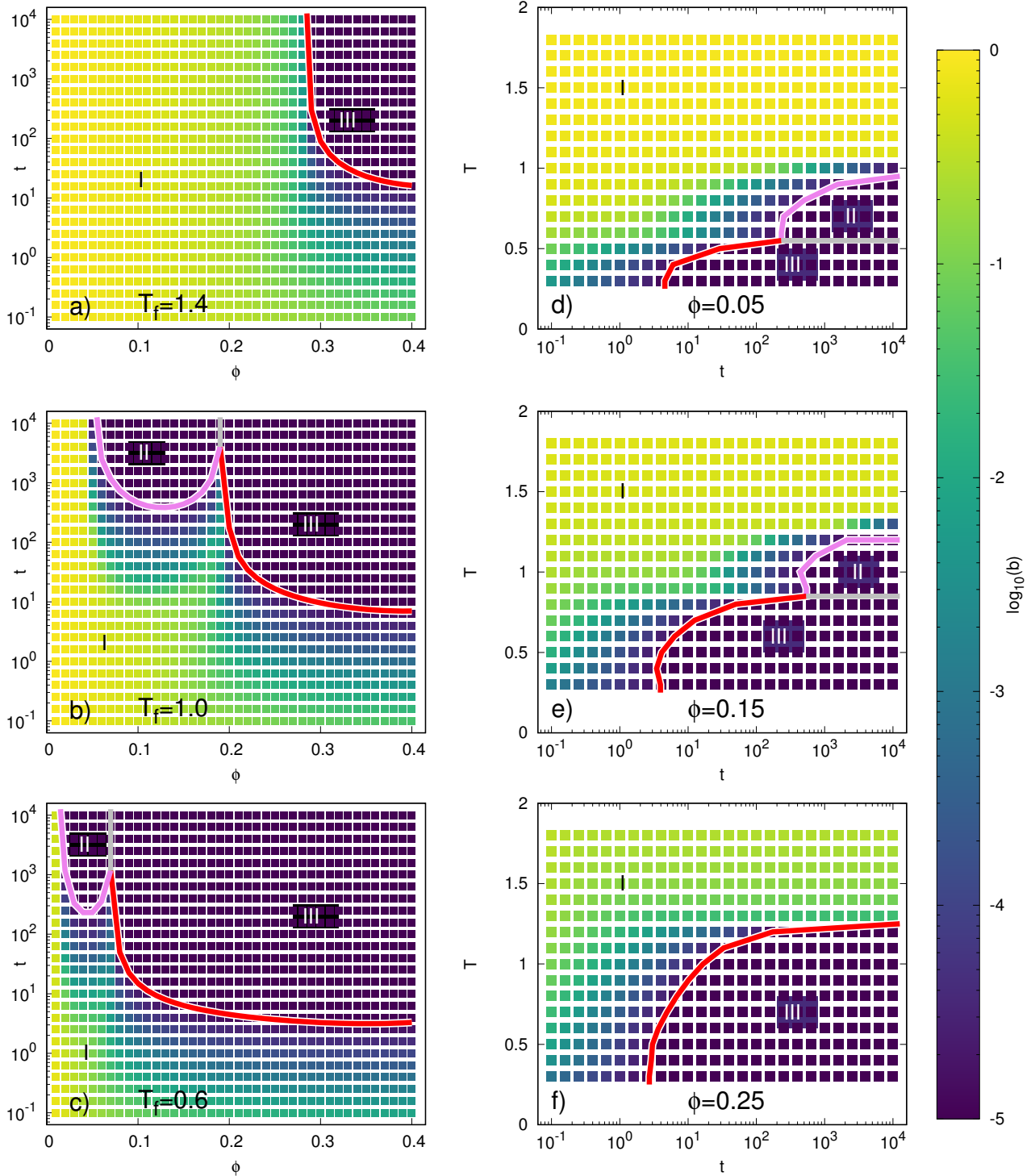


Figure 5.3: ϕ - t planes at constant $T_f = 1.4$ (a), 1.0 (b) and 0.6 planes and t - T planes at constant $\phi = 0.05$ (d), $\phi = 0.15$ (e) and $\phi = 0.25$ (f) of $b(t; \phi, T)$. Fluid states are expected at region I in each of the diagrams, with $b(t; \phi, T) > 10^{-5}$ boundary condition. The solid red and pink lines corresponds to the $b(t; \phi, T) = 10^{-5}$ boundary, while segregating glass-like (red enclosing region III) from the gel-like (pink enclosing region II) arrested states.

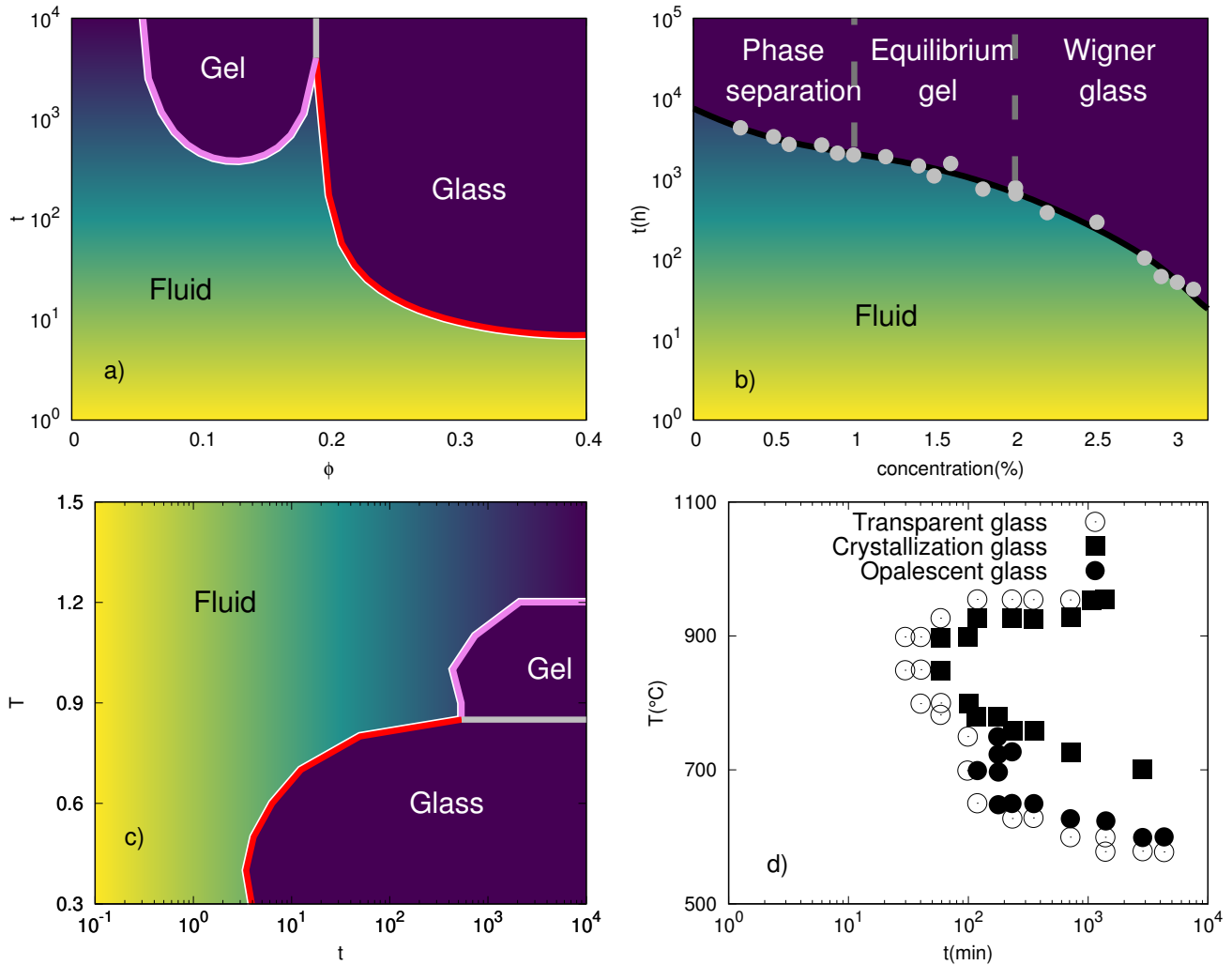


Figure 5.4: a) Time-dependent non-equilibrium phase diagram for the HSSW system at $T = 1.0$. b) Laponite time dependent diagram sketched from the experimental data in Ref. [28] where time is measured in hours after filtering the sample which was immediately obtained after 30 minutes of stirring, and concentration is weight concentration. c) Time-dependent non-equilibrium phase diagram for the HSSW system at $\phi = 0.15$. d) Non-equilibrium state transformation of the borosilicate glass $65\text{SiO}_2 \cdot 25\text{B}_2\text{O}_3 \cdot 10\text{Na}_2\text{O}$, reproduced from the time-temperature transformation (TTT) diagram in fig. 1 of Ref. [31]

being just a numerical fit for the data. This shows how the NE-SCGLE theory is able to generate essentially the same time-dependent information required for the description of non-equilibrium transformations in a quenched liquid. A similar comparison can be made for diagrams at constant ϕ which are comparable to the experimental TTT diagrams previously mentioned in Fig. 5.4 d), reproduced from ref. [31].

From these qualitative comparisons, it can be implied that some of the general features of these transitions are maintained even though obvious differences exist within the systems. On the one hand, the Laponite system is made of electrically charged non-spherical particles, while the borosilicate glass is a molecular mixture system. Nevertheless, similar states to the NE-SCGLE predictions are observed within the Laponite system in the same kind of order, a glass region at higher densities and a gel region for moderate and low densities. On the other hand, although the phase separation is not strictly predicted within the theory, one could make the case that such a process could be estimated as has been previously done [25, 29]. In terms of the Borosilicate system, the transparent glass phases could be interpreted as homogeneous phases, waiting for the transitions to develop. In such terms, the crystallization glass could be interpreted as a vitrification process in which the full crystallization of the system is frustrated, while the opalescent glass region is reminiscent of a frustrated spinodal decomposition process.

5.3 Summary

As a conclusion, the methodology just described is capable of describing the general characteristics of the time-dependent transformations of materials. Such methodology consists in following the solution of the NE-SCGLE equations for the mobility. This is done thoroughly across the thermodynamic parameter space of the system. In addition, the practical threshold, $b^a = 10^{-5}$, allows us to track dynamical arrested states through a relaxed condition. This allows us to estimate a practical time in which a system transition towards a non-equilibrium state is expected to occur. As a consequence, we are able to obtain the *waiting-time dependent glass transition diagrams*.

In particular, the described procedure applied to a Lennard-Jones like system allows us to follow such characteristics along the frustrated spinodal decomposition predicted by the theory. The resulting *waiting-time dependent glass transition diagrams* qualitatively agree with experimental reports of different systems undergoing similar processes. It is then within our expectations, that the methodology just described, to work similarly for systems with interactions more similar to the experimental ones, as is the case of mixture and non-spherical interacting systems. Although the theoretical extension to such kind of system is a reality [21, 64], they fall out of the scope of the current work. Thus, they conform a promising perspective for the further development of these time dependent diagrams.

Chapter 6

NE-SCGLE description of density linear deviations.

In this chapter, we discuss an extension of the NE-SCGLE theoretical framework which allows for the description of the mean value evolution of the local density, $\bar{n}(\mathbf{r}, t)$, after an instantaneous isochoric quench in a fluid is considered. This quantity plays an important role in a system description as, in principle, it allow us to describe the morphological characteristics of a system. Such characteristics are in fact relevant in non equilibrium processes such as the spinodal decomposition of metallic alloys and polymer systems [65]. In general, morphology analysis can be employed to obtain physical insight, as well as to present a visual aid for a system structural description. Hence, as in the previous chapters, here we exemplify the solutions for $\bar{n}(\mathbf{r}, t)$ of a HSSW system undergoing distinct instantaneous isochoric quench processes along the (ϕ, T) parameters space.

This final chapter is organized in three sections. In the first of them, we discuss the theoretical approximations involved in the derivation of an equation that describes the time evolution of the mean local density fluctuations (we refer to Eq. (6.7) below). As shown in what follows, such equation is obtained from considering the linear deviations of the mean local density, which is described by the generalized Fick's equation employed within the NE-SCGLE (*i.e.*, Eq. (2.59)). The resulting linearized equation, however, requires for an initial condition in addition to the solution of the NE-SCGLE equations previously discussed. This initial condition is discussed in the second section of the present chapter along with a method proposed to visualize the results. Finally, in the third section some concrete theoretical predictions for the evolution of $\bar{n}(\mathbf{r}, t)$ are presented and discussed for a HSSW model. More specifically, the time-evolving morphology of this system is studied for a collection of different isochoric quench processes and discussed in the context of the *waiting-time dependent non-equilibrium glass transition diagram* and the dynamical arrest transitions previously characterized.

6.1 Theoretical approximation.

Recalling the full non-equilibrium SCGLE theory in its most general version, summarized by Eqs. (2.59) and (2.61), the central elements of the theory are the time evolution equations describing the kinetics for $t > 0$ of the mean value $\bar{n}(\mathbf{r}, t)$, and the covariance $\sigma(\mathbf{r}, \mathbf{r}'; t) \equiv \overline{\delta n(\mathbf{r}, t) \delta n(\mathbf{r}', t)}$ of the fluctuations $\delta n(\mathbf{r}, t) = n(\mathbf{r}, t) - \bar{n}(\mathbf{r}, t)$, of the instantaneous local density $n(\mathbf{r}, t)$. The growth and arrest of spatial heterogeneities, which are characteristic of the process of arrested spinodal decomposition [27, 48] (*i.e.*, quenching inside the spinodal) can be described from the solution of

Eq. (2.59) for the mean local density. Such equation reads

$$\frac{\partial \bar{n}(\mathbf{r}, t)}{\partial t} = D_0 \nabla \cdot b(\mathbf{r}, t) \bar{n}(\mathbf{r}, t) \nabla \beta \mu[\mathbf{r}; \bar{n}(t)], \quad (6.1)$$

presented here again for clarity and practical convenience. In order to unveil the evolving morphology of a quenched system, however, the previously assumed homogeneous-fluid approximation, $\bar{n}(\mathbf{r}, t) \neq cte$, must be disregarded and replaced, instead, by a non-trivial solution for Eq. (6.1).

In general, such non-trivial solutions become remarkably difficult to be treated both mathematically and numerically. In the absence of external fields, however, a simple strategy that provides a glimpse on the most general features of such solutions might be devised. This strategy starts by writing $\bar{n}(\mathbf{r}, t)$, $b(\mathbf{r}, t)$, and $\sigma(k; \mathbf{r}, t)$ as the sum of their homogeneous mean (or bulk) values \bar{n} , $b(t)$, and $\sigma(k; t)$, plus their deviations from homogeneity, $\Delta \bar{n}(\mathbf{r}, t)$ ($\equiv \bar{n}(\mathbf{r}, t) - \bar{n}$), $\Delta b(\mathbf{r}, t)$ ($\equiv b(\mathbf{r}, t) - b(t)$), and $\Delta \sigma(k; \mathbf{r}, t)$ ($\equiv \sigma(k; \mathbf{r}, t) - \sigma(k; t)$). It is at the zeroth order in these deviations when the spatially-homogeneous version of the NE-SCGLE theory is recovered. Under such condition, among other properties, the zeroth-order mobility function $b(t)$ is recovered (see Eq. (2.68)). Unfortunately, in this spatially-uniform version of the theory, the morphological information embodied in $\bar{n}(\mathbf{r}, t)$ is lost when neglecting $\Delta \bar{n}(\mathbf{r}, t)$.

In order to retain at least some of the morphological information, we might rewrite equation (6.1) to include the deviations $\Delta \bar{n}(\mathbf{r}, t)$. Expanding Eq. (6.1) to linear order one gets

$$\frac{\partial [\bar{n}(t) + \Delta \bar{n}(\mathbf{r}, t)]}{\partial t} = D_0 \nabla \cdot [b(t) + \Delta b(\mathbf{r}, t)] [\bar{n}(t) + \Delta \bar{n}(\mathbf{r}, t)] \nabla \left[\int \frac{\delta \beta \mu[\mathbf{r}; \bar{n}(t)]}{\delta \bar{n}(\mathbf{r}', t)} \Delta \bar{n}(\mathbf{r}, t) d\mathbf{r} + \mathcal{O} \Delta \bar{n}^2(\mathbf{r}, t) \right],$$

which, by neglecting the mobility fluctuations $\Delta b(\mathbf{r}, t)$ and considering only the linear terms of $\bar{n}(\mathbf{r}, t)$, we may write

$$\frac{\partial \Delta \bar{n}(\mathbf{r}, t)}{\partial t} = D_0 b(t) \bar{n} \nabla^2 \int d\mathbf{r}' \mathcal{E}(|\mathbf{r} - \mathbf{r}'|) \Delta \bar{n}(\mathbf{r}', t). \quad (6.2)$$

This last equation can then be easily solved in Fourier space. Applying the FT to this last equation follows

$$\frac{\partial \Delta \bar{n}(\mathbf{k}, t)}{\partial t} = -k^2 D_0 b(t) \bar{n} \mathcal{E}(k; \bar{n}, T_f) \Delta \bar{n}(\mathbf{k}, t), \quad (6.3)$$

where $\mathcal{E}(k; \bar{n}, T)$ is the FT of the functional derivative $\mathcal{E}[|\mathbf{r} - \mathbf{r}'|; n, T] \equiv [\delta \beta \mu[\mathbf{r}; n, T] / \delta n(\mathbf{r}')]$, evaluated at the uniform density and temperature profiles $n(\mathbf{r}) = \bar{n}$ and $T(\mathbf{r}) = T_f$. Thus, the solution of Eq. (6.3) reads

$$\Delta \bar{n}(\mathbf{k}, t) = w[k; u(t)] \Delta \bar{n}(\mathbf{k}, t = 0), \quad (6.4)$$

where the transformation $u(t) \equiv \int_0^t b(t') dt'$ has been employed and where the function $\Delta \bar{n}(\mathbf{k}, t = 0)$ is the FT of the initial condition $\Delta \bar{n}(\mathbf{r}, t = 0)$, and where the propagator $w[k; u]$ is the solution of

$$\frac{\partial w[k; u]}{\partial u} = -k^2 D_0 b(t) \bar{n} \mathcal{E}(k; \bar{n}, T_f) w[k; u], \quad (6.5)$$

i.e.,

$$w[k; u] \equiv \exp[-k^2 D_0 \bar{n} \mathcal{E}(k; \bar{n}, T_f) u]. \quad (6.6)$$

Hence, up to its linear order from deviations, the non-equilibrium evolution of the mean local density, is given by

$$\bar{n}(\mathbf{r}, t) = \bar{n} + \frac{1}{(2\pi)^d} \int d\mathbf{k} e^{-i\mathbf{k}\cdot\mathbf{r}} w[k; u(t)] \Delta\bar{n}(\mathbf{k}, t = 0), \quad (6.7)$$

which is the main result of this section. To use this expression, together with Eqs. (2.69) and (6.6), we need an initial condition $\Delta\bar{n}(\mathbf{k}, t = 0)$, as well as to determine the function $\mathcal{E}(k; \bar{n}, T_f)$ being $u(t)$ and $b(t)$ self-contained within the NE-SCGLE theory. Thus, the NE-SCGLE formalism provides a closed system of equations, whose solution provides the evolution of the mean local number density. By imagining a virtually divided space, this result can be employed to solve for $\bar{n}(\mathbf{r}_i, t) \equiv \bar{n}_i(t)$, the mean density value of a subspace centered at \mathbf{r}_i in a linear approximation.

Even though the physical meaning of the local density can be considered a well-known concept (in essence, a function which describes the spatial distribution of particles), the expression just derived actually describes its *average*. The *average* of this and all previously defined quantities refers to an ensemble average, *i. e.*, an average over all possible realizations, which is typically defined in terms of the particles configurations of positions and momenta. In this regard, even if an heterogeneous initial condition is given as a frozen configuration at $t = 0$, the current formalism is unable to predict a particular trajectory that this configuration might follow. In contrast, the evolution of the mean local density predicted by the theory, is but an average over all possible trajectories that an initial density configuration might follow. Such initial configuration, as shall be later discussed, can be as simple as the average number of particles contained in a virtually divided space, for example the number of particles present in two halves of a container.

6.2 Initial state condition of a hard sphere system.

In chapter 3 a procedure for the determination of the thermodynamic function $\mathcal{E}(k; \bar{n}, T_f)$ for the HSSW system was presented. With this in mind, all that is left to do is to obtain an initial condition for the local density profile $\Delta\bar{n}(\mathbf{r}, t = 0)$. In equilibrium, the initial local density distribution of a system is given by the inherent thermal fluctuations. For a fluid system, a density fluctuation is given by the diffusion of the particles within their available space. For example, for a system of N punctual non-interacting particles that are contained within a volume V , hence having a bulk number density $\bar{n} \equiv N/V$. In such system, the density fluctuations can only be noticed by looking a frozen configuration of the system, thus observing the specific local position of the system particles.

For this system, a given density fluctuation can be partitioned in order to be able to describe the density in several regions of the volume. This is done by dividing the containment space and looking into the resultant subspaces, *i.e.* when dividing the the total space in m subspaces, with volume $V_i \equiv V/m$ for the i -esim subspace. Such partition of the space allow us to measure the number density $n_i(t)$ for the i -th subspace. In general, the measurement of any of the subspaces can differ from the bulk density \bar{n} at any particular time, as particles are free to enter and leave each of the subspaces. This happens even though the average measurement is consistent with the mean density, as random events take place.

In practice, such distributions can actually be obtained from experimental and simulation data. On the other hand, theoretical approaches that directly describe the density fluctuations exist in the form of thermodynamic fluctuations theory [66]. In this work, the initial density fluctuations

are modeled after a purely repulsive hard sphere system in the simplest form possible, where only two options are considered, having a particle in a given subspace or not.

Let us consider a system of N particles confined in a total volume given by a box of size L . By following the same exercise previously described, let us now divide the containment in sub-space boxes of size $l = \sigma$ (with σ being the diameter of each particle). Given the size of the sub-spaces boxes used, the proposal consist in the consideration that the density in each of the sub-spaces is a result of a non-correlated binomial distribution, which only accounts for two different events, a sub-space which can either fully contain a particle or that is totally empty. With such simplification, the probability p_1 of finding a particle in a sub-space is given by

$$p_1 = \bar{n}, \quad (6.8)$$

with $p_0 = 1 - \bar{n}$ being the probability of finding an empty subspace, and whose mean value is \bar{n} . Specifically, for all the results presented in what follows, we will consider $L = 2^7\sigma$.

In Fig. 6.1 a) the probability function is plotted for the HS initial condition $\phi = 0.10$, with $\phi \equiv n\pi\sigma^3/6$, while in Fig. 6.1 b) we show a slab of width $\Delta z = \sigma$ and area $\Delta x\Delta y = (100\sigma)^2$, obtained for one realization. Such slab is, therefore, a cross section of the total system, contained in a three dimensional box conformed by $(L/l)^3 = 2^{21}$ smaller boxes. but a face of the total system, which consists of a three dimensional arrange of $(L/l)^3 = 2^{21}$ total density boxes. In addition, Fig. 6.1 b) presents the density in a gray scale for the system volume fraction, centered around its equilibrium value, with white reserved for the lowest value $\phi = 0$, and black for $\phi > 2\phi$. In the presented case, each of the sub-spaces can either have a volume fraction of $\phi = 0$ (white) or $\phi = \pi/6$ (black). Although the adopted visual representation is limited to a binary color for the current case, from now we will employ this convention as it will be relevant in what follows. In addition, we will stick to slabs of the same size ($10^4\sigma^2$) to discuss our results.

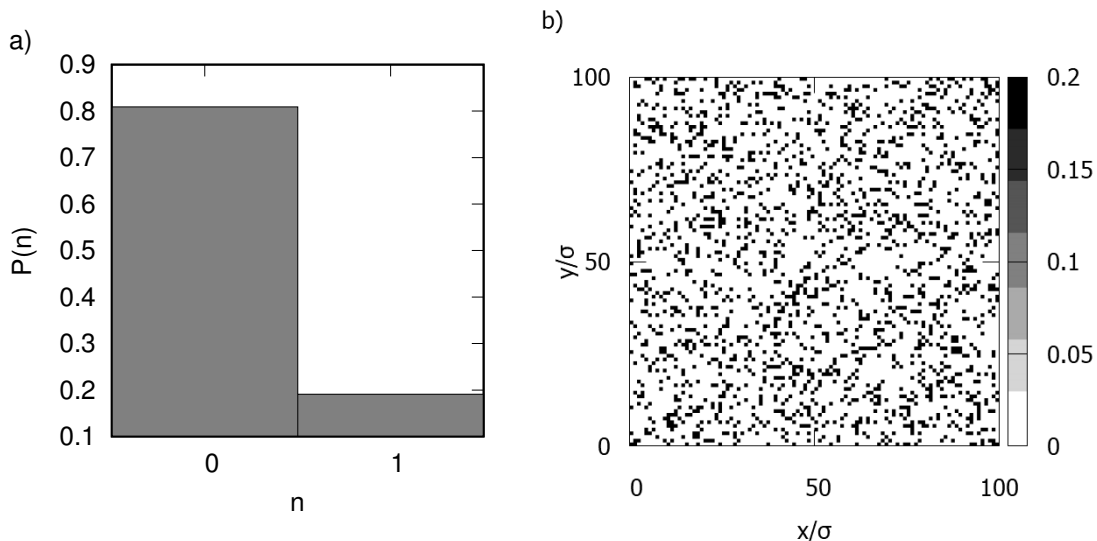


Figure 6.1: a) Probability distribution for the HS system at $\phi = 0.10$ equilibrium state for boxes of size $l = \sigma$. b) A slab of width σ of the pseudo Montecarlo realizations for a window of size 100σ . As explained in the text, the complete system is composed of 2^{21} boxes of size σ

6.3 Evolution of density fluctuations.

In this section, the results of solving Eq. (6.7) are shown for several quenching processes. Thus, the format just described in the previous section allow us to distinguish fine details in the evolution of the density fluctuations at different stages of each of the quench process considered. The predicted evolution of the mean local density is shown along Figs. 6.2-6.8, which corresponds to a sequence of snapshots of this quantity at waiting times $t = 0, 10^{-1}, 10^0, 10^1, 10^2, 10^3$ and 10^4 , respectively. For reference, the snapshot for the visualization of $\Delta\bar{n}(\mathbf{r}, t)$ are displayed along these figures using the (ϕ, T) plane in the background, where the center of each snapshot corresponds to the state point investigated. It is worth to mention that additional data treatment has been considered to account for physical limits that are not explicitly contained in the above NE-SCGLE equations (see Appendix B).

Fig. 6.2 in particular, considers the initial values of the density fluctuations along the previously discussed non-equilibrium glass transition diagram (see Fig. 3.5) resulting *non-equilibrium glass transition diagram* (see Fig. 3.5). Recall that this asymptotic diagram ($t \rightarrow \infty$) emphasizes the three main scenarios predicted by the NE-SCGLE for the relaxation of the HSSW after a quench, corresponding to: Equilibration, for final states that lie in the fluid (region I); gelation, for the final states enclosed by the gray and black thick solid lines in Figs. 3.5 and 6.2 (region II); and vitrification, for final states below the black solid line of the same figures (region III). Thus, the asymptotic (thick solid) lines shown in Fig. 6.2 serve the purpose of identifying the kind of process expected for each of the quenches, whereas the snapshots in Figs. 6.3-6.8 describe the predicted evolution of the morphology during all the processes considered. For reference, the mobility at *nearby* states (*i. e.*, states points in the vicinity of each snapshot) is displayed using the same color format as in Fig. 5.2. This, for instance, emphasizes (in yellow color) the high diffusivity of the constitutive particles in the initial states.

Let us now discuss each of the expected processes one by one starting with the equilibration processes. From the asymptotic diagram in Fig. 6.2, we know that the equilibration of the HSSW system is expected for quenches that consider a sufficiently large final temperature. These kind of processes are represented along Figs. 6.2-6.8 by the three upper panels, corresponding to three isochoric quenches ($\phi = 0.10, 0.15, 0.20$) towards the final temperature $T_f = 1.40$. In general, one expects that the mobility of the particles would not decrease significantly after the equilibration of the system. Along Figs. 6.3-6.8, this is observed by noticing the evolution of the iso-mobility line $b = 10^{-1}$ (black lines with solid circles) which always lies below the equilibrium states described in the upper panels. Thus, it is expected that, at $t = 10^1$, the particles should have diffused at least a distance greater than that of their radius. Such description is captured by the theory in terms of the relaxation of the density fluctuations towards the equilibrium density. One notices, for instance, that any relevant change is predicted for the mean local density (with respect to the initial configuration) for $t \leq 10^{-1}$. At waiting times $t = 10^0$, however, the beginning of a homogenization process of the gray color is observed in the three equilibrium quenches. These homogenization finally ceases at $t \sim 10^2$, but with a different evolution and final equilibrium value for each process, thus emphasizing the influence of each initial condition.

The equilibration processes of the mean local density, which starts from the heterogeneous distribution represented by the black and white regions shown in Fig. 6.2, is rather intuitive and can be, hence, easily understood. To this endeavor, let us mention that one possible interpretation of $\bar{n}(\mathbf{r}; t)$ is as a sort of probability distribution. Such idea results simply due to an expected correlation between the particles' distribution function and the density in each of the regions of the space, even if the concrete relation remains unknown. Nevertheless, a naive model can be

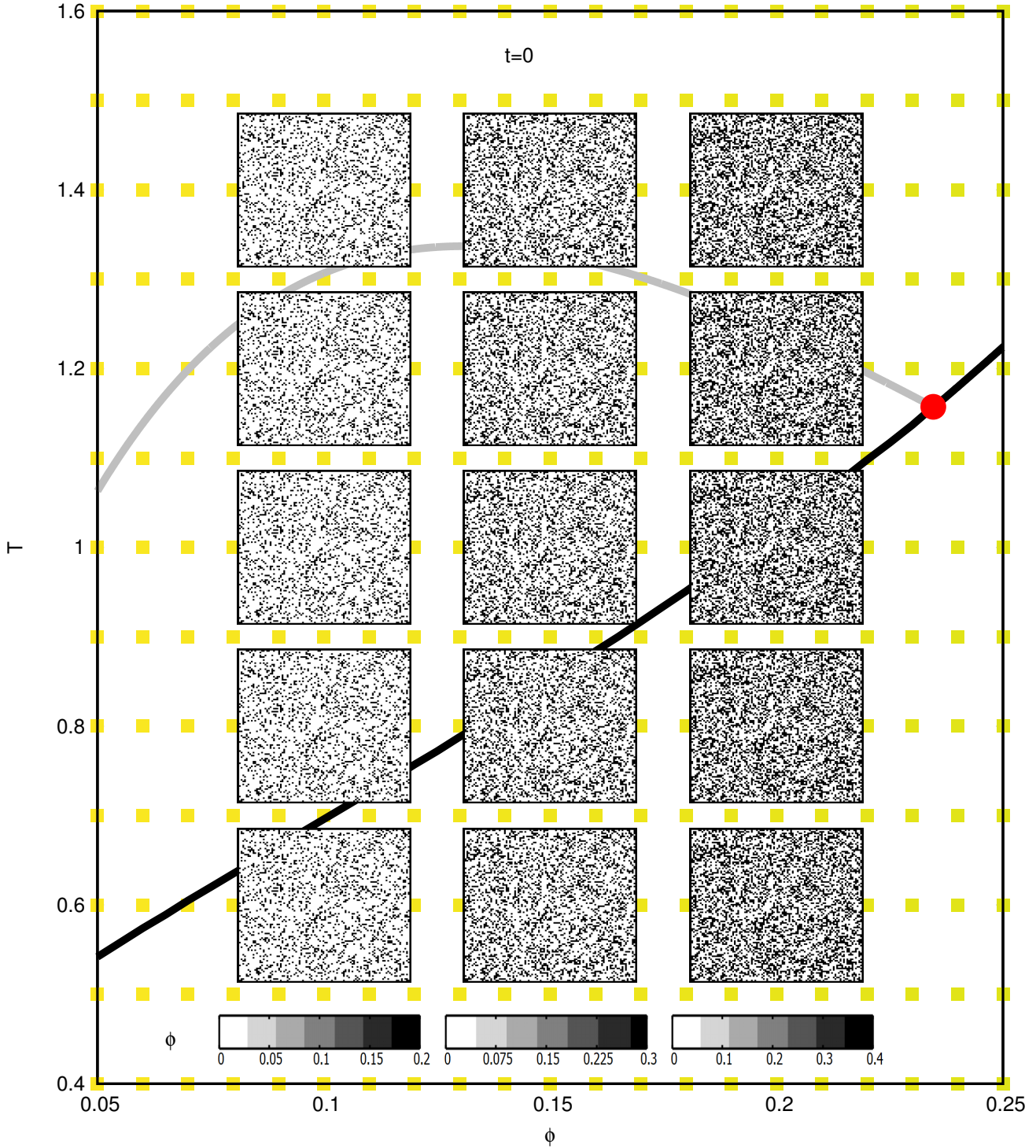


Figure 6.2: Initial local density distributions for multiple quenching process from the HS limit ($T_i = \infty$) at the isochores $\phi = 0.10, 0.15$ and 0.20 , for whose final temperatures are $T_f = 0.60, 0.80, 1.00, 1.20$ and 1.40 . Each fluctuation is centered in its corresponding state, while the employed grayscale for each isochore is at the bottom. The presented curves along the diagram correspond to the curves of the *non-equilibrium glass transition diagram* presented in 3 (see Fig. 3.5). In addition, the mobility of the states is presented in the same format and scale as in Fig. 5.2.

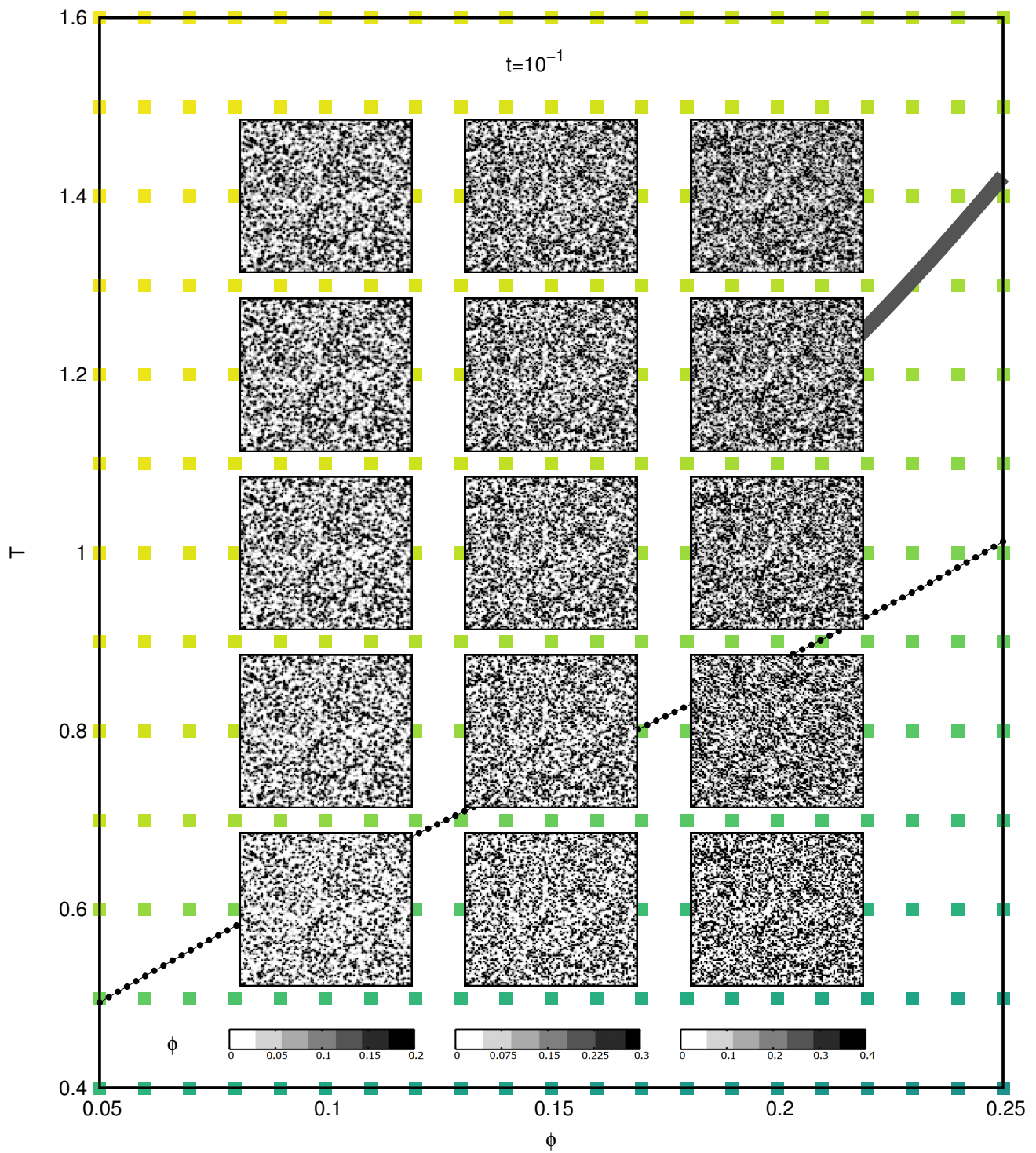


Figure 6.3: Evolution of the local density distribution for $t = 10^{-1}$ for the same states as 6.2. The time-dependent phase diagram for the same time is shown as a background with the same notation as 5.2.

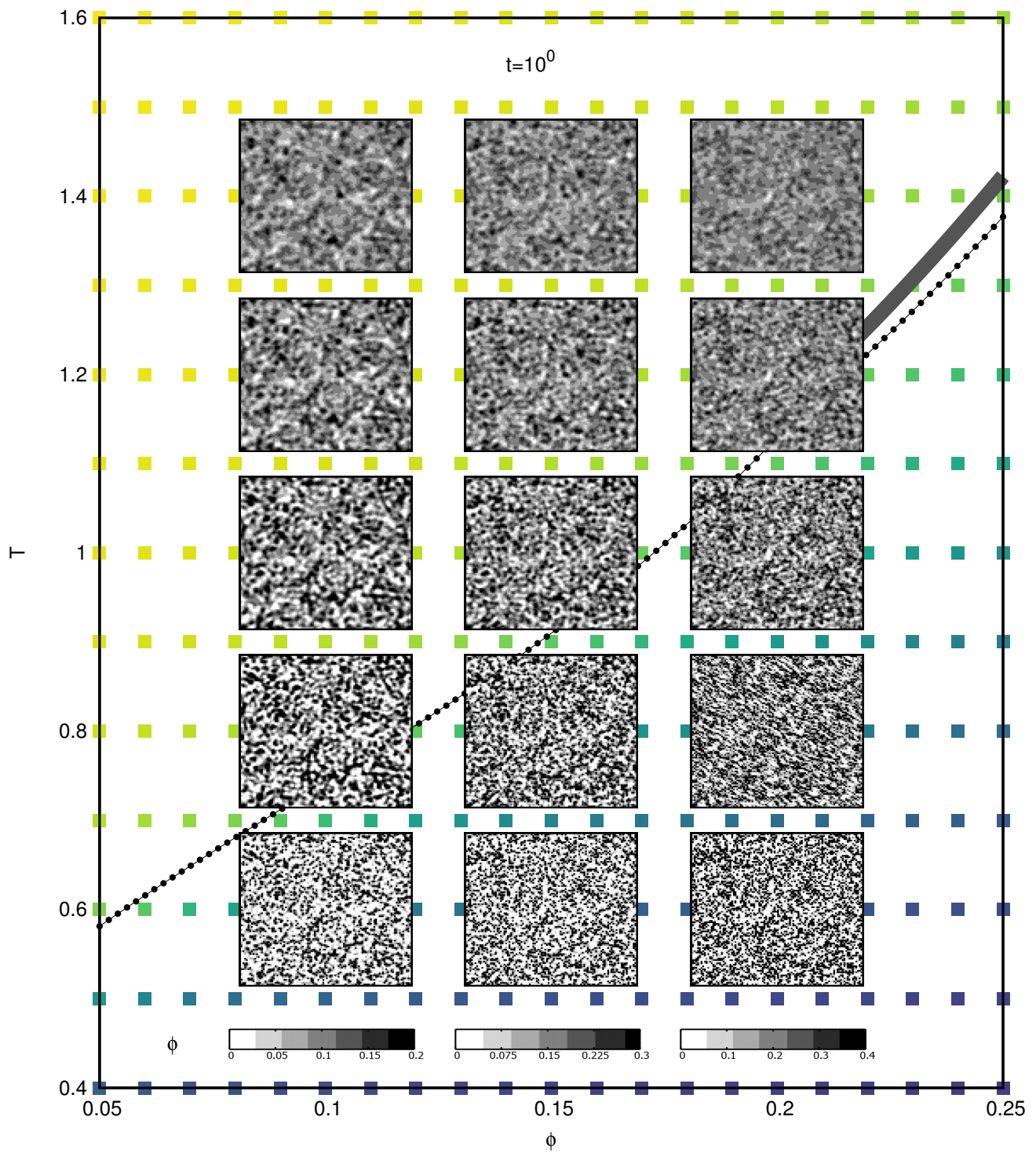


Figure 6.4: Evolution of the local density distribution for $t = 10^0$ for the same states as 6.2. The time-dependent phase diagram for the same time is shown as a background with the same notation as 5.2.

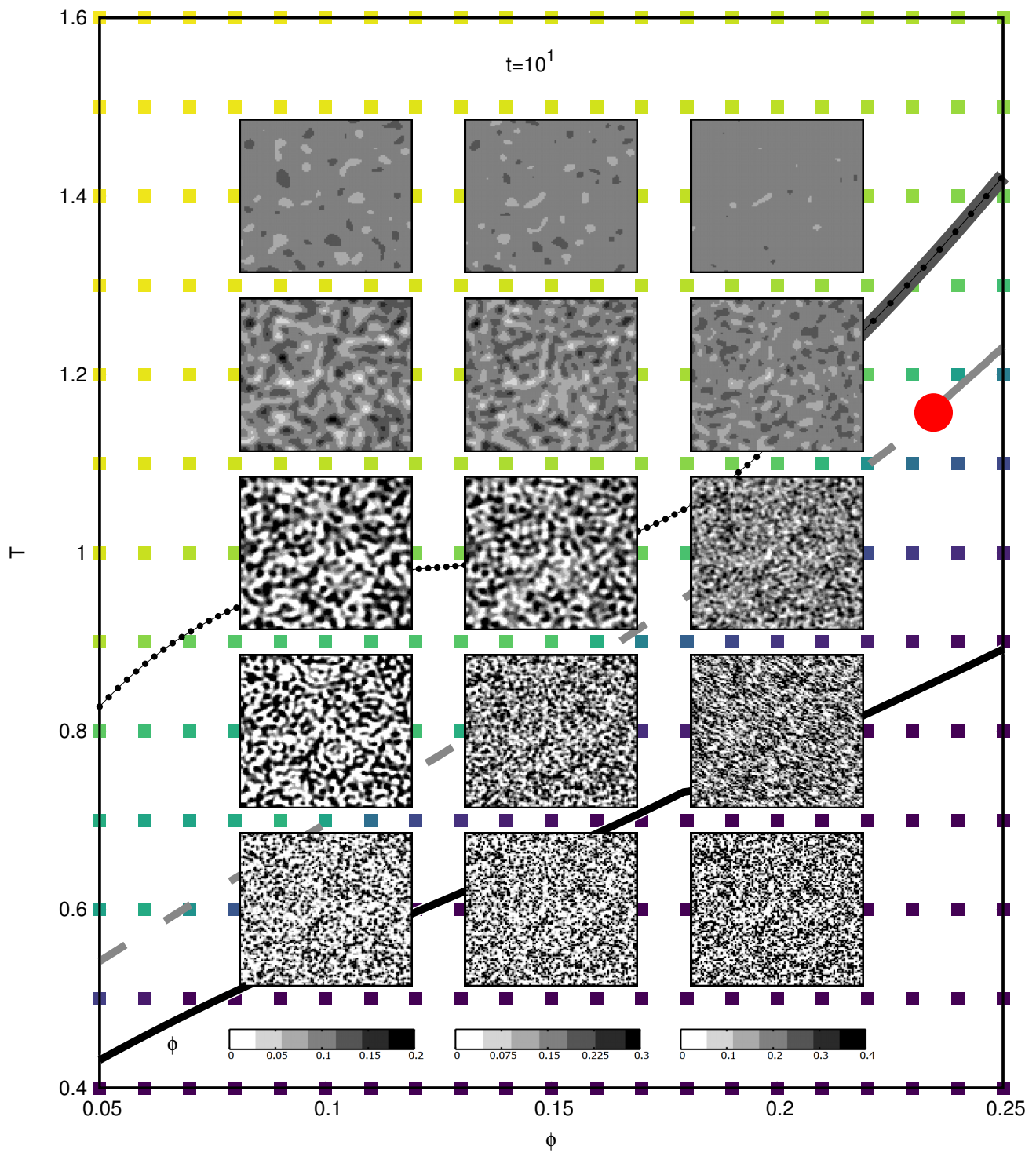


Figure 6.5: Evolution of the local density distribution for $t = 10^1$ for the same states as 6.2. The time-dependent phase diagram for the same time is shown as a background with the same notation as 5.2.

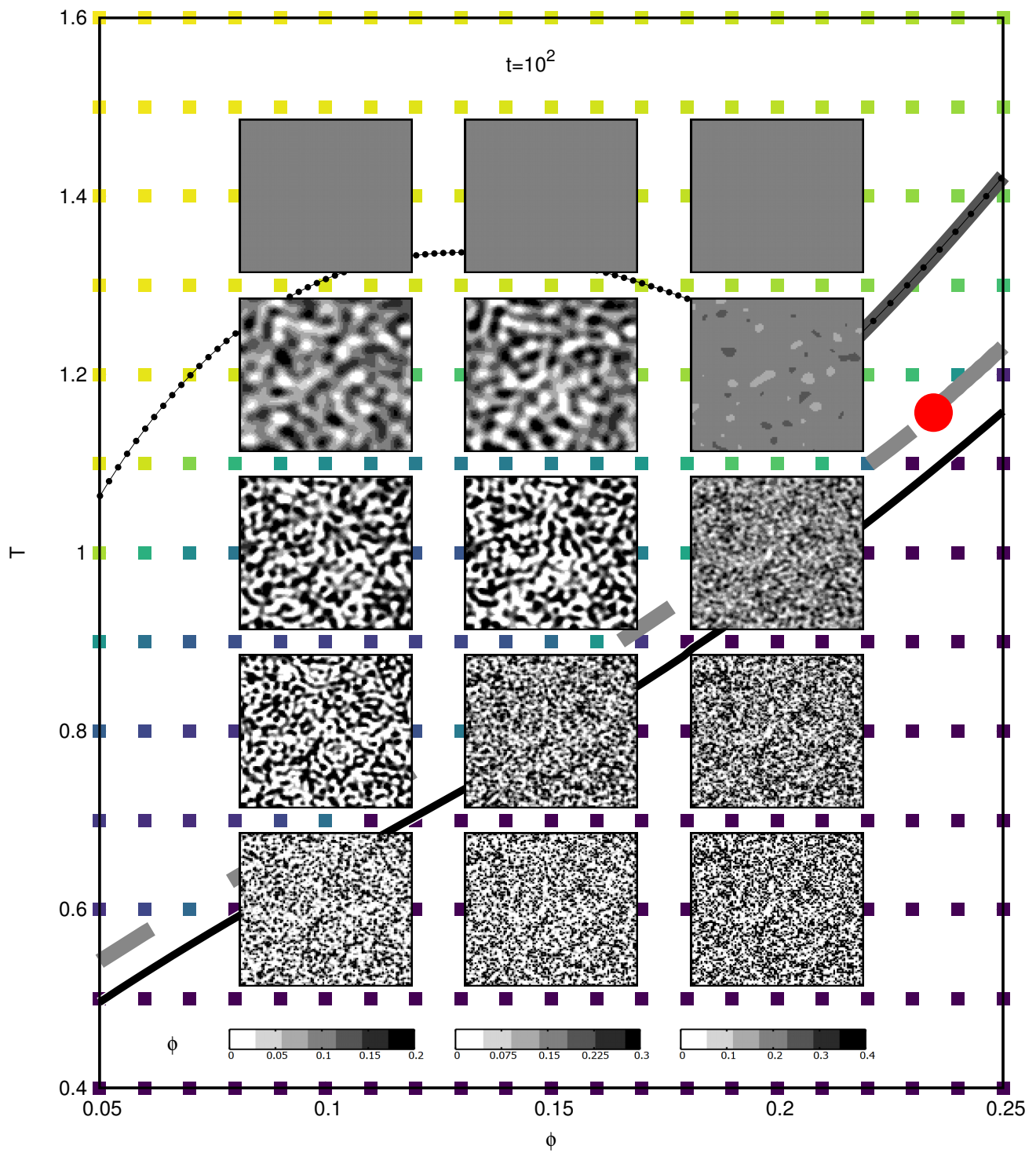


Figure 6.6: Evolution of the local density distribution for $t = 10^2$ for the same states as 6.2. The time-dependent phase diagram for the same time is shown as a background with the same notation as 5.2.

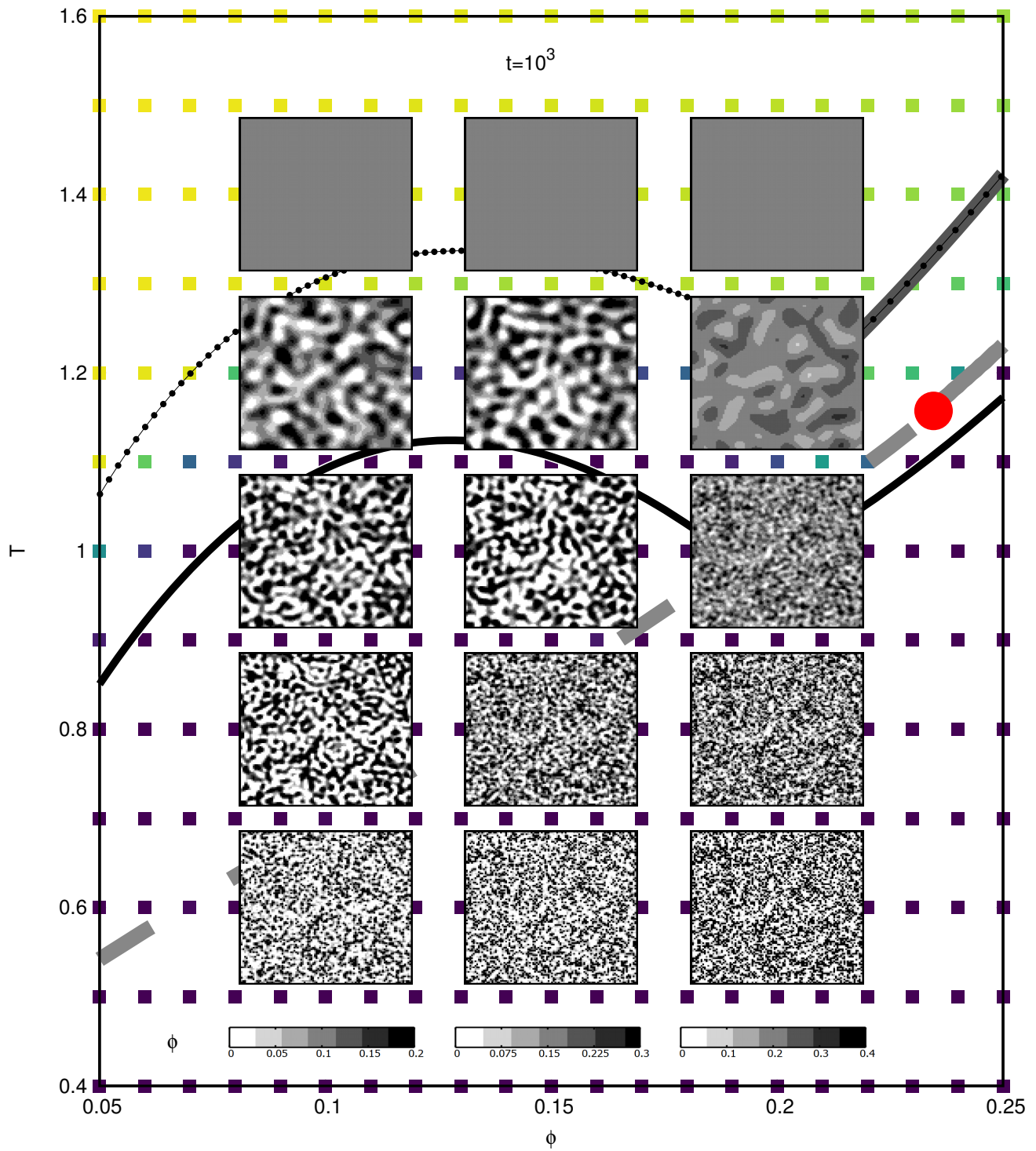


Figure 6.7: Evolution of the local density distribution for $t = 10^3$ for the same states as 6.2. The time-dependent phase diagram for the same time is shown as a background with the same notation as 5.2.

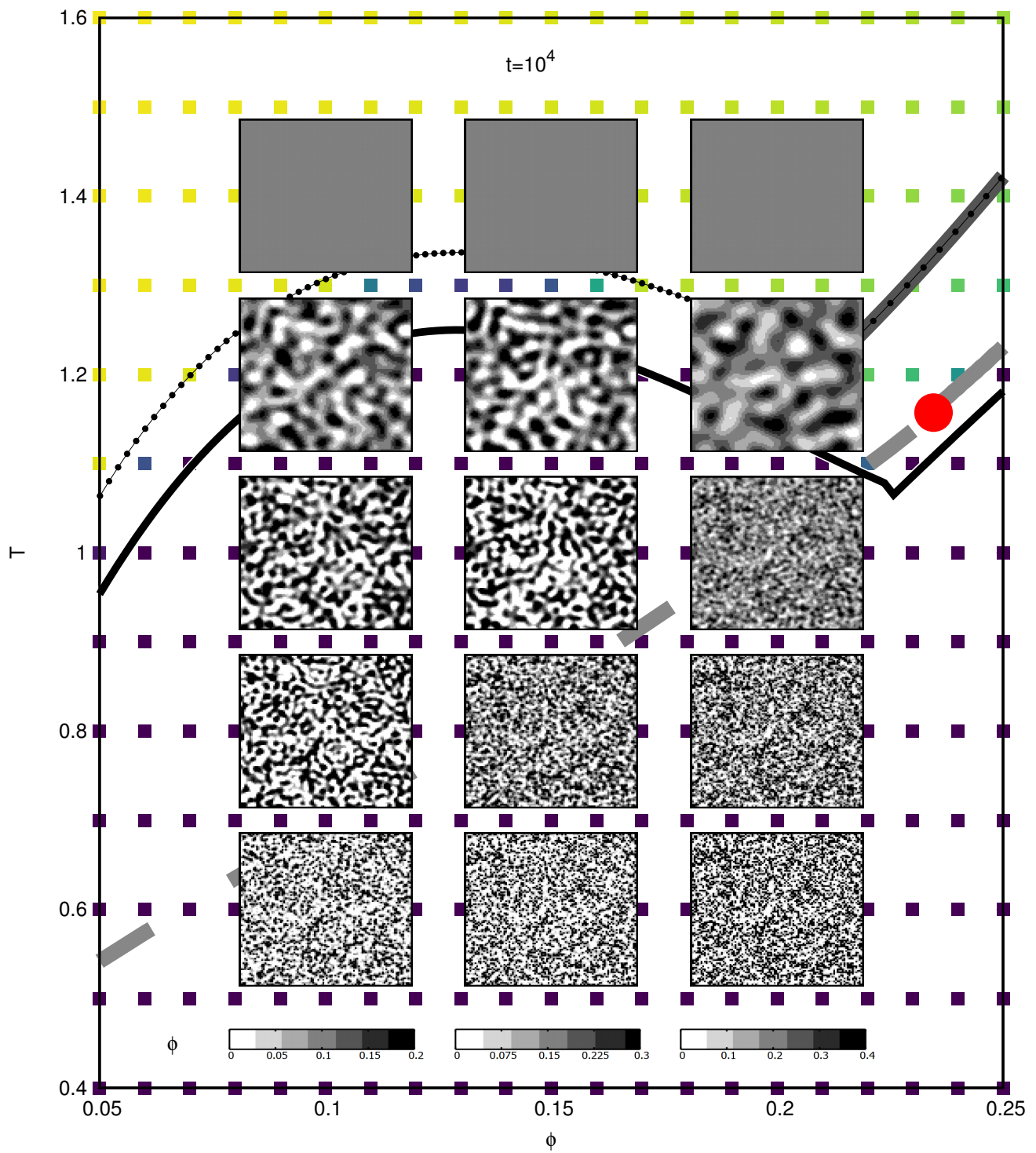


Figure 6.8: Evolution of the local density distribution for $t = 10^4$ for the same states as 6.2. The time-dependent phase diagram for the same time is shown as a background with the same notation as 5.2.

employed in order to translate the number density in terms of the volume fraction to a probability of finding a particle in a given region.

Recall that, in the concrete example under consideration, the total volume is conformed by cubes of size σ which, at most, can contain one particle inside. When a particle is fully contained, it yields a volume fraction of $\phi = \pi\sigma^3/6$ for the respective cube. In terms of the aforementioned occupation probability, this translates into a probability of 1 of finding a particle inside the region. Thus, the simple linear approximation $p_i(t) = 6\phi_i(t)/\pi$ for the i -th cube, can be proposed in order to obtain the probability in terms of the predicted density. Hence, the evolution of the mean density towards its equilibrium bulk value is described as an homogenization process of such (occupancy) probability distribution over the whole space, explicitly represented by the uniform gray scale obtained for $n(\mathbf{r}; t \approx 10^2)$ in all the space. Thus, for $t \geq 10^2$, the probability of finding a particle in certain space region is the same and independent of the initial condition. In summary, this interpretation allow us to think in the theoretical results simply as the spatial localization of low and high probable density regions.

Let us now describe the features of the process of gelation in terms of the spatial resolution provided by the fluctuations in the mean local density. According to Fig. 3.5 (or, equivalently, Fig. 6.2), these process are expected for quenches with final temperatures $T_f = 1.2$ and slightly below. For these processes, essentially three distinct regimes are observed in the evolution of the mean local density. These are a pseudo-equilibration regime, phase separation and aging. The pseudo-equilibration regime is characterized by a transient overall homogenization (of a gray scale), which occurs in the early stage of the gelation processes. For the isochores $\phi = 0.1$ and $\phi = 0.15$, this occurs during a time scale of order $t = 10^1$, whilst for $\phi = 0.2$ this time scale becomes one order of magnitude larger. This is reminiscent of the proximity of each of the final states to the spindodal line which, according to the discussion of chapter 4, increases the latency effects.

On the other hand, the pseudo-equilibration regime ends with the development of the phase separation. This process takes place at some point near the end of the latency time. It is in this regime when large heterogeneous structures are clearly formed, resembling those obtained through spinodal decomposition processes. Nevertheless, those quick changes are found to practically stop almost as soon as they started. This occurs as the heterogeneity appears to freeze in time, which occurs once the inverse mobility increases as a power law, as discussed before in Sec 4.1 of chapter 4. Thus, when such apparent freeze in the mean density occurs, the system enters to the aging regime. In this last aging regime, the the mobility gradually decreases as it enters to a never ending relaxation towards ideal glass value $b = 0$. As this occurs in each of the dynamically arrested states, the isomobility line $b^{(a)} = 10^5$ (black solid line) evolves increasing the region of arrest, so the state points considered lie below such line and satisfy the empirically defined condition for dynamic arrest. Once this occurs, the heterogeneous density distribution are expected to become frozen.

The evolution of the morphology during vitrification is in stark contrast to the scenario observed for equilibration and gelation. In general, for this process the evolution of the initial distribution appears to be negligible, almost frozen since the beginning of the evolution. This is a consequence of the remarkably faster decrease in the mobility (whose inverse follows a power law of waiting time from the beginning). Thus, within the presented regime it would appear that the particles are only able to diffuse through a small neighboring region. Allow us to remark that this occurs for every fluctuation regardless of the neighbor mean density values as we have neglected possible fluctuations in the mobility.

Within the theoretical model, the local mobility of each mean density heterogeneity is approximated to be the same bulk mobility *i. e.*, $b(\mathbf{r}, t) = b(t)$. As a consequence, the aging effects are applied across the whole system irrespective of the evolution of the mean density in the sur-

rounding sub-volumes. In general, such approximation is thought to be appropriate, at least, for moderate densities, such as the ones presented in this work, where the interparticle distance could be considered small in terms of the particle sizes, *i.e.* $l < 2\sigma$. For these cases, the predicted asymptotic scenario reveals the final mean traveling distance of the particles to be roughly around 10% of the inter particle distance (see Fig. 3.6). Thus, the diffusion of the particles under the entirety of the process could be estimated to be near the mean particle distance. In return, the predicted morphology of the states undergoing a glass transition process could be understood simply as a first neighbor diffusive process.

Although this might be the first time that a first principles theory is employed for the description of the time-evolving morphology of a liquid during the formation of non-equilibrium states, the study of such evolution has been the subject of previous studies describing the morphology of a liquid during the formation of non-equilibrium states [48, 67, 68]. In this regard, the work of Testard *et. al.* [48] is of special interest to us due to the system similarities. In the referred work the authors studied the morphology of a Lennard-Jones binary mixture system with molecular dynamics for several quenches inside the spinodal region. The morphology description is then discussed in terms of a contracted description of the particle densities, which allows them to follow an iso-surface of the density set at $\bar{\rho} = 0.42$. The followed surface is set empirically as it allows them to distinguish between low and high density regions which they distinguish between gas and liquid phases.

In Fig. 6.9 some of Testard's general results[48] are presented across the system's thermodynamic phase space for the largest evolution time considered. The inset of the figure shows the thermodynamic region of interest, in which the analysis is made, where the spinodal, binodal and the glass transition lines are shown as a guide. In the main frame of this figure, the iso-surface of $\bar{\rho} = 0.42$ is shown for several states with two differently colored regions, namely a yellow region, which delimits the smaller density region, and a green region for the high density region. In these states, aging glass-like features are reported to occur and the spinodal decomposition process is predicted to be interrupted due to the change in the particles diffusive behavior. For such cases, a bi-continuous state dependent structure is found, where the dense-phase's size grows at higher temperatures and densities.

Similar to Testard's surfaces, our theoretical predictions can also be presented in order to distinguish a mean density cut. For example, by selecting a binary view on the color map density for a given threshold value, the boundary between white and black would be the surface projection within the observed slab. This procedure is done in Fig. 6.10, where the threshold value is set at $\phi_c = 0.15$ cut volume fraction, at a waiting time $t = 10^4$. From the theoretical predictions, the role of the temperature and density can be very well discern. In general, quenching to larger temperature and density values leads to the development of increasingly larger dense structures, which agrees qualitatively with the physical scenario that emerges from the results of Testard *et. al.*, despite some quantitative differences, such as the region in the (ϕ, T) where interrupted spinodal decomposition phenomena is expected to occur. Such differences may be attributed to the intrinsic differences of the two systems considered, having a slightly different interaction between particles.

Even though the comparison is qualitative, these results surely add another underlying feature of the arrested spinodal decomposition process that the NE-SCGLE theory is able to describe. The visual nature of the system's morphology allow us to complement the evolution of the other resulting theoretical properties. Thus, the visualization of the density fluctuations could be employed as a base for the generation of a better physical insight of non-equilibrium processes. On the other hand, it is precisely due to the generalities found within these processes across multiple

systems, what has allowed to establish a connection between the NE-SCGLE theory predictions of such simple theoretical model and more complex models, as well as with real life systems.

In the presented results, the practically defined arrest condition b^a sets a time scale in which aging behavior is expected to take place. In Figs. 6.2-6.8 these aging effects are manifested in the interrupted evolution for the density fluctuations, arising from the increasingly smaller value of $b(t)$ as t increases. A way to quantify such changes can be easily devised by predicting the asymptotic (waiting) time limit of the density fluctuations. Such fluctuations can actually be obtained through the simple evaluation of the propagator $w(u, k)$ at the material time u_a (see Eq. (6.7)). Such time corresponds to the asymptotic waiting time which has been employed to find the *non-equilibrium glass transition diagram* in chapter 2. Thus, in Fig. 6.11, these asymptotic solutions are presented within the *non-equilibrium glass transition diagram*.

Figure 6.11 assures that the density fluctuations subjected at the practical arrest condition $b(t) < b^a = 10^{-5}$, remains almost constant along the whole process. In addition, the asymptotic solutions can be employed to analyze the general characteristics and trends of the morphology along the system's thermodynamic parameters. This procedure allow us to momentarily forget about the time description, which would otherwise increase the amount of variables to take into account. For example, for states inside region II, as the final state of a quench approaches the spinodal line, the resulting arrested state appears more homogeneous, while the characteristic length of the local density heterogeneities increases. Thus, an statistical analysis of the mean density evolution of these asymptotic states could provide a quantifiable measurement of the observed morphology across the non-equilibrium states.

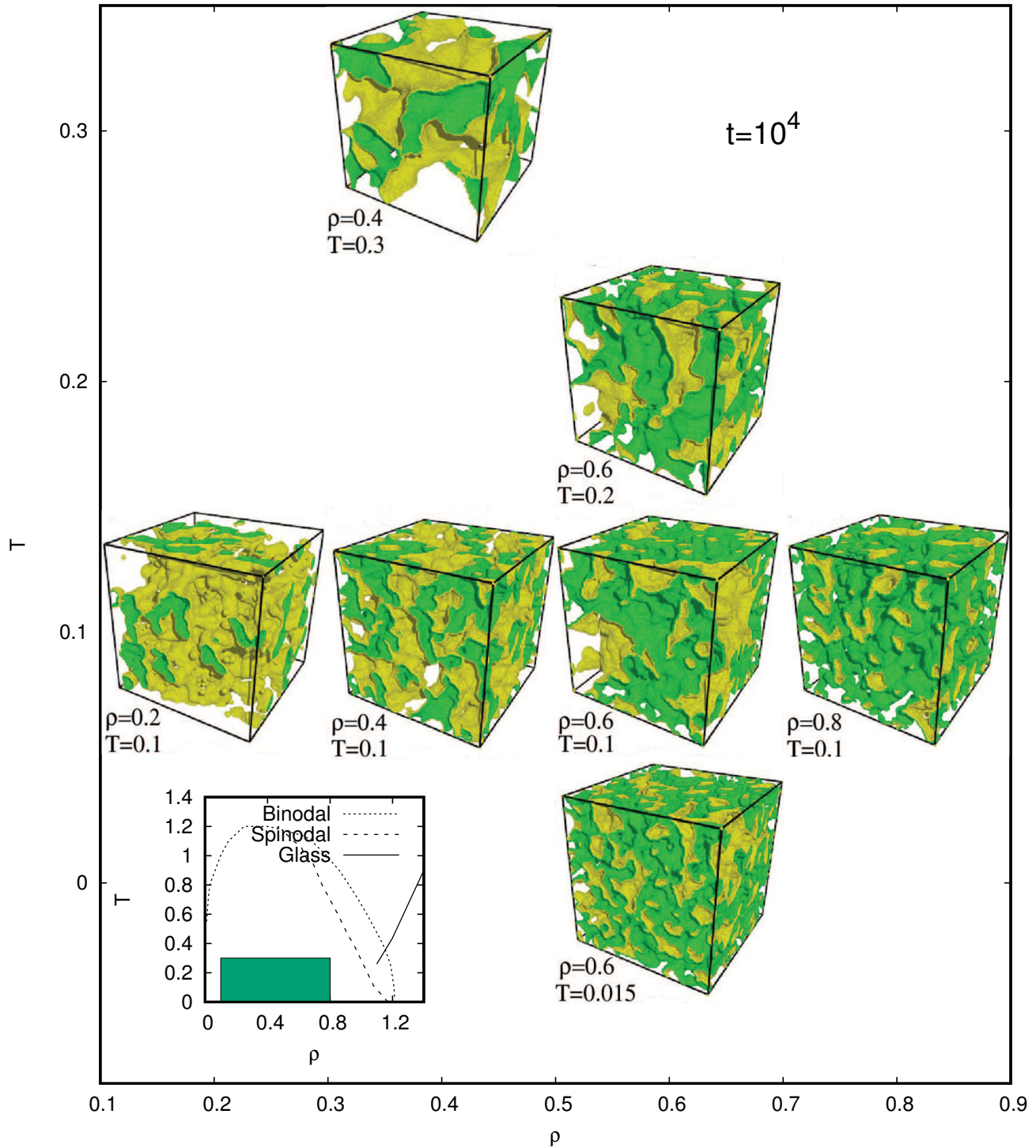


Figure 6.9: Number density iso-surface at the threshold value $\bar{\rho} = 0.42$ of a Lennard-Jones 80 : 20 (large and small species respectively) binary mixture. The iso-surfaces were obtained from molecular dynamics simulations undergoing quenches at different final states for $t^* = 10^4$ in units $\sqrt{m\sigma^2}/\epsilon$ where σ refers to the large particles diameter, ϵ to the large particles energy scale and m to the large particles mass. The phase diagram of the system is shown as an inset, where the localization of the final thermodynamic states are localized within the green region. The surfaces and the phase diagram data were obtained from ref. [48].

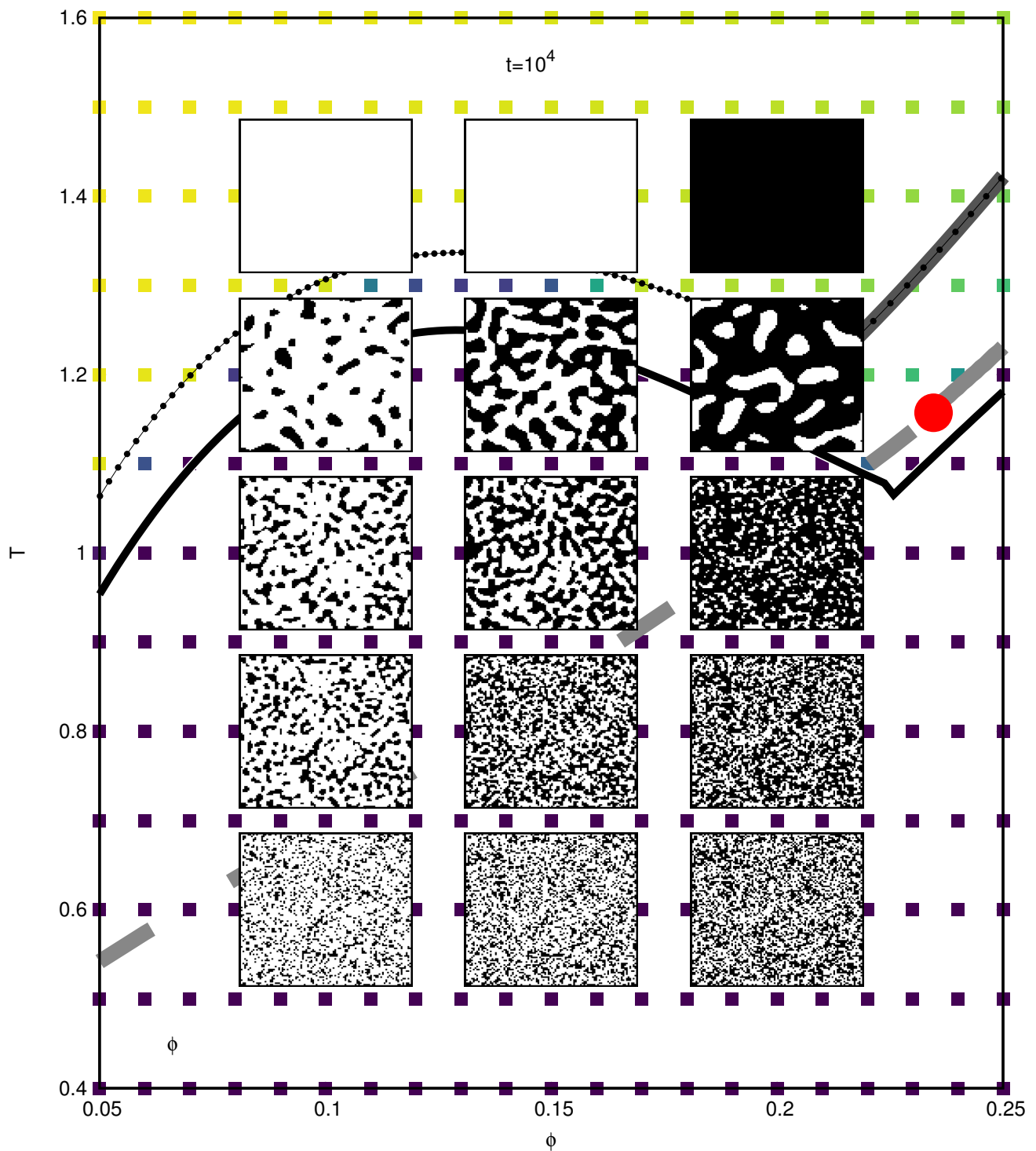


Figure 6.10: Evolution of the local density distribution for $t = 10^4$, equivalent to Fig. 6.8. For this case, the density color map has been selected to be in a binary state with densities either lower than the threshold $\phi = 0.15$ (white regions) or higher (black regions).

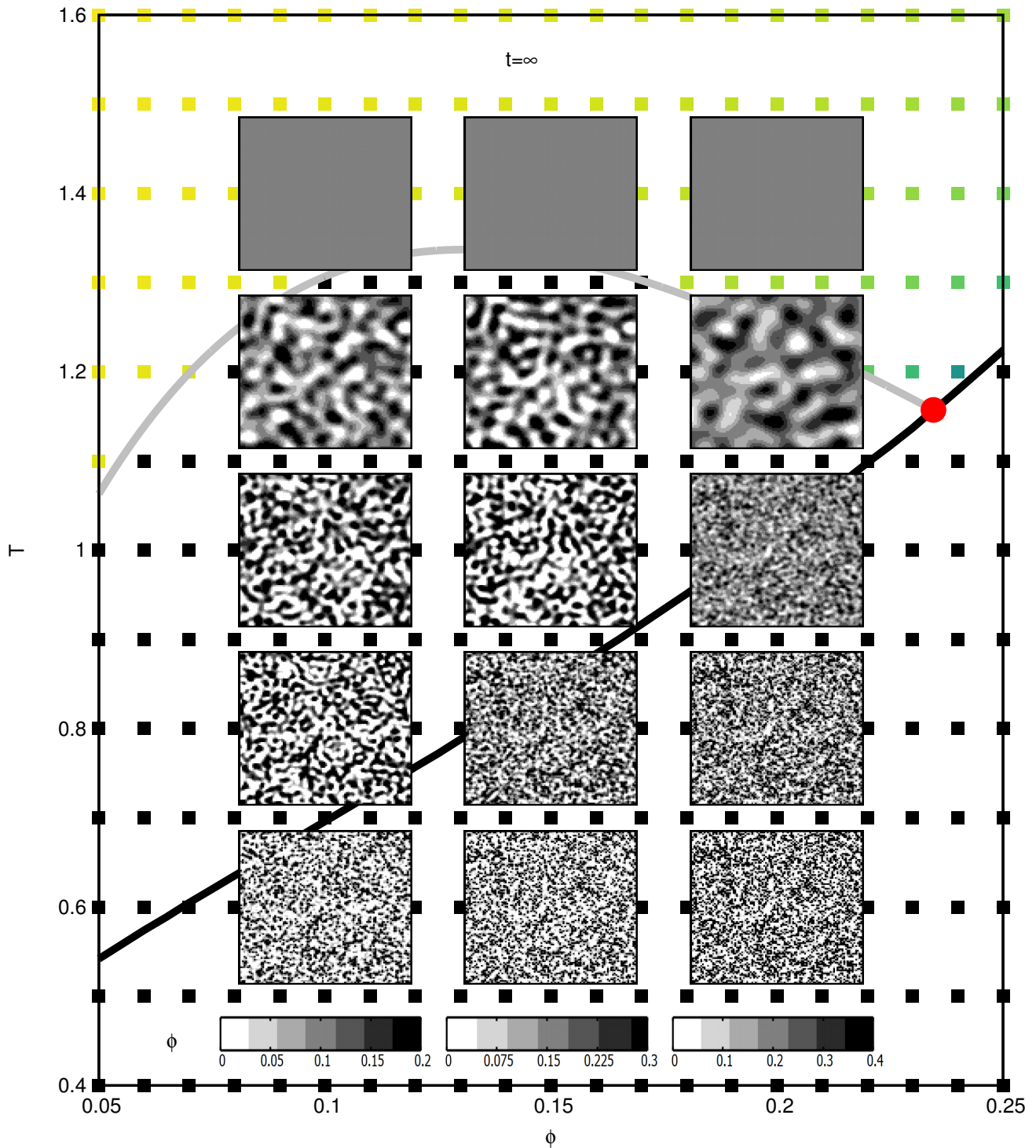


Figure 6.11: Asymptotic local density distributions for multiple quenching process from the HS limit ($T_i = \infty$) at the isochores $\phi = 0.10, 0.15$ and 0.20 to the final temperature $T_f = 0.60, 0.80, 1.00, 1.20$ and 1.40 for the isochores $\phi = 0.10, 0.15$ and 0.20 . Each fluctuation is centered in its corresponding state within the asymptotic non-equilibrium glass transition diagram and each isochore has its own color scale at the bottom.

In particular, we are interested in providing an statistical analysis capable of describing the

magnitude and spatial distribution of the local mean densities. For these purposes, the covariance of the local mean density can be employed. In particular, for the coarse-grained description, this quantity is defined as

$$\sigma_{nn'}(\mathbf{r}, \mathbf{r}', t, t') \equiv \langle \Delta n(\mathbf{r}, t) \Delta n(\mathbf{r}', t') \rangle, \quad (6.9)$$

in which $\Delta n(\mathbf{r}, t)$ indicates the density fluctuation of a subspace spatially located at \mathbf{r} at the waiting time t . Additionally, under the assumption of spatial homogeneity and isotropy, $\sigma_{nn'}(\mathbf{r}, \mathbf{r}', t, t') \equiv \sigma_{nn'}(|\mathbf{r} - \mathbf{r}'|, t, t')$, the definition allow us to compute an average in the covariance for different distances. The covariance just defined, in the limit $r = 0$ and $t = t'$, results in the square of the standard deviation of the densities distribution $\sigma_0(t)$, allowing us to statistically quantify the states distributions.

On the other hand, the density covariance, in its current form, is a rarely used property to describe the structure of a fluid. For this reason, we define a coarse-grained two time-dependent radial distribution function as

$$g_{nn'}(r, t, t') = \frac{\sigma_{nn'}(r, t, t') + \bar{n}^2}{\bar{n}^2} \quad \text{for } r > l, \quad (6.10)$$

whose significance is similar to that of the radial distribution function when considering $t = t'$. The main difference to the common interpretation of a liquid radial distribution function, is that it now refers to the probability of having a fluctuation at a distance r given that there exist an initial fluctuation at $r = 0$, in contrast with the typical definition involving a particle located at a distance r from a reference particle.

In figure 6.12, the results for these statistical properties and the propagator are shown. In this statistical analysis, the propagator (see Eq. (6.6)) is computed in order to provide an insight of how does the theory impact these quantities. In Fig. 6.12 a), we show the normalized standard deviation $\sigma_0(t = \infty; T_f) / \sigma_0(t = 0; T_i)$ for each of the three isochores across different final quenching temperatures. Full symbols are employed for the glass-like arrested states, while empty symbols are used to represent states inside the gel-like arrest region.

The standard deviation is a statistical parameter that allow us to quantify the dispersion of data. For the mean density displayed in Fig. 6.11 such dispersion can be directly correlated with the distribution contrast, where high and low density regions leads to a high contrast image, and an homogeneous systems to a low contrast image. Thus, the homogenization tendency as the final temperature of a quench increases is corroborated by this property. In particular, for every asymptotic equilibrium state a zero standard deviation is expected. As for the dynamical arrested states, with the exception of the near gel-glass transition states, the general trend for the standard deviation is to decay as the final temperature becomes larger. Such tendency is found for the whole gel region, where the standard deviation reaches the zero equilibrium value as the final state becomes closer to the spinodal, as well as for most of the glass transition states. On the other hand, at the gel-glass transition, the standard deviation is predicted to have a sudden change in its behavior, reminiscent of the γ discontinuity which occurs upon such transition.

In Fig. 6.12 b) the same time correlation function $g(r, t = t' = \infty)$ is shown for selected quenches. Particularly, in order to follow the temperature behavior, the quenches at $\phi = 0.10$ for $T_f = 0.60$ (purple solid line), 0.80 (blue solid line), 1.00 (green solid line) and 1.20 (yellow solid line) where selected. Similarly to follow the density behavior, the quenches at $\phi = 0.15$ (blue dashed line) and 0.20 (purple dashed line) for $T_f = 1.00$ where chosen. In these plots, correlations above 1 indicate a positive correlation, where the surrounding densities are expected to be similar, or at least to have the same sign. Conversely, correlations below 1 indicate negative correlations.

Then, in terms of $g(r, t = t' = \infty)$, the heterogeneities sizes are directly correlated to the distance of this property first minimum, as it indicates the most probable distance to find a negatively correlated density.

Hence, Fig. 6.12 b), allow us to follow the long-distance correlation of the gel-like states (non-purple color lines) as well as the short-distance correlations formed by the glass-like states (purple color lines). Within these results, the correlation function captures a systematic increase in the first minimum distance as the temperature becomes larger and the density decreases. Although the density behavior might appear counter intuitive at first glance due to the previous analysis, let us remind that the heterogeneity sizes captured by this property are fixed, and relative to the mean bulk density of the system, which is in contrast to the threshold set in the previous discussion. Additionally, for the selected final temperature, the increase in the density results in a state closer to the glass transition line. Thus, the heterogeneity sizes are found to be dependent on the proximity of each state to the spinodal and glass transition lines. In particular, for near to spinodal states bigger heterogeneity sizes are found.

These theoretical predictions derive from the propagator influence over the initial distribution. As a matter of fact, the simple analysis of the propagator Eq. 6.6 reveals that *for any finite u time, the mean of the density distribution must remain constant* due to the limit $\lim_{k \rightarrow 0} w(k, u) = 1$. Hence, a way to understand the nature of these predictions is to follow the behavior of the propagator, which it is done in Fig. 6.12 c) for the same states of Fig. 6.12 b). From the propagator expression, under equilibrium normal circumstances, an exponential decay is expected. Such behavior is the result of having a negative defined exponent, as $1/\bar{n}\varepsilon$ and the mobility b are positive (non-zero) defined for equilibrium states. On the other hand, for states inside the spinodal region, an expected divergence in $1/\bar{n}\varepsilon$ occurs, which leads to the exponential to become positive for large wave lengths [25]. It is precisely due to the appearance of such growth at large wave lengths the reason behind a much richer morphology.

Figure 6.12 serves the purpose of establishing patterns across the thermodynamic phase space for the predicted asymptotic states. From this figure, a clear difference can be observed from gel and glass states. For gel states, a large wave length peak in $w[k, u^a]$ is formed, while having a quick decay at smaller wave lengths. In comparison, for glass states, the large wave vector growth in $w[k, u^a]$ is found to be rather insignificant and a much more slow decay for smaller wave lengths is predicted. In this property, it is its decay towards zero what yields to the homogenization in an equilibrium state. In return, it is the interplay between the relaxation and growth of different wave lengths what causes the morphology of gel states, where a clear tendency towards larger wave lengths and a smaller peak width is observed for states closer to the spinodal. In this regard, the growth of the heterogeneity sizes can be explained as the peak as the shift of the main peak towards larger k values, while the overall behavior of the standard deviation is a result of the peak width becoming smaller, thus allowing more wave lengths to relax. On the other hand, for glassy states, the slow decay of most wavelenghts, even as small as the particle size for states deeper within the transition, produces the small observed variations from that of the initial state.

The theory propagator reveals that the morphology of the asymptotic states is given by the relevant arrested wave-length modes in the processes. For gel-like states, these wave-length modes are large, located near the maximum of the propagator, and leads to an increase in the magnitude of the associated local densities. For the glass transition, the relevant wave-length modes also include the comparables to inter-particles distances. On the other hand, and in stark contrast to the arrested states, for equilibrium states the propagator is expected to relax to zero for any finite wave-length.

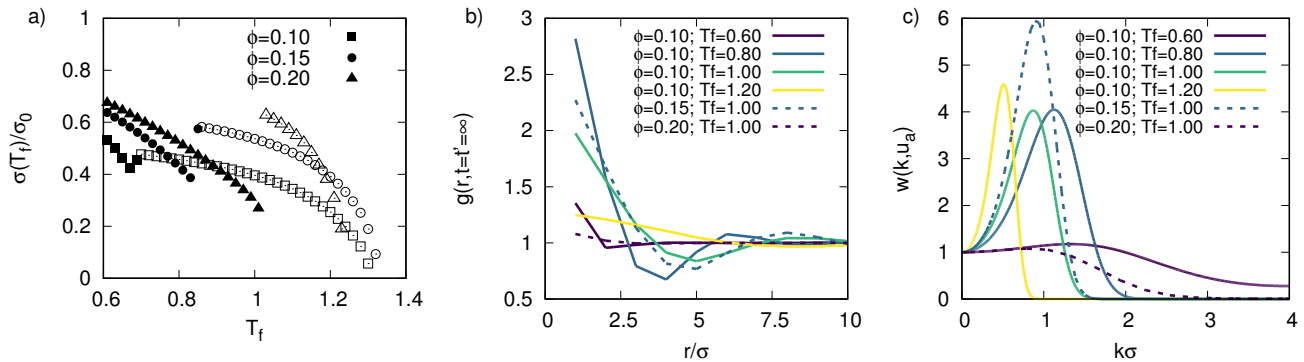


Figure 6.12: Density distribution properties for the asymptotic evolution at different final temperatures. a) Asymptotic standard deviation σ_n vs final quenching temperature for the isochores $\phi = 0.10, 0.15$ and 0.20 . b) Same time correlation $g(r, t = t')$ vs distance for several final states. c) Asymptotic propagator for several final states.

6.4 Summary

In this chapter we have extended the NE-SCGLE theory in order to describe the evolution of the mean local density. This was done through a linear approximation in the generalized Fick's law. Additionally, and in order to apply the NE-SCGLE evolution description, we have devised a simple proposal for the determination of the initial mean density fluctuation. The predicted results were analyzed and discussed in the context of the *waiting-time dependent non-equilibrium phase diagrams*, where different morphologies are predicted depending on the specific features of the quench process. In particular, large heterogeneous structures are expected for states inside the gel-like region. For such states, the size of the heterogeneities is found to increase the closer the final state is to the spinodal, while the magnitude of their fluctuations is expected to decrease (involving more homogenous structures). For states inside the glass region, the slow dynamics lead to an apparent lack of evolution of the property, hence, morphologies similar to the initial ones are found. The just described tendencies of both gel- and glass-like arrested states, qualitatively agrees with simulation data[48].

Additionally, we have analyzed the asymptotic solutions of the theory, obtained in the limit $t \rightarrow \infty$. This allowed us to corroborate the near end state predictions done along the evolution of the mean density. On the other hand, such asymptotic limit allow us to establish overall behaviors in terms of the thermodynamic variables of the system. Such behaviors are then quantified through an statistical analysis which corroborates the previous simple observations. Specifically, this is done through the standard deviation and $g(r, t, t')$ correlation function. Finally, the theoretical results provided by this analysis are explained in terms of the propagator, allowing us to obtain a better physical insight of our theoretical model.

Chapter 7

Conclusions

In this work we have achieved each and every of the previously set objectives stated in the introduction. In this regard, the NE-SCGLE theoretical framework has proven to be a sound theoretical approach capable of describing several nuances of the dynamic and structural behaviors of the arrested spinodal decomposition processes. Allow us now to conclude with this chapter by simply stating the most relevant results, and highlight the most relevant contributions.

In this sense, we shall only mention briefly the first three chapters, as they summarize the state of the art previous to the current original contributions. Particularly, chapter one served to state the general context of this work, while chapter two reviews the NE-SCGLE theoretical framework. In chapter three, the concepts of *thermodynamic equilibrium phase diagram*, *glass transition diagram* and *non-equilibrium glass transition diagram* were introduced and exemplified for the HSSW fluid. In these diagrams, the phase of a material is stated in terms of its thermodynamic state, where gel-like and glass-like arrested states are found inside the thermodynamical instability region, enclosed by the spinodal line.

From chapter four onward, original contributions are discussed. Particularly, within the fourth chapter, the dynamics evolution across the arrested phases in the *non-equilibrium glass transition diagram* is discussed. In such evolution, latency effects were observed in the evolution of the mobility for gel-like arrested states. These effects were found to increase as the states were closer to the spinodal line and disappeared for glass-like arrested states. In addition, a double-step relaxation was found for inside gel region states when approaching the glass transition. These theoretical predictions were found to agree with experimental observation of same or similar quantities. Hence, in this chapter the second aim of the present work is accomplished.

In chapter five, we accomplished the main aim of the present dissertation through the development of a *waiting-time dependent non-equilibrium glass transition diagram*. In stark contrast to the discussed diagrams of chapter three, this diagram introduces the waiting time t as a variable in the description of the phase transformation. This is done by the proposal of the practical mobility threshold $b^{(a)} = 10^{-5}$, which is followed along time for several quenching processes. The variable dependence of the process makes for a richer phase space, being some planes being commonly represented for certain applications. In addition, the theoretical predictions, are found to have qualitative similarities to diagrams obtained by experiments for systems exhibiting similar phenomena.

The similarities found across such different systems serve as a cornerstone to explore and study systems with more complex interactions. Although not as developed as for the current mono component repulsive plus attractive spherical interacting system, extensions to the NE-SCGLE formalism in order to describe mixtures, non-spherical interactions as well as atomic systems.

Hence, such advances allows for the theory development towards more real gel and glass forming systems to be a nearby possibility.

Lastly, in chapter six we provided a theoretical description for the morphology evolution, thus attending the last aim set at the introduction. Such description is based on a linear approximation to the general Fick's law contained within the NE-SCGLE framework, whose major result is summarized by the evolution equation for mean density $\bar{n}(\mathbf{r}, t)$ (see Eq. (6.7)). From this quantity we were able to describe both, equilibration and dynamical arrested processes morphology. In these last processes, stark differences are found depending on the expected final state. For states inside the gel-like arrested region, large density heterogeneities are found, with sizes increasing when approaching the spinodal line. On the other hand, for states inside the glass-like arrested region, the evolution of the density is predicted to be frozen at very early stage of the process. In return, this leads to a very similar morphology to that of the initial state. These theoretical predictions are then compared with simulation data, for which a qualitative agreement is met. In addition, an statistically analysis over the mean density corroborated the otherwise simple observations, and allowed us to quantify the predicted morphology tendencies. In this regard, the visual representation of the evolution towards dynamical arrested states proved to be a valuable and powerful tool for the description and physical interpretation of the phenomenology.

As a conclusion, the NE-SCGLE theory has proven to be a formalism capable of describing the evolution of non-equilibrium states such as gel and glasses. The analysis and interpretation of such description has allowed us to propose ways to tackle real life issues, be it through the *waiting-time dependent non-equilibrium diagrams* proposal or the prediction of morphology changes of non-equilibrium processes. Thus, the development and application of the NE-SCGLE formalism can be said to be a fruitful endeavor for the understanding of non-equilibrium phenomena, and this work is but a step in the long road ahead to reach Anderson's goal.

Appendices

Appendix A

Solution algorithm for the SCGLE equations

In general, the solution of the SCGLE coupled set of equations (Eqs. (2.32)-(2.37)) is a highly involving mathematical problem. In this sense, a numerical algorithm that allow us to solve for a similar set of equations have been previously proposed within the framework of MCT theory [69, 70]. The concrete task of such numerical algorithm is to find a solution for the dynamical properties at new correlation times by the discretization of the coupled equations where previous values of these quantities are taken into account. Thus, in this appendix, we shall now discuss such algorithm in the framework of the SCGLE coupled equations, which can be broken down into three major approximations for distinct $\tau^* \equiv \tau\sigma^2/D_0$ correlation time regimes: a short, medium and large time regimes.

Allow us to recall the SCGLE theory set of coupled equations for *homogeneous isotropic and monocomponent* systems, which we rewrite in this appendix for convenience reading

$$\Delta\zeta^*(\tau) = \frac{D_0}{24\pi^3\bar{n}} \int_V k^2 \left[\frac{S(k) - 1}{S(k)} \right]^2 F(k, \tau) F_s(k, \tau) d\mathbf{k}, \quad (\text{A.1})$$

$$\hat{F}(k, z) = \frac{S(k)}{z + \frac{k^2 D_0 S^{-1}(k)}{1 + \lambda(k) \hat{\Delta}\zeta^*(z)}}, \quad (\text{A.2})$$

$$\hat{F}_s(k, z) = \frac{1}{z + \frac{k^2 D_0}{1 + \lambda(k) \hat{\Delta}\zeta^*(z)}}, \quad (\text{A.3})$$

where the hat symbol in \hat{F} , \hat{F}_s and $\hat{\Delta}\zeta^*$ indicates the Laplace transform in the time correlation variable. In these equations, the task ahead requires for the set of properties $\{\Delta\zeta^*(\tau); F(k, \tau); F_s(k, \tau)\}$ to be a solution for any given τ . Thus, let us first rewrite Eqs. A.2 and A.3 in order to easily recognize the inverse Laplace transform (ILT) of these equations by multiplying each of these for their respective right side common denominator, hence leading to

$$\left\{ z \left[1 + \lambda(k) \hat{\Delta}\zeta^*(z) \right] + k^2 D_0 S^{-1}(k) \right\} \hat{F}(k, z) = S(k) \left[1 + \lambda(k) \hat{\Delta}\zeta^*(z) \right], \quad (\text{A.4})$$

$$\left\{ z \left[1 + \lambda(k) \hat{\Delta}\zeta^*(z) \right] + k^2 D_0 \right\} \hat{F}_s(k, z) = 1 + \lambda(k) \hat{\Delta}\zeta^*(z). \quad (\text{A.5})$$

These last two expressions allow us to directly employ the derivative relation and convolution the-

orem for the ILT of a function $F(\tau) = \mathcal{L}^{-1}\{\hat{F}(z)\}$, which respectively read as

$$\mathcal{L} \left\{ \frac{dF(\tau)}{d\tau} \right\} = z\hat{F}(z) - F(0), \quad (\text{A.6})$$

$$\mathcal{L} \left\{ \int_0^\tau F(\tau')G(\tau - \tau')d\tau' \right\} = \hat{F}(z)\hat{G}(z), \quad (\text{A.7})$$

and where the former one for the case of a convolution can be employed by taking into account Leibniz integral rule

$$\frac{d}{d\tau} \int_{a(\tau)}^{b(\tau)} f(\tau, \tau')d\tau' = f(\tau, b(\tau))\frac{db(\tau)}{d\tau} - f(\tau, a(\tau))\frac{da(\tau)}{d\tau} + \int_{a(\tau)}^{b(\tau)} \frac{f(\tau, \tau')}{d\tau}d\tau' \quad (\text{A.8})$$

which leads to

$$\mathcal{L} \left\{ \frac{d}{d\tau} \int_0^\tau F(\tau')G(\tau - \tau')d\tau' \right\} = z\hat{F}(z)\hat{G}(z). \quad (\text{A.9})$$

Hence, using above results in the ILT of Eqs. (A.4) and (A.5) we may write

$$\frac{dF(\tau)}{d\tau} = \lambda\Delta\zeta^*(\tau)S - k^2D_0S^{-1}F(\tau) - \lambda\frac{d}{d\tau} \int_0^\tau \Delta\zeta^*(\tau - \tau')F(\tau')d\tau', \quad (\text{A.10})$$

$$\frac{dF_s(\tau)}{d\tau} = \lambda\Delta\zeta^*(\tau) - k^2D_0F_s(\tau) - \lambda\frac{d}{d\tau} \int_0^\tau \Delta\zeta^*(\tau - \tau')F_s(\tau')d\tau', \quad (\text{A.11})$$

where we have omitted the wave-vector dependence of $F(k, \tau)$, $F_s(k, \tau)$, $\lambda(k)$ and $S(k)$ for clarity reasons, and where we have employed the fact that $F(\tau = 0) = S$ and $F_s(\tau = 0) = 1$. In these last two expressions, Leibniz integral rule can be applied in order to obtain

$$\frac{dF(\tau)}{d\tau} = \lambda [\Delta\zeta^*(\tau)S - \Delta\zeta^*(0)F(\tau)] - k^2D_0S^{-1}F(\tau) - \lambda \int_0^\tau \frac{d\Delta\zeta^*(\tau - \tau')}{d\tau} F(\tau')d\tau', \quad (\text{A.12})$$

$$\frac{dF_s(\tau)}{d\tau} = \lambda [\Delta\zeta^*(\tau) - \Delta\zeta^*(0)F_s(\tau)] - k^2D_0F_s(\tau) - \lambda \int_0^\tau \frac{d\Delta\zeta^*(\tau - \tau')}{d\tau} F_s(\tau')d\tau', \quad (\text{A.13})$$

which allow us to easily consider the short time limit of both equations, in which the convolutions and the difference in the square braces can be neglected, *i.e.*, $\Delta\zeta^*(\tau) \approx cte.$ and $\Delta\zeta^*(\tau)S \approx \Delta\zeta^*(0)F(\tau)$, leading to

$$\frac{dF(\tau)}{d\tau} \approx -k^2D_0S^{-1}F(\tau), \quad (\text{A.14})$$

$$\frac{dF_s(\tau)}{d\tau} \approx -k^2D_0F_s(\tau), \quad (\text{A.15})$$

These last two expressions have analytical solutions, namely

$$F(k, \tau) = S(k) \exp [-k^2D_0\tau S^{-1}(k)], \quad (\text{A.16})$$

$$F_s(k, \tau) = \exp [-k^2D_0\tau], \quad (\text{A.17})$$

that can be straightforwardly computed for any $S(k)$ proposal, which in return enables the computation of $\Delta\zeta^*(\tau)$ with Eq. (A.1). Hence, expressions (A.16) and (A.17) conforms the solution employed in the short time regime of the numerical computation, for which the only constrain is

for $k^2 D_0 \tau \ll 1$. In this sense, although there is not any real upper limit, for the current work we employ the short time approximation for correlation times $\tau^* \leq 10^{-6}$, which allows for a significant wave-vector domain.

In what follows, we shall devise a numerical approximation that allow us to compute the full solution the coupled set of equations for any given correlation time, namely Eqs. (A.1), (A.12) and (A.13). This is done through the implementation of local approximations to the functions in order to be able to compute the differential and integral operators. In particular, we will consider a grid of the independent variables k and τ for the functions to solve.

For the wave-vector grid we consider the domain $k/\sigma \in [0 : 40.96]$. In such domain, we approximate the functions integrals with two Clenshaw-Curtis quadrature[71], one for the sub-domain $k/\sigma \in [0 : 4.096]$, and another for $k/\sigma \in [4.096 : 40.96]$, in which $N = 512$ nodes (points) are considered. For the correlation time grid, we start by considering the domain $\tau D_0/\sigma^2 \in [1E - 7 : 5.12E - 5]$ with $N = 512$ points evenly spaced by $h = 1E - 7$ time difference. These correlation time grid characteristics are just for the first iteration of the whole algorithm, where the short time regimes are employed for the first 11 points, prior to the medium time approximation takes place, while for the large time regimes, the considered domain and time difference shall change accordingly through what is known as a decimation algorithm [69]. In particular, for the correlation time variable, we shall consider Newton-Cotes quadratures for integrals [71], while for the differentiation we simply abide to approximate its definition.

For context, a quadrature is simply the approximation of an integral $\int f(x)dx \approx \sum_i^N f(x_i)w_i$ through a finite sum of the function evaluated in the nodes x_i multiplied by the weights w_i . In particular, for the Clenshaw-Curtis quadrature, the main idea consists in approximating the function through a finite cosine series, for which the employed nodes corresponds to evenly spaced values of the angle variable of the cosine transformation. On the other hand, Newton-Cotes quadratures consist in a polynomial approximation of the function for evenly spaced values of the independent variable, *i.e.*, the simplest zero order approximation yields $\int_{\tau_0}^{\tau_N} f(\tau)d\tau \approx \sum_{i=1}^N f(\tau_i)h$.

In what follows, we consider these approximations in order to obtain coupled recursive expressions for $F(\tau)$, $F_s(\tau)$ and $\Delta\zeta^*(\tau)$. We exemplify such procedure for Eq. (A.12), as similar steps can be taken for Eq. (A.13), while the implementation of Eq. (A.1) is straightforward. Thus, the objective of this procedure is to be able to represent the evaluation of the function F at a correlation time τ in terms of prior known and same time values of F and $\Delta\zeta^*$ through a non-linear relationship. Thus, the next steps are centered around establishing such relationship in terms.

Let us start by considering the differentiation for F in the right side of Eq. (A.12) as

$$\frac{dF(\tau)}{d\tau} \approx \frac{F(\tau) - F(\tau - h)}{h}, \quad (\text{A.18})$$

the differentiation for $\Delta\zeta^*(\tau)$ for the convolution of the same equation as

$$\frac{d\Delta\zeta^*(\tau)}{d\tau} \approx \frac{d\Delta\zeta^*(\tau + h) - d\Delta\zeta^*(\tau)}{h}, \quad (\text{A.19})$$

and a right side rectangle approximation for the convolution integral for the first and last interval of the correlation time $\tau_i \equiv ih$, reading as

$$\int_0^h f(\tau')d\tau' \approx f(h)h, \quad (\text{A.20})$$

and

$$\int_{(i-1)h}^{ih} f(\tau')d\tau' \approx f(ih)h, \quad (\text{A.21})$$

respectively. These approximations allow us to write eq. (A.12) as

$$\begin{aligned} \frac{F_i - F_{i-1}}{h} = & \lambda [\Delta\zeta_i^* S - \Delta\zeta_0^* F_i] - k^2 D_0 S^{-1} F_i - \lambda (\Delta\zeta_i^* - \Delta\zeta_{i-1}^*) F_1 \\ & - \lambda (\Delta\zeta_1^* - \Delta\zeta_0^*) F_i - \lambda \int_h^{(i-1)h} \frac{\Delta\zeta^*(ih + h - \tau') - \Delta\zeta^*(ih - \tau')}{h} F(\tau') d\tau', \end{aligned}$$

where the notation $f_i = f(\tau_i)$ is being employed. Thus, regrouping yields

$$\begin{aligned} \alpha F_i = & F_{i-1} + h\lambda\Delta\zeta_{i-1}^* F_1 - \lambda \int_h^{(i-1)h} [\Delta\zeta^*(ih + h - \tau') - \Delta\zeta^*(ih - \tau')] F(\tau') d\tau' \\ & + h\lambda\Delta\zeta_i^*(S - F_1), \end{aligned} \quad (\text{A.22})$$

where we have highlighted in red the terms at τ_i , and where

$$\alpha = 1 + hk^2 D_0 S^{-1} + h\lambda\Delta\zeta_1^*. \quad (\text{A.23})$$

The exact same procedure then can be followed for $F^{(s)} \equiv F_s$ (which we now denote and differentiate with the super index for clarity purposes), leading to

$$\begin{aligned} \alpha^{(s)} F_i^{(s)} = & F_{i-1}^{(s)} + h\lambda\Delta\zeta_{i-1}^* F_1^{(s)} - \lambda \int_h^{(i-1)h} [\Delta\zeta^*(ih + h - \tau') - \Delta\zeta^*(ih - \tau')] F^{(s)}(\tau') d\tau' \\ & + h\lambda\Delta\zeta_i^*(1 - F_1^{(s)}), \end{aligned} \quad (\text{A.24})$$

where the same highlight has been made and with

$$\alpha^{(s)} = 1 + hk^2 D_0 + h\lambda\Delta\zeta_1^*. \quad (\text{A.25})$$

The procedure up to this point, allow us to consider Newton-Cotes quadratures for the convolution interval $\tau \in [h : (i-1)h]$ of order as high as $i-2$, which could help for better evaluations of the integral. Nevertheless, in what follows we consider the simple right side rectangles approximation, leading to

$$\alpha F_i = F_{i-1} + h\lambda\Delta\zeta_{i-1}^* F_1 - h\lambda \sum_{j=2}^{i-1} [\Delta\zeta_{i+1-j}^* - \Delta\zeta_{i-j}^*] F_j + h\lambda\Delta\zeta_i^*(S - F_1), \quad (\text{A.26})$$

$$\alpha^{(s)} F_i^{(s)} = F_{i-1}^{(s)} + h\lambda\Delta\zeta_{i-1}^* F_1^{(s)} - h\lambda \sum_{j=2}^{i-1} [\Delta\zeta_{i+1-j}^* - \Delta\zeta_{i-j}^*] F_j^{(s)} + h\lambda\Delta\zeta_i^*(1 - F_1^{(s)}), \quad (\text{A.27})$$

which together with Eq. (A.1) allows us to establish a relatively simple system of equations.

In principle, all that is left to do is to solve the system of equations. This may be achieved through a solution proposal, *i.e.*, a test value for the memory function, namely $\Delta\zeta_i^* = \Delta\zeta_{test}^*$, as it allow us to compute F_i and $F_i^{(s)}$ with Eqs. (A.26) and (A.27) respectively, and in return can be employed in Eq. (A.1) to assure the validity or quantify an error of the proposal. A simple, yet instructional path to find the solutions might be devised by simply exploring the space of solutions given by the proposals, *i.e.*, proposing a grid of test values, where solutions exists as long as zeros for $\Delta\zeta_{test}^* - \Delta\zeta_i^*$ can be found, in which $\Delta\zeta_i^*$ is the result of the aforementioned procedure.

Nevertheless, such path to the solution is impractical, whereas an algorithm which can be automated is desirable. For such reason, a Picard iteration method is employed instead. For such

method, we start by approximating the test value for the memory function by its immediately previous value, namely $\Delta\zeta_{test}^* = \Delta\zeta_{i-1}^*$. This is due to an expected smoothness in the functions, yet one can propose different starting points. Then, we proceed to obtain $\Delta\zeta_i^*$ as previously described. After that, the relative error

$$\epsilon = \left| \frac{\Delta\zeta_i^* - \Delta\zeta_{test}^*}{\Delta\zeta_{test}^*} \right|, \quad (\text{A.28})$$

is computed and compared with an acceptance tolerance tol , which for the current work is set at $tol = 10^{-7}$. Next, if $\epsilon > tol$, the new value is proposed as the new test value, $\Delta\zeta_{test}^* = \Delta\zeta_i^*$, which in return, initiates another iteration of the procedure. This is done until an error value lower than the set tolerance is found, and extended to the whole correlation time grid.

Thus, the above described procedure allow us, in principle, to solve for F , F_s and $\Delta\zeta^*$ for any time, given that we know at least some prior values of the functions. On the other hand, as one may notice from the convolution sums of Eqs. (A.26) and (A.27), this procedure becomes computationally costly very fast as new correlation times are considered, where a new convolution involving the previous plus the new terms needs to be done. In addition, we are interested to solve these expressions in a logarithmic scale, as the description of arrest or near-arrest dynamics requires the description of longer and longer times. Thus, in practice, this procedure is only employed for a finite not-so big grid of correlation times, which is what we refer to as medium times.

In this regard, as has been previously stated, the decimation algorithm takes place for larger times. The decimation algorithm consist in the storage of half of the points considered in the correlation time grid once the full N points in time have been computed. This is done by considering a two times greater time step, thus overwriting the properties as

$$\begin{aligned} F_{2i} &\rightarrow F_i, \\ F_{2i}^{(s)} &\rightarrow F_i^{(s)}, \\ \Delta\zeta_{2i}^* &\rightarrow \Delta\zeta_i^*, \\ h &\rightarrow 2h. \end{aligned}$$

This procedure essentially allow us to continue applying the medium times procedure, but starting at the middle times of the grid and now considering the double of the previous maximum correlation time. In the current work, this procedure is done until a convergence is found for the dynamic properties, for which we particularly make use of b , computed from Eq. (2.48) once $\Delta\zeta^*$. Such convergence is established in a similar fashion as it has been done for $\Delta\zeta^*$, thus defining a relative error for the mobility

$$\epsilon_b = \left| \frac{b_p - b}{b_p} \right|, \quad (\text{A.29})$$

where b_p is the computed mobility prior to applying the current decimation, and where b is the computed mobility after the decimation. In order to accept convergence, a tolerance $tol = 10^{-7}$ is employed. In addition, the condition $b \leq 10^{-7}$ is employed to stop the decimation, as it would imply a practically arrested state.

This thorough review upon the numerical algorithm to solve for the SCGLE coupled set of equations resulted in an efficient algorithm implementation. The implementation is available to the public within the repository https://github.com/LANIMFE/HS_HSSW_quench_NESGLE, where one can contact the author for further details.

Appendix B

Additional data treatment for the density fluctuations

This appendix main concern is the preservation of physical boundaries when solving the NE-SCGLE theory equations for the description of mean local density time dependence of isochoric instantaneous quenches, discussed in chapter 6. Specifically, the evolution of the mean local density is modeled after Eq. (6.3), where its evolution explicitly depends upon the propagator Eq. (6.6). In this regard, one should expect for the evolution of $\bar{n}(\mathbf{r}, t)$ to respect simple physical boundaries, such as mass conservation, restricted to positive values, and the denied possibility of overly high values of hard core systems (due to volume exclusion). Nevertheless, such considerations are not strictly taken into account within the proposed equations and solutions. Thus, at extreme cases, such as when a spinodal decomposition process occurs, some of these physical restrictions might be violated.

Thus, let us first consider the physical information that can be acquired from the aforementioned equations, or more specifically, from their solutions for the mean local density(6.7) and the propagator (Eq. (6.6)) propagator solution , which we rewrite for clarity purposes, respectively reading

$$\bar{n}(\mathbf{r}, t) = \bar{n} + \frac{1}{(2\pi)^d} \int d\mathbf{k} e^{-i\mathbf{k}\cdot\mathbf{r}} w[k; u(t)] \Delta\bar{n}(\mathbf{k}, t = 0), \quad (\text{B.1})$$

$$w[k; u] \equiv \exp[-k^2 D_0 \bar{n} \mathcal{E}(k; \bar{n}, T_f) u]. \quad (\text{B.2})$$

In these equations, a relevant limit is obtained at $k \rightarrow 0$, where infinitely large distance are considered. In such limit, $w[k; u]$ is expected to be 1, for whatever value of u , including the $u(t = 0) = 0$ value, which allow us to consider that at such wave-vector, the quantity $\bar{n}(\mathbf{k} \rightarrow 0, t)$ remains constant. This basically implies the conservation of the mean value \bar{n} at any given time, as the initial value of the fluctuations correlations for the wavelength $1/k \rightarrow \infty$ are expected to be totally uncorrelated, thus the net sum over all fluctuations at such wavelength is expected to be zero.

Nevertheless, the fluctuations evolution is actually governed by the propagator, which as discussed in the main text, can increase the magnitude of certain fluctuations for inside spinodal states. Thus, the issue arise when such growth goes beyond the physical limits, being that there is not an explicit consideration for them. Specifically, there is the possibility for the i -mean local density value $\phi^{(i)} \equiv \phi(\mathbf{r} = \mathbf{r}_i, t)$ (referred to the i position) to have a value $\phi^{(i)} < 0$ or $\phi^{(i)} > \phi_{RCP}$, with ϕ_{RCP} being the random close package of the system ($\phi_{RCP} \approx 0.64$ for HS systems). Hence, an additional data treatment is proposed in order to take into account for such limits.

Allow us now to explain a simple procedure which is capable of constraining the physical limits. Let us consider a system divided in N sub-spaces, described by the evolution of the mean local density $\phi^{(i)}$, with $i = 1, 2, 3, \dots, N$, and where the mean bulk value $\bar{\phi}$ can be approximated as $\bar{\phi} \approx \sum_i \phi^{(i)}/N$. The first step in the data treatment protocol is to distinguish if any non-physical value for each of the $\phi^{(i)}$ exist, so we can further proceed. Once it has been established that such non-physical values are present, the next step is to establish which of the physical limits presents a bigger issue. This can be estimated in terms of the mean bulk value $\bar{\phi}$, by simply asking which boundary is closest to, *i.e.*, if $\bar{\phi} < \phi_{RCP}/2$ then negative values are more prominent to be an issue.

Once the closest physical limit is considered, we then proceed to change the non-physical values that violate said limit to the physical threshold, *i.e.*, if $\bar{\phi} < \phi_{RCP}/2$, then all $\phi^{(i)} \leq 0$ are set to 0. This procedure does in fact modify the mean value of the distributions, which as previously stated, was the only thing that we could have assured to be constant, hence, we now need to fix this problem to at least recover the mean of the densities distributions. Therefore, in order to maintain the mean value, we make a linear modification to each fluctuation along the less problematic domain, which for the stated example is every $\phi^{(i)} > \bar{\phi}$. Such linear modification is the simple multiplication of each local densities by a positive constant A , where A must satisfy that $A \sum \Delta\phi_i^{(+)} + \sum \Delta\phi_i^{(-)} = 0$, where $\Delta\phi^{(+)} = \phi_i^+ - \bar{\phi}$ is a positive fluctuation ($\phi_i^+ \geq \bar{\phi}$), and where $\Delta\phi^{(-)} = \phi_i^- - \bar{\phi}$ is a negative one ($\phi_i^- < \bar{\phi}$).

The previous proposal does have the disadvantage of modifying the variance of the mean local densities affected distributions, nevertheless assures for them to at least to respect the physical boundaries and their mean value. Thus, this procedure is implemented in the results of chapter 6 when needed, which is only for certain states in region II of the non-equilibrium glass transition diagram of the considered HSSW system.

Bibliography

- [1] P. E. Ramírez-González and M. Medina-Noyola, “General nonequilibrium theory of colloid dynamics,” *Phys. Rev. E*, vol. 82, no. 6, p. 061503, 2010.
- [2] Herbert B. Callen, *Thermodynamics and Introduction to Thermostatistics*. ”Wiley”, 1985.
- [3] Leopoldo García-Colín, *Introducción a la termodinámica clásica*. ”Trillas”, 1970.
- [4] Donald A. McQuarrie and John D. Simons, *Molecular Thermodynamics*. ”University Science Books”, 1999.
- [5] Flake C. Campbell, *Phase Diagrams—Understanding the Basics*. ”ASM International”, 2012.
- [6] Lee W. J. and J. A. Lucey, “Formation and physical properties of yogurt,” *Asian-Australas J. Anim. Sci.*, vol. 23, no. 9, pp. 1127–1136, 2010.
- [7] Ph. Colomban, “Gel technology in ceramics, glass-ceramics and ceramic-ceramic composites,” *Ceramics International*, vol. 15, no. 1, pp. 23–50, 1989.
- [8] E. D. Zanotto and P. K. Gupta, “Do cathedral glasses flow?—additional remarks,” *Ceramics International*, vol. 67, no. 3, pp. 260–262, 1999.
- [9] W. Götze, “Dynamical phenomena near the liquid-glass transition,” *Zeitschrift für Physikalische Chemie*, vol. 156, no. 1, pp. 3–22, 1988.
- [10] G. Szamel and H. Löwen, “Mode-coupling theory of the glass transition in colloidal systems,” *Phys. Rev. A*, vol. 44, no. 12, pp. 8215–8219, 1991.
- [11] L. Yeomans-Reyna and M. Medina-Noyola, “Self-consistent generalized langevin equation for colloid dynamics,” *Phys. Rev. E*, vol. 64, no. 6, p. 066114, 2001.
- [12] L. Yeomans-Reyna, M. Chávez-Rojo, P. E. Ramírez-González, R. Juárez-Maldonado, M. Chávez-Páez, and M. Medina-Noyola, “Dynamic arrest within the self-consistent generalized langevin equation of colloid dynamics,” *Phys. Rev. E*, vol. 76, no. 4, p. 041504, 2007.
- [13] U. Bengtzelius, W. Götze, and A. Sjölander, “Dynamics of supercooled liquids and the glass transition,” *J. Phys. C: Solid State Phys.*, vol. 17, no. 33, pp. 5915–5934, 1984.
- [14] C. A. Angell, K. L. Ngai, G. B. McKenna, P. F. McMillan, and S. W. Martin, “Relaxation in glassforming liquids and amorphous solids,” *J. Appl. Phys.*, vol. 88, no. 6, pp. 3113–3157, 2000.

- [15] M. D. Ediger, C. A. Angell, and Sidney R. Nagel, “Supercooled liquids and glasses,” *J. Phys. Chem.*, vol. 100, no. 31, pp. 13200–13212, 1996.
- [16] L. M. C. Janssen, “Mode-coupling theory of the glass transition: A primer,” *Frontiers in Physics*, vol. 6, no. 1, p. 97, 2018.
- [17] M. Sperl, “Dynamics in colloidal liquids near a crossing of glass- and gel-transition lines,” *Phys. Rev. E*, vol. 69, no. 1, p. 011401, 2004.
- [18] H. Guo, S. Ramakrishnan, J. L. Harden, and R. L. Leheny, “Gel formation and aging in weakly attractive nanocolloid suspensions at intermediate concentrations,” *J. Chem. Phys.*, vol. 135, no. 15, p. 154903, 2011.
- [19] A. Latz, “Non-equilibrium mode-coupling theory for supercooled liquids and glasses,” *Condens. Matter*, vol. 12, no. 29, pp. 6353–6363, 2000.
- [20] L. E. Sánchez-Díaz, P. Ramírez-González, and M. Medina-Noyola, “Equilibration and aging of dense soft-sphere glass-forming liquids,” *Phys. Rev. E*, vol. 87, no. 5, p. 052306, 2013.
- [21] L. E. Sánchez-Díaz, E. Lázaro-Lázaro, J. M. Olais-Govea, and M. Medina-Noyola, “Non-equilibrium dynamics of glass-forming liquid mixtures,” *J. Chem. Phys.*, vol. 140, no. 23, p. 234501, 2014.
- [22] P. Mendoza-Méndez, E. Lázaro-Lázaro, L. E. Sánchez-Díaz, P. Ramírez-González, Pérez-Ángel, and M. Medina-Noyola, “Crossover from equilibration to aging: Nonequilibrium theory versus simulations,” *Phys. Rev. E*, vol. 96, no. 2, p. 022608, 2017.
- [23] E. Cortés-Morales, L. F. Elizondo-Aguilera, and M. Medina-Noyola, “Equilibration and aging of liquids of non-spherically interacting particles,” *J. Phys. Chem. B*, vol. 120, no. 32, pp. 7975–7987, 2016.
- [24] L. F. Elizondo-Aguilera, E. Cortés-Morales, P. F. Zubieta-Rico, M. Medina-Noyola, R. Castañeda-Priego, T. Voigtmann, and G. Pérez-Ángel, “Arrested dynamics of the dipolar hard sphere model,” *Soft Matt.*, vol. 16, no. 1, pp. 170–190, 2020.
- [25] José Manuel Olais-Govea, Leticia López-Flores, and Magdalena Medina-Noyola, “Non-equilibrium theory of arrested spinodal decomposition,” *J. Phys. Chem.*, vol. 143, no. 17, p. 174505, 2015.
- [26] E. Zaccarelli, “Colloidal gels: equilibrium and non-equilibrium routes,” *J. Phys. Cond. Matt.*, vol. 19, no. 32, p. 323101, 2007.
- [27] T. Gibaud and P. Schurtenberger, “A closer look at arrested spinodal decomposition in protein solutions,” *J. Phys. Condens. Matter*, vol. 21, no. 32, p. 322201, 2009.
- [28] B. Ruzicka and E. Zaccarelli, “A fresh look at the laponite phase diagram,” *Soft Matter*, vol. 7, no. 4, pp. 1268–1286, 2011.
- [29] J. M. Olais-Govea, L. López-Flores, J. B. Zepeda-López, and M. Medina-Noyola, “Interference between the glass, gel, and gas-liquid transitions,” *Sci. Rep.*, vol. 9, no. 1, p. 16445, 2019.

- [30] J. M. Olais-Govea, L. López-Flores, and M. Medina-Noyola, “The subtle kinetics of arrested spinodal decomposition: Colloidal gels and porous glasses,” *MRS Adv.*, vol. 3, no. 1, p. 3817–3825, 2018.
- [31] K. Nakashima, K. Noda, and K. Mori, “Time–temperature–transformation diagrams for borosilicate glasses and preparation of chemically durable porous glasses,” *J. Am. Ceram. Soc.*, vol. 80, no. 5, pp. 1101–1110, 1997.
- [32] B. Ruzicka, E. Zaccarelli, L. Zulian, R. Angelini, M. Sztucki, A. Moussaïd, T. Narayanan, and F. Sciortino, “Observation of empty liquids and equilibrium gels in a colloidal clay,” *Nat. Mat.*, vol. 10, no. 1, pp. 56–60, 2011.
- [33] J. B. Zepeda-López and M. Medina-Noyola, “Waiting-time dependent non-equilibrium phase diagram of simple glass- and gel-forming liquids,” *J. Phys. Chem.*, vol. 154, no. 17, p. 174901, 2021.
- [34] Stephen M. Kosslyn, “Through the glass lightly,” *Science*, vol. 267, no. 5204, pp. 1615–1615, 1995.
- [35] M. Medina-Noyola and J. L. del Rio-Correa, “The fluctuation-dissipation theorem for non-markov processes and their contractions: The role of the stationarity condition,” *Phys. A: Stat. Mech. and its Apls.*, vol. 146, no. 3, pp. 483–505, 1987.
- [36] M. Medina-Noyola, “The generalized langevin equation as a contraction of the description,” *Faraday Discuss. Chem.*, vol. 83, no. 0, pp. 21–31, 1987.
- [37] R. Juárez-Maldonado, M. Chávez-Rojo, P. E. Ramírez-González, L. Yeomans-Reyna, and M. Medina-Noyola, “Simplified self-consistent theory of colloid dynamics,” *Phys. Rev. E*, vol. 76, no. 6, p. 062502, 2007.
- [38] L. Onsager and S. Machlup, “Fluctuations and irreversible processes,” *Phys. Rev.*, vol. 91, no. 6, pp. 1505–1512, 1953.
- [39] L. Onsager and S. Machlup, “Fluctuations and irreversible process. ii. systems with kinetic energy,” *Phys. Rev.*, vol. 91, no. 6, pp. 1512–1515, 1953.
- [40] M. Medina-Noyola, “Generalized onsager-machlup’s theory of thermal fluctuations for non-equilibrium systems,” *arXiv*, vol. 1, no. 0, pp. –, 2009.
- [41] P. E. Ramírez-González and M. Medina-Noyola, “Aging of a homogeneously quenched colloidal glass-forming liquid,” *Phys. Rev. E*, vol. 82, no. 6, p. 061504, 2010.
- [42] Jean-Pierre Hansen and I. R. McDonald, *Theory of Simple Liquids.* “Academic Press”, 2006.
- [43] M. S. Wertheim, “Exact solution of the percus-yevick integral equation for hard spheres,” *Phys. Rev. Lett.*, vol. 10, no. 8, pp. 321–323, 1963.
- [44] Loup Verlet and Jean-Jacques Weis, “Equilibrium theory of simple liquids,” *Phys. Rev. A*, vol. 5, no. 2, pp. 939–952, 1972.
- [45] Jean-Pierre Hansen and Loup Verlet, “Phase transitions of the lennard-jones system,” *Phys. Rev.*, vol. 184, no. 1, pp. 151–161, 1969.

- [46] Hartmut Löwen, Thomas Palberg, and Rolf Simon, “Dynamical criterion for freezing of colloidal liquids,” *Phys. Rev. Lett.*, vol. 70, no. 10, pp. 1557–1560, 1993.
- [47] T. Voigtmann, “Multiple glasses in asymmetric binary hard spheres,” *EPL*, vol. 96, no. 3, p. 36006, 2011.
- [48] V. Testard, L. Berthier, and W. Kob, “Intermittent dynamics and logarithmic domain growth during the spinodal decomposition of a glass-forming liquid,” *J. Chem. Phys.*, vol. 100, no. 16, p. 164502, 2014.
- [49] S. Cocard, J. F. Tassin, and T. Nicolai, “Dynamical mechanical properties of gelling colloidal disks,” *J. Rheol.*, vol. 44, no. 3, pp. 585–594, 2000.
- [50] H. M. Wyss, S. Romer, F. Scheffold, P. Schurtenberger, and L. J. Gauckler, “Diffusing-wave spectroscopy of concentrated alumina suspensions during gelation,” *J. Col. Int. Sci.*, vol. 241, no. 1, pp. 89–97, 2001.
- [51] M. Pilavtepe, S. M. Recktenwald, R. Schumann, K. Emmerich, and N. Willenbacher, “Macro- and microscale structure formation and aging in different arrested states of laponite dispersions,” *J. Rheol.*, vol. 62, no. 2, pp. 593–605, 2018.
- [52] F. Sciortino and P. Tartaglia, “Glassy colloidal systems,” *Adv. Phys.*, vol. 54, no. 6-7, pp. 471–524, 2005.
- [53] P. Poesio, A. M. Lezzi, and G. P. Beretta, “Evidence of convective heat transfer enhancement induced by spinodal decomposition,” *Phys. Rev. E*, vol. 75, no. 6, p. 066306, 2007.
- [54] Y. Li and T. Tanaka, *Effects of Shear Modulus of Polymer Gels*, pp. 471–524. 1991.
- [55] N. Khalil, A. de Candia, A. Fierro, M. P. Ciamarra, and A. Coniglio, “Dynamical arrest: interplay of glass and gel transitions,” *Soft Matter*, vol. 10, no. 27, pp. 4800–4805, 2014.
- [56] P. Chaudhuri, L. Berthier, P. I. Hurtado, and W. Kob, “When gel and glass meet: A mechanism for multistep relaxation,” *Soft Matter*, vol. 81, no. 4, p. 040502, 2010.
- [57] P. Chaudhuri, P. I. Hurtado, L. Berthier, and W. Kob, “Relaxation dynamics in a transient network fluid with competing gel and glass phases,” *J. Chem. Phys.*, vol. 142, no. 17, p. 174503, 2015.
- [58] Sourya Banik and G. B. McKenna, “Isochoric structural recovery in molecular glasses and its analog in colloidal glasses,” *Phys. Rev. E*, vol. 97, no. 6, p. 062601, 2018.
- [59] E. R. Weeks, “Introduction to the colloidal glass transition,” *ACS Macro Lett.*, vol. 6, no. 1, pp. 27–34, 2017.
- [60] D. A. Weitz, *Colloidal Glasses*, pp. 25–39. 2011.
- [61] G. L. Hunter and E. R. Weeks, “The physics of the colloidal glass transition,” *Rep. Prog. Phys.*, vol. 75, no. 6, p. 066501, 2012.
- [62] T. Voigtmann, M. Siebenbürger, C. P. Amann, S. U. Egelhaaf, S. Fritschi, M. Kröger, M. Laurati, K. J. Mutch, and K. H. Samwer, “Rheology of colloidal and metallic glass formers,” *Colloid Polym. Sci.*, vol. 298, no. 7, p. 681–696, 2020.

- [63] E. Zaccarelli, G. Foffi, K. A. Dawson, S. V. Buldyrev, F. Sciortino, and P. Tartaglia, “Confirmation of anomalous dynamical arrest in attractive colloids: A molecular dynamics study,” *Phys. Rev. E*, vol. 66, no. 4, p. 041402, 2002.
- [64] L. F. Elizondo-Aguilera, P. F. Zubieta-Rico, H. Ruiz-Estrada, and O. Alarcón-Waess, “Self-consistent generalized langevin-equation theory for liquids of nonspherically interacting particles,” *Phys. Rev. E*, vol. 90, no. 5, p. 052301, 2014.
- [65] W. J. MacKnight and F. E. Karasz, *4 - Polymer Blends*, pp. 111–130. 1989.
- [66] R. F. Greene and H. B. Callen, “On the formalism of thermodynamic fluctuation theory,” *Phys. Rev.*, vol. 83, no. 6, pp. 1231–1235, 1951.
- [67] A. Hodroj, P. Simon, P. Florian, M. H. Chopinet, and Y. Vails, “Phase separation and spatial morphology in sodium silicate glasses by afm, light scattering and nmr,” *J. Am. Ceram. Soc.*, vol. 96, no. 8, pp. 2454–2460, 2013.
- [68] X. Li, Y. Wang, X. Lu, and C. Xiao, “Morphology changes of polyvinylidene fluoride membrane under different phase separation mechanisms,” *J. Membr. Sc.*, vol. 320, no. 1, pp. 477–482, 2008.
- [69] W. Götze, “Bifurcations of an iterated mapping with retardations,” *J. Stat. Phys.*, vol. 83, no. 5, p. 1183–1197, 1996.
- [70] M. Fuchs, W. Götze, I. Hofacke, and A. Latz, “Comments on the alpha -peak shapes for relaxation in supercooled liquids,” *J. Phys. Cond. Matt.*, vol. 3, no. 26, pp. 5047–5071, 1991.
- [71] P. K. Kythe and P. Puri, *Computational Methods for Linear Integral Equations*. ”Springer Scienc+Business Media, LLC”, 2002.